ANNALS OF CARNEGIE MUSEUM

VOL. 74, NUMBER 2, PP. 91—150 30 JUNE 2005

CRANIAL ANATOMY AND RELATIONSHIPS OF A NEW CTENODACTYLOID (MAMMALIA, RODENTIA) FROM THE EARLY EOCENE OF HUBEI PROVINCE, CHINA

JOHN R. WIBLE
Curator, Section of Mammals
5800 Baum Blvd., Pittsburgh, PA 15206-3706 (WibleJ@CarnegieMNH.Org)

YUANQING WANG
Institute of Vertebrate Paleontology and Paleoanthropology, Chinese Academy of Sciences, Beijing 100044, China
(wangyuanqing@pa.ivpp.ac.cn)

CHUANKUI LI
Research Associate, Section of Vertebrate Paleontology;
Institute of Vertebrate Paleontology and Paleoanthropology, Chinese Academy of Sciences, Beijing 100044, China
(lichuankui@pa.ivpp.ac.cn)

MARY R. DAWSON
Curator Emeritus, Section of Vertebrate Paleontology
4400 Forbes Avenue, Pittsburgh, PA 15213-4080 (DawsonM@CarnegieMNH.Org)

ABSTRACT

Two remarkably complete skulls and associated mandibles from the late early Eocene of the Yuhuangding Formation of Hubei Province, central China, are described as a new genus and species of rodent, *Exmus mini*, and referred to the early ctenodectyloid family Cocomyidae. This is a small rodent in the size range of the early Eocene Asian *Cocomys*. Dental characters that link *Exmus* with other cocomyids include: non-molariform P4; cheek teeth increasing in size posteriorly; lower molar ectolophid weak or absent; and lower molar hypoconulid distinct, enlarged on m3. Cranial characters linking *Exmus* and *Cocomys* include: skull shape and proportions, including a short rostrum and large orbit; sagittal crest absent; large optic canal, confluent between the orbits; and no petrosal shelf posterior to the caudal tympanic process of the petrosal. Differences from *Cocomys* are numerous and include: absence of conules on P4 and loss of the protoconule on the upper molars; tiny metacone and hypocone on P4; molariform p4: and auditory bulla tightly attached, rather than loose as in *Cocomys. Exmus* also displays a number of autapomorphies that distinguish it from all other Eocene rodents examined in this study, such as substantial orbital roof formed by lacrimal and frontal, and a suture between the parietals that is nearly completely fused. A phylogenetic analysis based on characters of the skull, mandible, and dentition supports the concept of two clades within the ingroups, one composed of Eocene paramyids, sciuravids, and theridomyids and the other composed of *Bandaomys, Exmus, Cocomys, Tamquammys, Advenimus,* and *Yuomys* as stem taxa to ctenodactylids and hystricognaths. This dichotomy, which has been suggested by others prior to the discovery of *Exmus,* is here considered to represent an accurate assessment of Eocene rodent evolution and makes good paleogeographic sense. However, the desirability of adding more taxa to a phylogenetic analysis of early rodents is clearly recognized.

KEY WORDS: early Eocene, Rodentia, ctenodactyloid, cranial morphology

INTRODUCTION

From their first appearance in the earliest Eocene Wutu, Lingcha, and Bumban faunas of Asia the ctenodactyloid rodents exhibited a diversity indicative of an initial radiation into a new level of gliriform adaptation (Li et al. 1979; Dashzeveg 1990a; Tong and Dawson 1995; Dashzeveg et al. 1998). These faunas have yielded the ctenodactyloid rodents *Cocomys, Tsagankhushumys, Sharomys,* and *Bumbanomys,* of which the best known is *Cocomys.* Excellently preserved skulls and jaws of *Cocomys lingchaensis* (Li et al. 1989) have yielded important details on dental, cranial, and mandibular characteristics of this basal rodent, thus providing significant insights into early (if not the earliest) rodent evolution.

The Yuhuangding Formation of central China's Hubei Province has been an important source of information on the next younger phase of ctenodactyloid rodent diversity, in the late early Eocene (Li and Ting, 1983). Three rodent taxa have previously been described from near Dajian village in the Yuhuangding Formation, *Advenimus hubeiensis, Hohomys lii,* and cocomyid gen. indet. (Dawson et al. 1984; Hu 1995). The new rodent described here makes the fourth ctenodactyloid taxon from this locality. Two remarkably well preserved skulls and associated lower jaws of this animal document some interesting changes in ctenodactyloid skull morphology. It is notable that the gliriform eurymylid *Rhombomylus* is also very well represented in the Dajian village locality (Meng et al. 2003), giving still more variety among the small herbivores present in the fauna. An additional, although geographically separated, locality of similar age in the Yuhuangding Formation (Guo et al. 2000) produced another ctenodactyloid, *Hannanomys lini.*

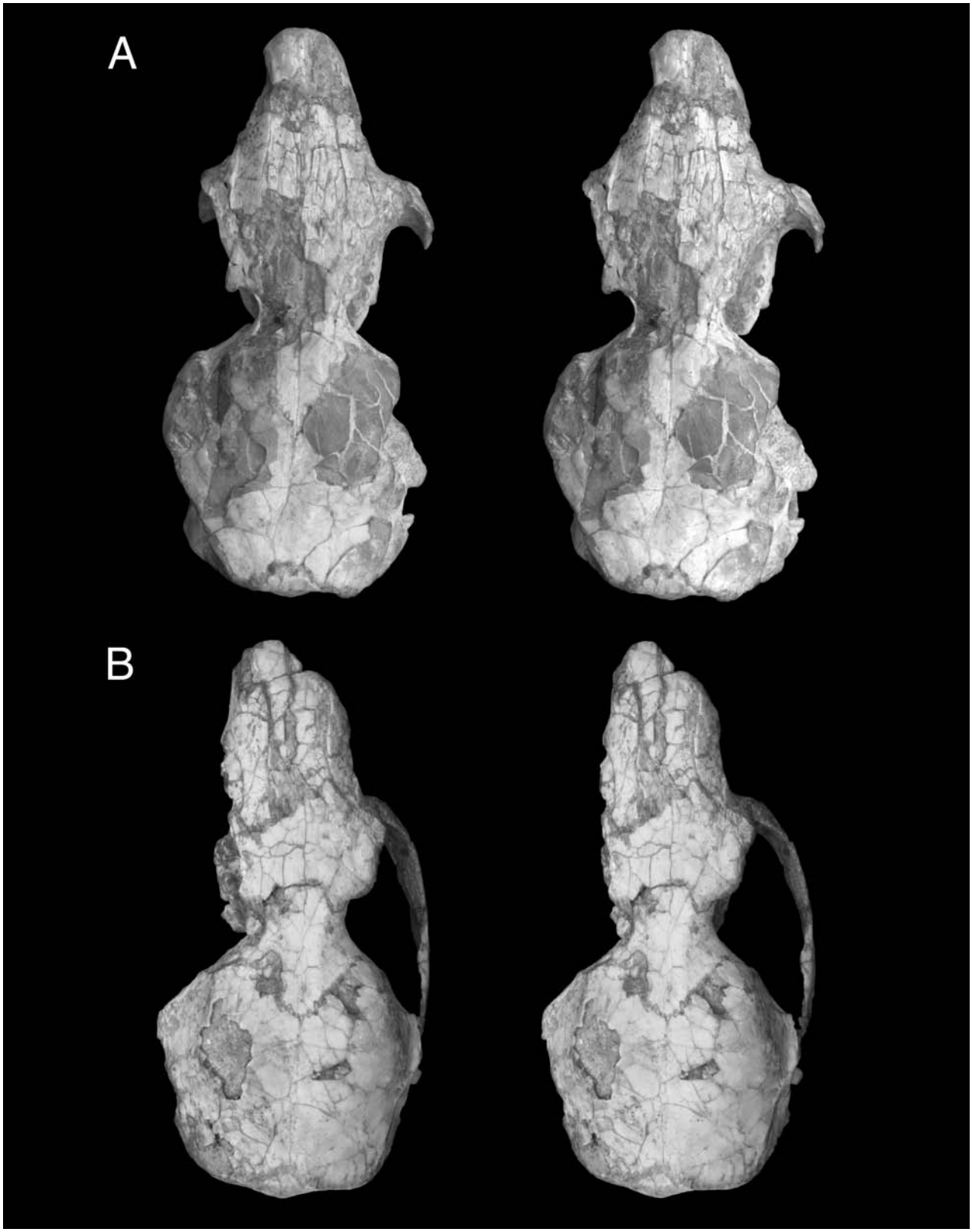
A
B

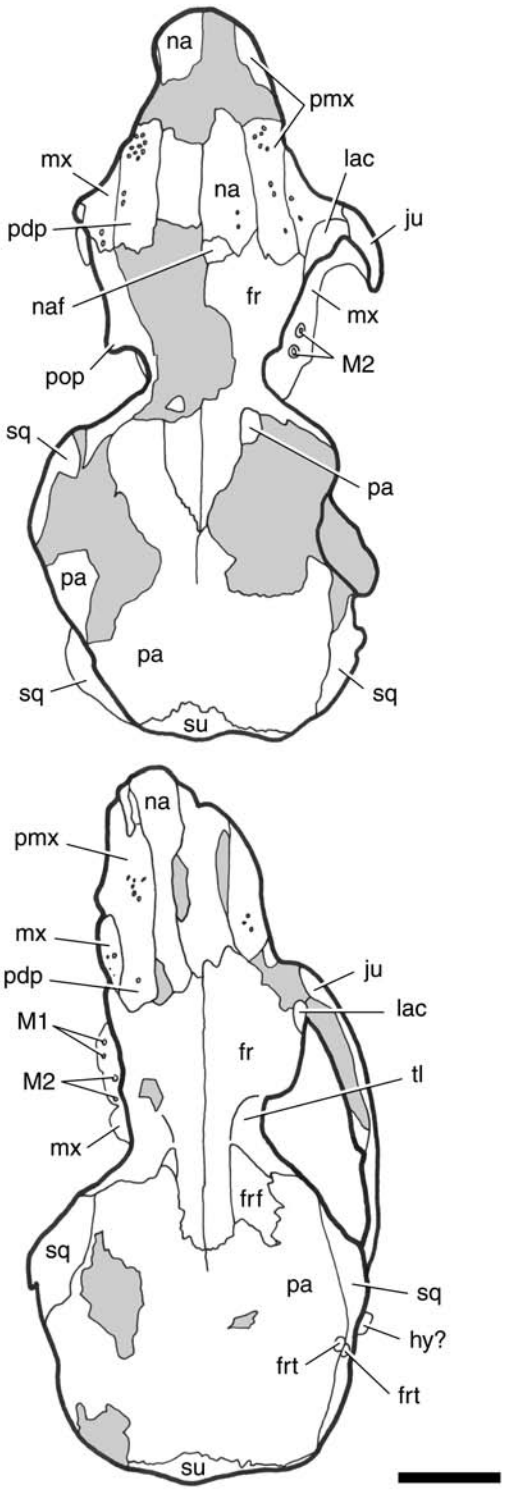

The new rodent taxon is compared with its somewhat older and more primitive relative *Cocomys* as well as with selected younger ctenodactylids. The new evidence provided by this taxon on cranial, mandibular, and dental morphology is then used in a phylogenetic analysis aimed at clarifying relationships among the earliest rodents.

INSTITUTIONAL ABBREVIATIONS

AMNH—Department of Vertebrate Paleontology, American Museum of Natural History, New York, New York; CM—Section of Mammals, Carnegie Museum of Natural History, Pittsburgh, Pennsylvania; IVPP—Institute of Vertebrate Paleontology and Paleoanthropology, Beijing; MAE—Collections of joint Mongolian Academy of Sciences—American Museum of Natural History Expeditions; USNM—Department of Paleobiology, United States National Museum, Smithsonian Institution, Washington, D.C.

SYSTEMATIC PALEONTOLOGY

Order Rodentia Bowdich, 1821

Superfamily Ctenodactyloidea Simpson, 1945

Family Cocomyidae De Bruijn, Hussain, and Leinders, 1982

Genus *EXMUS,* gen. nov.

(Figures 1–6 and 8–16)

Type and only known species.—*Exmus mini,* sp. nov.

Age and locality.—Late early Eocene, Hubei Province, China.

Diagnosis.—As for species.

EXMUS MINI, sp. nov.

Holotype.—IVPP V7429. Skull with lower jaws; right I2, P3, dP4, M1-3; left I2, dP4, M1-M3; right i2, dp4, m1-m3; left i2, dp4, m1-m3.

Hypodigm.—Type and IVPP V7430, skull with articulated lower jaws; right P3 (broken), dP4, P4 in crypt, M1-3; left I2, M1-3; right i2, dp4, m1-3; left i2, p4, m1-m3. Of the two specimens, V7429 is a slightly younger individual, with M3 not completely out of its crypt, but both individuals retain deciduous teeth. IVPP V7430 has larger cheek teeth, but this is here regarded as individual variation because skull, jaw, and tooth morphologies of the two individuals are essentially the same.

Fig. 1.—*Exmus mini* IVPP V7429 (A) and IVPP V7430 (B), dorsal view of skull, stereophotograph and accompanying line drawing. Grey represents matrix. Scale = 5 mm. Abbreviations: **fr**, frontal; **frf**, frontal facet on parietal; **frt**, foramen for ramus temporalis; **hy?**, possible hyoid arch element; **ju**, jugal; **lac**, lacrimal; **M1**, roots of upper first molar; **M2**, roots of upper second molar; **mx**, maxilla; **na**, nasal; **naf**, nasal facet on frontal; **pa**, parietal; **pdp**, posterodorsal process of premaxilla; **pmx**, premaxilla; **pop**, postorbital process; **sq**, squamosal; **su**, supraoccipital; **tl**, temporal line.

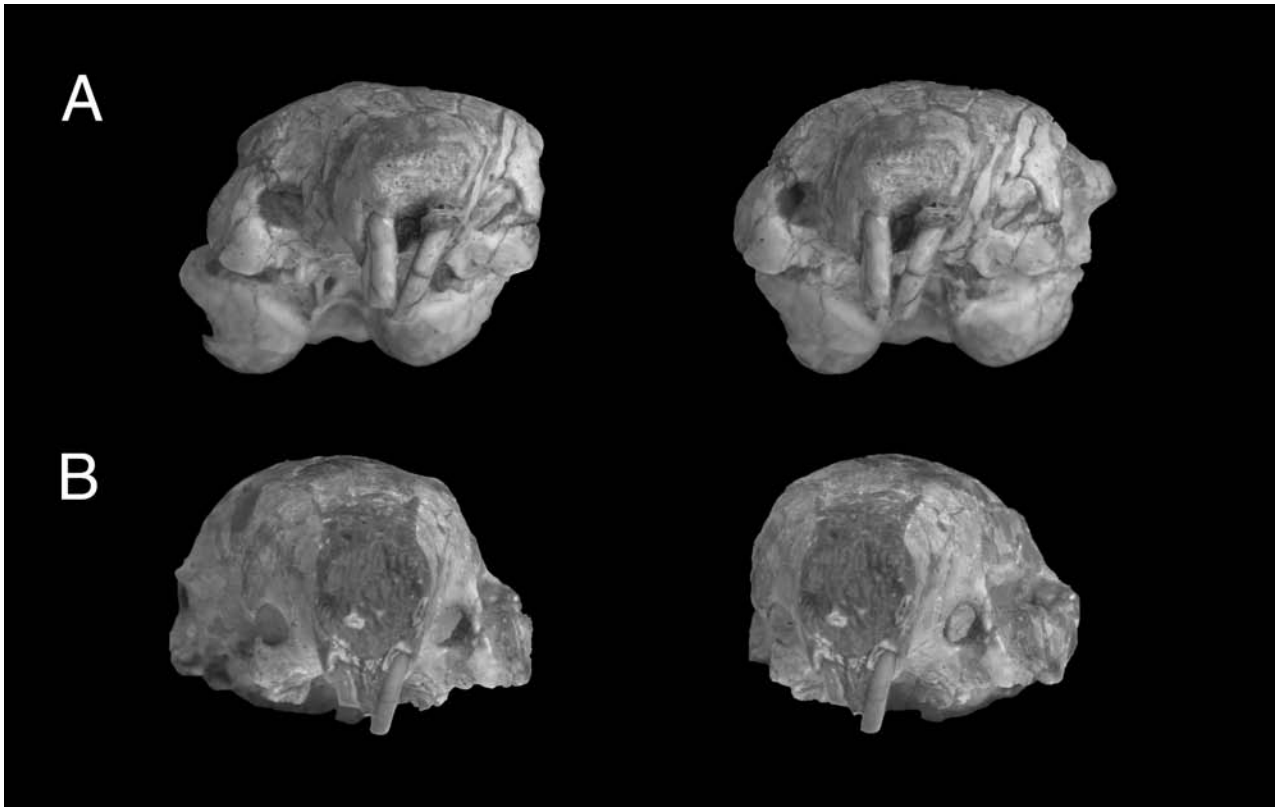

Fig. 2.—*Exmus mini* IVPP V7429 (**A**) and *Cocomys lingchaensis* IVPP V7399 (**B**), anterior view of skull, stereophotograph and accompanying line drawing. Grey represents matrix. Scale = 5 mm. Abbreviations: **ec**, ectotympanic; **ena**, external nasal aperture; **I1**, upper second incisor; **iof**, infraorbital foramen; **ju**, jugal; **lac**, lacrimal; **mx**, maxilla; **na**, nasal; **pmx**, premaxilla.

Horizon and locality.—Late early Eocene: Dajian locality, Yuhuangding Formation, Xichuan Basin (or Liquanqiao Basin), Hubei Province, IVPP locality IVPP 76006. Collected by Yuan Wang and Wei Zhou.

Diagnosis.—Small ctenodactyloid (cocomyid) rodent having bunodont cheek teeth, dental formula I/i, P3-M3/p4-m3, slight unilateral hypsodonty in P4-M3. P4 having single large buccal cusp (paracone) with very small metacone on its flank, and lacking conules on proto- and metaloph. Upper molars lacking protoconule (paraconule). The p4 talonid slightly wider than trigonid, with well developed entoconid, hypoconid, and hypoconulid. Auditory bullae inflated, firmly attached to skull. Differs from *Cocomys* in having small metacone and lacking conules on P4, lacking protoconule on upper molars, having relatively larger metaconule; anterior zygomatic root farther anterior in position and more vertical; more inflated auditory bulla relatively tightly attached to skull. Differs from *Advenimus hubeiensis* in slightly smaller size and more anteriorly placed masseteric fossa. Differs from *Hohomys lii* in much smaller size, relatively smaller incisive foramina, and simple P3. Differs from cocomyid gen. indet. in having talonid wider than trigonid on p4. Differs from *Hannanomys lini* in having p4 talonid wider than trigonid, lower molars lacking a well-developed posterior arm of protoconid and lacking a well-developed hypolophid, and having a more anteriorly placed masseteric fossa. These diagnostic features are treated in more detail and illustrated below.

Etymology.—Latin, *ex*-out of, and *mus*-mouse; species name is in memory of the late Professor Mingzhen Zhou, nicknamed Min, respected colleague and visionary director of the IVPP.

DESCRIPTIONS

Below is a bone-by-bone description of the external surfaces of individual cranial bones and lower jaws of the two specimens of *Exmus,* following the format of Wible (2003) and Wible and Gaudin (2004), and then a description of the dentition. Unfortunately, a common anatomical terminology has not been employed by researchers publishing on extinct and extant rodents. For our descriptions, wherever possible, we employ the Latin term or anglicized version thereof from the fourth edition of the Nomina Anatomica Veterinaria (1994). For the dental terminology, we follow Wood and Wilson (1936). The abbreviations "I,

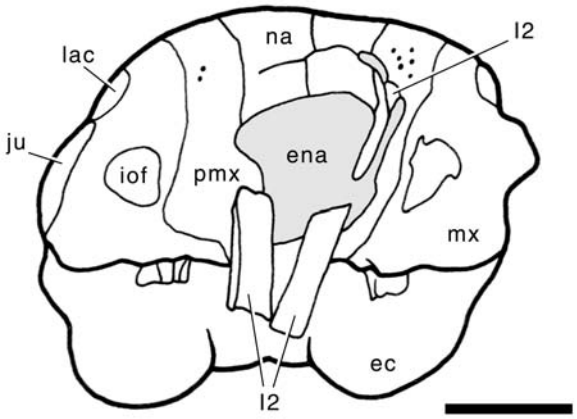

P, M" and "i, p, m" are used to refer to upper and lower incisors, premolars, and molars, respectively. We identify the enlarged upper and lower incisors of *Exmus* as I2 and i2, respectively, accepting these as homologous with the enlarged, retained deciduous second incisor of extant rodents (Moss-Salentijin 1978; Luckett 1985).

Most of the illustrations are stereophotographs with accompanying line drawings. The stereophotographs in Figures 1–5, 7, 10–12, and 15 were taken with a Nikon D-1 and those in Figures 6, 8, 9, and 13 employed the Auto-Montage Pro software (Syncroscopy, Frederick, MD). IVPP V7430 was subjected to high resolution micro-computer tomography (CT scan), both to reveal the morphology of the right P4, which was hidden above dP4, and to confirm some interpretations of cranial foramina. Two scans of the skull were made with Universal System's HD-100 micro CT scanner at the Center for Quantitative Imaging, Pennsylvania State University. The whole skull was scanned with an interslice resolution (z-axis) of 0.03458 mm and XY pixel size of 0.0275 mm. The area of the unerupted P4 was scanned at much higher resolution, with z-spacing at 0.016921 mm and XY pixel size at 0.0125 mm. The resulting data for both scans were archived as slices in 1024×1024 16-bit tiff format. Three-dimensional reconstruction of the unerupted tooth was performed using the interactive segmentation editor in Amira 3.1 (TGS Template Graphics Software, Inc., San Diego, CA) and two views are included in figure 14. Finally, the microstructure of the lower incisor enamel was studied by Professor Wighart von Koenigswald, Rheinischen Friedrich-Wilhelms-Universität Bonn, Germany; two scanning electron micrographs provided by him are included in Figure 16.

The skulls of IVPP V7429 and V7430 are remarkably complete, although sutures are not always clear even in these young individuals due in part to many post-mortem cracks on the surfaces of the bones. In the former specimen, both zygomata are missing as is bone in the confluence of the right alisphenoid, squamosal, and parietal. The latter specimen is less complete and not as thoroughly prepared; the left zygoma, basioccipital, and exoccipitals are missing. The presence of auditory bullae in both specimens hindered the full preparation of the ear region, although a remarkable amount of the right middle ear of IVPP 7429 has been painstakingly prepared as have the left malleus and incus. For comparisons, we had access to a specimen of *Cocomys lingchaensis,* IVPP V7399 (skull 1 of Li et al. 1989).

In many dimensions, the skull of *Exmus mini* is remarkably similar to that of *Cocomys lingchaensis* (Table 1). Viewed laterally (Figs. 3, 4), the skull of *Exmus* is long and low with a short, slightly heavy rostrum that reduces in width anteriorly, similar to that of *Cocomys.* Li et al. (1989) reported the ratio of the length of the facial region (from the posterior margin of the upper incisor to the protocone of the last molar) to that of the cranial region (from the protocone of the last molar to the posterior end of the occipital condyle) to be 0.80–0.84 for *Cocomys,* 1.0 for *Paramys,* and 1.08 for *Sciuravus*; the ratio in the type of *Exmus,* V7429, is 0.79. Also as in *Cocomys,* the zygoma preserved on the right side of V7430 is not expanded laterally, but is nearly parallel to the long axis of the skull, slightly wider posteriorly (Fig. 1B). Among the principal differences between *Exmus* and *Cocomys,* the former has moderately inflated, firmly attached auditory bullae, whereas the bullae in *Cocomys* are smaller and more loosely attached to the petrosal (of 20 skulls reported by Li et al. [1989], bullae are preserved and then incompletely in only four). Also, the incisive foramina and the diastema between the upper incisor and postcanines are slightly larger in *Exmus* than in *Cocomys.* Finally, *Cocomys* has an interparietal bone, which is wholly absent in *Exmus,* and a slightly higher and more rounded braincase.

Nasal

The nasal bones form the roof of the snout. They are damaged in both specimens. The anterior one-third of the nasal, best preserved on the left side of V7429 (Fig. 1A), has a gently convex external surface; the posterior two-thirds is best preserved on the right side of V7430 (Fig. 1B) and is essentially flat. In dorsal view, the nasal is roughly quadrangular, long and thin. The anterior border is slightly convex and has a slight overhang of the external nasal aperture (Figs. 3, 4). The posterior border, which is at a level anterior to the postorbital process, is also slightly convex, with the nasal overlapping the frontal (Fig. 1). The lateral border of the nasal includes the long suture with the premaxilla and the short suture with the frontal. Along the lateral border, the nasal is widest at two points, at its rostral end and at the level of the anterior orbital margin. Between these two points the nasal is slightly concave and the premaxilla slightly convex. The dorsal surface of the nasal is poorly preserved, but in the posterior part in V7429 there are some tiny foramina, presumably nutritive in nature (Fig. 1A).

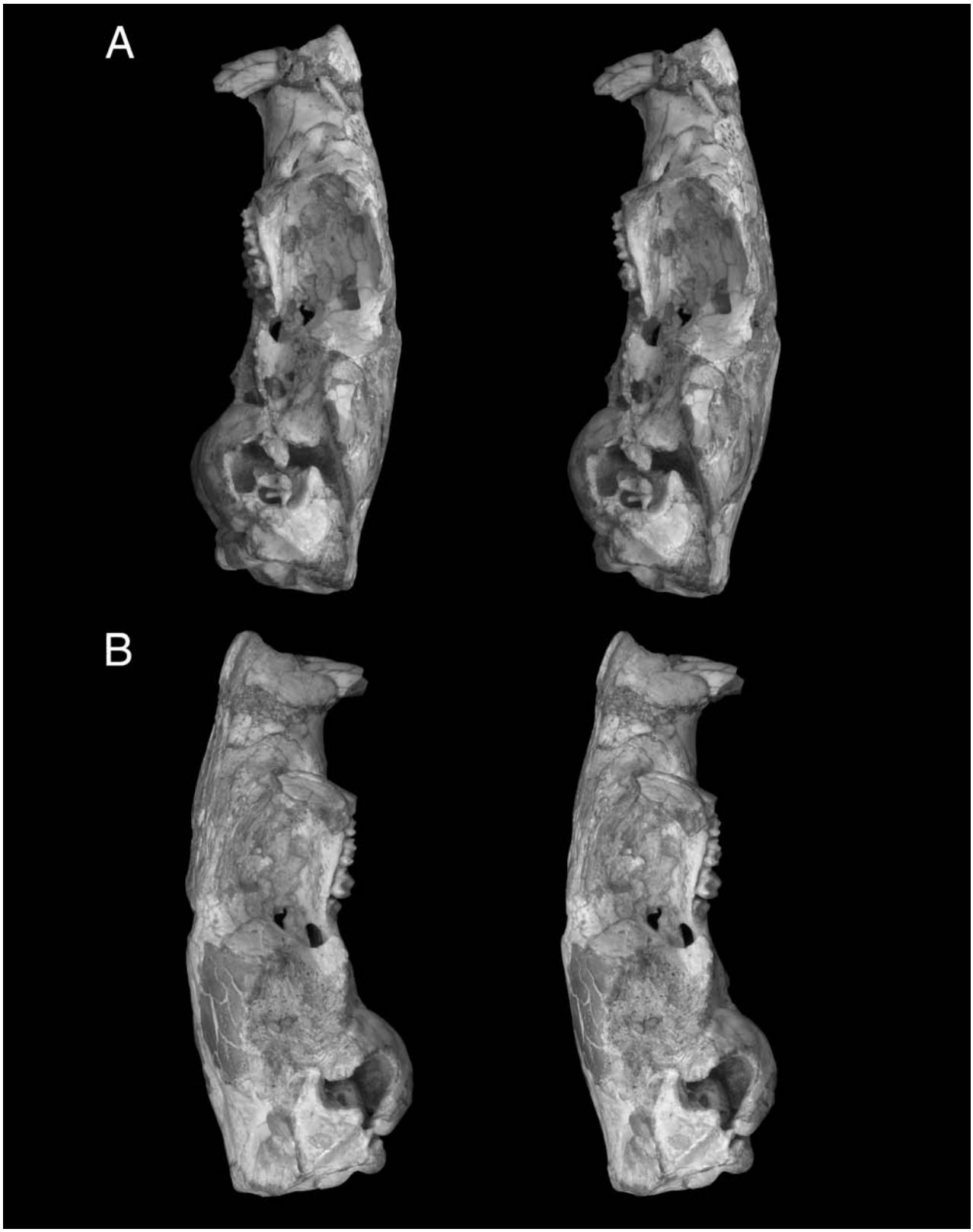
A
B

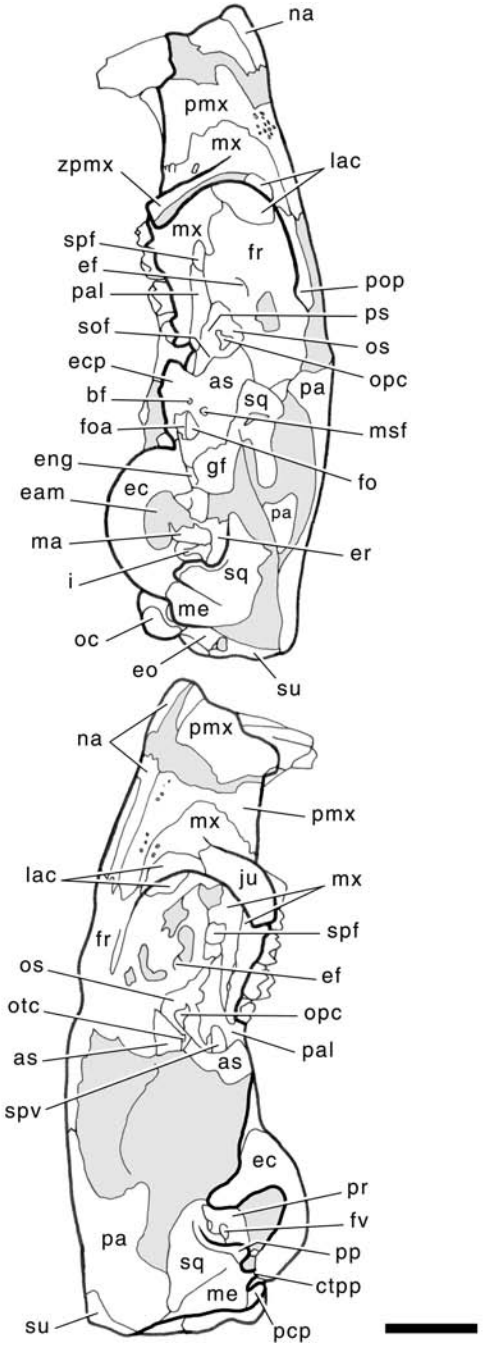

Premaxilla

The premaxillae house the pair of enlarged upper incisors and are the principal elements of the walls and floor of the rostrum and of the enlarged upper diastemata. The premaxillae are preserved in both specimens, but are more complete and less distorted in V7429. With the anterior border of the nasals, the anterior border of the premaxillae complete the external nasal aperture, which is ovoid, wider than high (Fig. 2A). The premaxilla has a facial process that forms roughly the anterior two-thirds of the lateral wall of the rostrum and a palatal process that forms about the anterior one-third of the hard palate. The facial and palatal processes grade into one another and are not delimited in any particular way.

The facial process includes an elongate, digitiform posterodorsal process that is slightly narrower than the adjacent nasal bone and contacts the frontal just posterior to the frontonasal suture (Fig. 1). The medial and lateral sides of the posterodorsal process are essentially parallel and the posterior border is convex. The dorsal surface of the posterodorsal process in V7429 is riddled with dozens of minute foramina (Fig. 1A); anteriorly are a dozen or so more substantial, small foramina in both specimens (Fig. 1). All of these foramina are presumably nutritive in function. Ventral to the posterodorsal process, the posterior border of the facial process is concave at its suture with the maxilla (Figs. 3, 4).

The palatal process includes the alveolus for the enlarged upper incisor and behind that forms most of the border for the elongate incisive foramen, the premaxilla forming the anterior three-fourths and the maxilla the posterior one-fourth (Fig. 5). The incisive foramen is ovoid, pointed anteriorly; the ratio of length of the incisive foramen to length of the upper diastema is 48% in V7429 and 51% in V7430; Li et al. (1989) reported this ratio as 48–65% for *Cocomys*. The part of the premaxilla in the medial border of the incisive foramen is the medial palatine process. This process is narrow ventrally, but it is expanded dorsolaterally to form a broad wing visible within the medial aspect of the incisive foramen, based on the right side of V7429, which was prepared more extensively than the others (Fig. 5A). The anterior half of the lateral edge of the incisive foramen is formed by a sharp crest that posteriorly diverges laterally from the incisive foramen and continues onto the maxilla, ending anteromedial to P3 (Fig. 5). This crest likely marks the attachment of part of the buccinator muscle (Meinertz 1941). The suture between the palatal process of the premaxilla and maxilla

Fig. 3.—*Exmus mini* IVPP V7429, left (**A**) and right (**B**) lateral views of skull, stereophotograph and accompanying line drawing. Contact between the frontal and squamosal in A is not natural, but results from displacement of the squamosal. Grey represents matrix. Scale = 5 mm. Abbreviations: **as**, alisphenoid; **bf**, buccinator foramen; **ctpp**, caudal tympanic process of petrosal; **eam**, external acoustic meatus; **ec**, ectotympanic; **ecp**, ectopterygoid crest; **ef**, ethmoidal foramen; **eng**, entoglenoid process; **eo**, exoccipital; **er**, epitympanic recess; **fo**, foramen ovale; **foa**, foramen ovale accessorius; **fr**, frontal; **fv**, fenestra vestibuli; **gf**, glenoid fossa; **i**, incus; **ju**, jugal; **lac**, lacrimal; **ma**, malleus; **me**, mastoid exposure; **msf**, masticatory foramen; **mx**, maxilla; **na**, nasal; **oc**, occipital condyle; **opc**, optic canal; **os**, orbitosphenoid; **otc**, anterior opening of orbitotemporal canal; **pa**, parietal; **pal**, palatine; **pcp**, paracondylar process; **pmx**, premaxilla; **pop**, postorbital process; **pp**, paroccipital process; **pr**, promontorium; **ps**, presphenoid; **sof**, sphenorbital fissure; **spf**, sphenopalatine foramen; **spv**, sphenopalatine vacuity; **sq**, squamosal; **su**, supraoccipital; **zpmx**, zygomatic process of maxilla.

lateral to the incisive foramen is tightly interdigitated. Although the premaxillae anterior to the incisive foramina are not pristinely preserved in either V7429 or V7430, it appears that an interpremaxillary foramen of Hill (1935) is absent.

Maxilla

The maxillae house the upper cheek teeth and have facial, zygomatic, palatal, and orbital processes. The maxillae are incomplete in both specimens, but enough is preserved between the two to reconstruct nearly the entire bone. The poorest preserved area is the orbital process, which is prepared on both sides of V7429.

The wedge-shaped facial process forms the posterior one-third of the snout's lateral wall (Figs. 3, 4). Its anterior suture with the premaxilla is the arcuate side of the wedge. The facial process extends onto the skull roof between the posterodorsal process of the premaxilla medially and the facial process of the lacrimal laterally (Fig. 1). It contacts the frontal posteriorly near the orbital margin at a suture that lies just anterior to that between the premaxilla and frontal. This part of the facial process adjacent to the posterodorsal process of the premaxilla has many small foramina in it (Fig. 1). The most conspicuous feature on the facial process is the somewhat enlarged infraorbital foramen (Fig. 2A), which lies anterodorsal to P3 wholly within the maxilla (Fig. 5B), where the facial and zygomatic processes meet. The facial process forms roughly the medial half of the infraorbital foramen and the zygomatic process the lateral half. As in *Cocomys* (Li et al. 1989), the infraorbital foramen is closer to the alveolar margin than to the skull roof, but it is slightly higher in *Exmus* (Fig. 2). The infraorbital canal is very short, and its anterior and posterior openings, the infraorbital and maxillary foramina respectively, are essentially confluent. The anteriorly facing infraorbital foramen, visible in ventral view (Fig. 5), is tilted so that its ventral border lies posterior to its dorsal border, as in *Cocomys* (Li et al. 1989). On the right side of both specimens, the infraorbital foramen is subcircular in anterior view, whereas on the left side of V7429 it is more ovoid, taller than wide (Fig. 2A). We think that the subcircular foramina best reflect the true condition and that the ovoid condition is distorted. The dorsoventral and lateral diameters in millimeters are 2.2/2.1 on the right side of V7429, 2.5/2.1 on the left of V7429, and 2.1/2.1 on the right side of V7430. In *Cocomys* IVPP V7399, the dimensions are 2.1/1.8 on the left side; Li et al. (1989) reported them for *Cocomys* as 1.8/2.1 dorsoventrally and 1.3/1.7 transversely. Regarding the infraorbital foramen in *Cocomys,* Li et al. (1989: p. 182) reported that "very little or no muscle penetrated the foramen. In skull V7399, just anterior to the infraorbital foramen, there is a very weak semicircular scar, which may be interpreted as a penetration of the muscle." Both specimens of *Exmus* have a weak ridge running anterodorsally from the ventral margin of the infraorbital foramen that might indicate the attachment of the pars anterior of the medial masseter muscle (Klingener 1964). However, if any muscle penetrated the infraorbital foramen in *Exmus*, as reported for *Cocomys,* it was probably not significant.

The zygomatic process is fully preserved only on the right side of V7430. In ventral view (Fig. 5B), its root lies at a right angle to the palate, opposite P3 and the anterior half of dP4, from which it curves posteriorly and slightly laterally opposite the metacone of M2, underlying the jugal bone. The ventral surface of the zygomatic process has a low process for attachment of the superficial masseter muscle on the anteroventral aspect of the root (Klingener 1964); lateral to that and extending opposite the metacone of M1 is a shallow depression for origin of the lateral deep masseter muscle (Klingener 1964). In lateral view, the zygomatic process forms the lateral half of the infraorbital foramen (Fig. 4) and contacts the facial process of the lacrimal and ventral to that, the jugal (Fig. 3). As the zygomatic process extends posteriorly, underlying the jugal, it tapers to a very thin splint (Fig. 5B). Within the orbit, based on the left side of V7429, the dorsalmost part of the zygomatic process forms the lateral and ventral aspect of the large, triangular lacrimal foramen, with the lacrimal forming the medial aspect.

The palatal processes of the maxilla contain the alveoli for the upper cheek teeth and form roughly the middle third of the hard palate, the anterior third being formed by the premaxilla and the posterior by the palatine (Fig. 5). The palatal process is best preserved in V7430 (Fig 5B); it is devoid of foramina, slightly concave anteriorly, behind the incisive foramen, and flat posteriorly, anterior to the palatine bone. The interdigitated anterior suture between the palatal process of the maxilla and the tongue-shaped horizontal process of the palatine bone is opposite the lingual root of the last premolar. Running lateral to the horizontal process of the palatine is the narrow alveolar margin of the palatal process of the maxilla, which tapers posteriorly and is all but missing from the lingual aspect of the last molar.

The orbital process forms the floor and the anteroventral wall of the orbit; the latter part is most complete in V7429, more so on the left side (Fig. 4A), but its surface is riddled with cracks that confound the identification of some sutures. The part of the maxilla in the orbital floor roofs the cheek teeth, although some molar roots are exposed in the orbital floor. In V7429, it is the lingual roots of the M2-3 that are exposed (M2 roots visible in Fig. 1A), whereas in V7430, it is the lingual roots of M1-3 (M1-2 roots visible in Figure 1B). In the anteromedial orbital floor on the right side of V7429, there is a small, oval, anteromedially directed foramen within the maxilla immediately behind the maxillary foramen and in front of the cheek teeth; the specimen's left side is damaged here, but preserves the foramen's posterior outline. Li et al.

(1989) reported a similar foramen for *Cocomys* and correctly identify it as the anterior alveolar foramen of Wahlert (1974) for the anterior superior alveolar nerve to I2 (Greene 1935). The most conspicuous feature of the anteroventral orbital wall is the elongate, ovoid sphenopalatine foramen, which lies opposite M1 (Fig. 3). The maxilla clearly forms the anterior border of the sphenopalatine foramen. The remaining borders of the foramen are formed by the frontal and palatine, although ventrally the palatine is overlain by the maxilla (Fig. 3A). The interval between the sphenopalatine and maxillary foramina is formed by the maxilla, which dorsally contacts the orbital processes of the frontal and lacrimal. The position of the suture with the frontal is well marked on the left side of V7429 (Fig. 3A). Its posterior part lies at the level of the dorsal edge of the sphenopalatine foramen, and its anterior part curves anterodorsally to the level of the lacrimal foramen. The suture between the maxilla and lacrimal, also well marked on the left side of V7429, is *V*-shaped in the interval between the frontomaxillary suture and the lacrimal foramen.

Palatine

The palatine bones have horizontal processes forming the posterior third of the hard palate (Fig. 5) and vertical processes, of which the lateral surface contributes to the posteroventral orbital wall (Fig. 3) and the medial surface to the internal nasal aperture or choanae and to the basipharyngeal canal, the nasopharyngeal passage behind the choanae (Fig. 5A). The horizontal processes are well preserved in both specimens, but the vertical processes can be studied only in V7429.

As mentioned above, the horizontal processes of the palatines have the shape of a tongue (Fig. 5). The most conspicuous feature on the horizontal process is the anteriorly directed major palatine foramen, which lies opposite the hypocone of M1. Extending anteriorly from the major palatine foramen nearly to the palatomaxillary suture is a deep sulcus for the contents of the foramen, the major palatine nerve and vessels. The posterior border of the horizontal process lies at the M2-M3 embrasure. It is not straight, but includes a distinct posterior nasal spine, which is flanked on either side by shallow notches. Based on the right side of V7429, the posterior border also includes a low postpalatine torus (Fig. 5A); this is damaged elsewhere. Extending posteriorly from and at the same level with the posterolateral border of the horizontal process is a bar of palatine that represents the ventralmost part of the vertical process; it is best seen in ventral view. The posteromedial and posterolateral surfaces of this bar are overlaid by the pterygoid and alisphenoid, respectively, and represent the base of the ento- and ectopterygoid crests (Fig. 5A). The posterior surface of this bar forms the anterior aspect of the deep pterygoid fossa, which lies between the ento- and ectopterygoid crests. Between the lateral surface of this bar and M3 is a deep notch, visible bilaterally in V7429 and on the left side of V7430 (Fig. 5B), resembling that described by Wahlert (1974) for the minor palatine nerve and vessels.

In lateral view (Fig. 3A), the main part of the vertical process of the palatine is quadrangular, long and thin, and its surface is essentially flat. Its short anterior border is concave and forms the posterior half of the sphenopalatine foramen. Its long ventrolateral border is the straight suture with the maxilla's contribution to the orbital floor, which is preserved best on the left side of V7429. Although poorly preserved on both sides of V7429, its long dorsomedial border appears to be roughly straight and to contact the frontal and the presphenoid. Its short posterior border is concave and forms the anterior and anteroventral border of the large vacuity that connects the basipharyngeal canal and the sphenorbital fissure (Fig. 3B), which we call the sphenopalatine vacuity following Hershkovitz (1962).

Lacrimal

The lacrimal is a sizeable element in the anterior orbital margin with facial and orbital processes. The facial process, incompletely preserved on both sides of V7429 and part of its impression on the right side of V7430, is small, arcuate, and flat (Fig. 1). It forms the orbital margin between the jugal and the frontal; its anterior border contacts the maxilla above the infraorbital foramen (Figs. 1A, 3). The orbital process is incompletely preserved on both sides of V7429, but enough is present to reconstruct its sutural relationships. The orbital process is a substantial quadrangular element in the anterodorsal orbital wall that contacts the frontal posteriorly, the jugal ventrally, and the maxilla anteroventrally. In the ventral part of the anterior border with the maxilla is the large lacrimal foramen for the nasolacrimal duct, whose triangular shape is unusual but is preserved on both sides of V7429 (not visible in the figures). The orbital process of the lacrimal forms the medial wall of the lacrimal foramen and the zygomatic process of the maxilla forms the lateral and ventral walls. The facial and orbital processes of the lacrimal meet at a very acute angle, such that the orbital process is recessed in from the orbital margin. Additionally, the surface of the orbital process near the orbital margin is concave. In this fashion, the lacrimal contributes to an orbital roof (some of which is visible in ventral view in figure 5), which continues onto the frontal behind the lacrimal. In *Cocomys* IVPP V7399, there is very little orbital roof on either the lacrimal or the frontal.

Jugal

The jugal is the principal element of the zygomatic arch. It

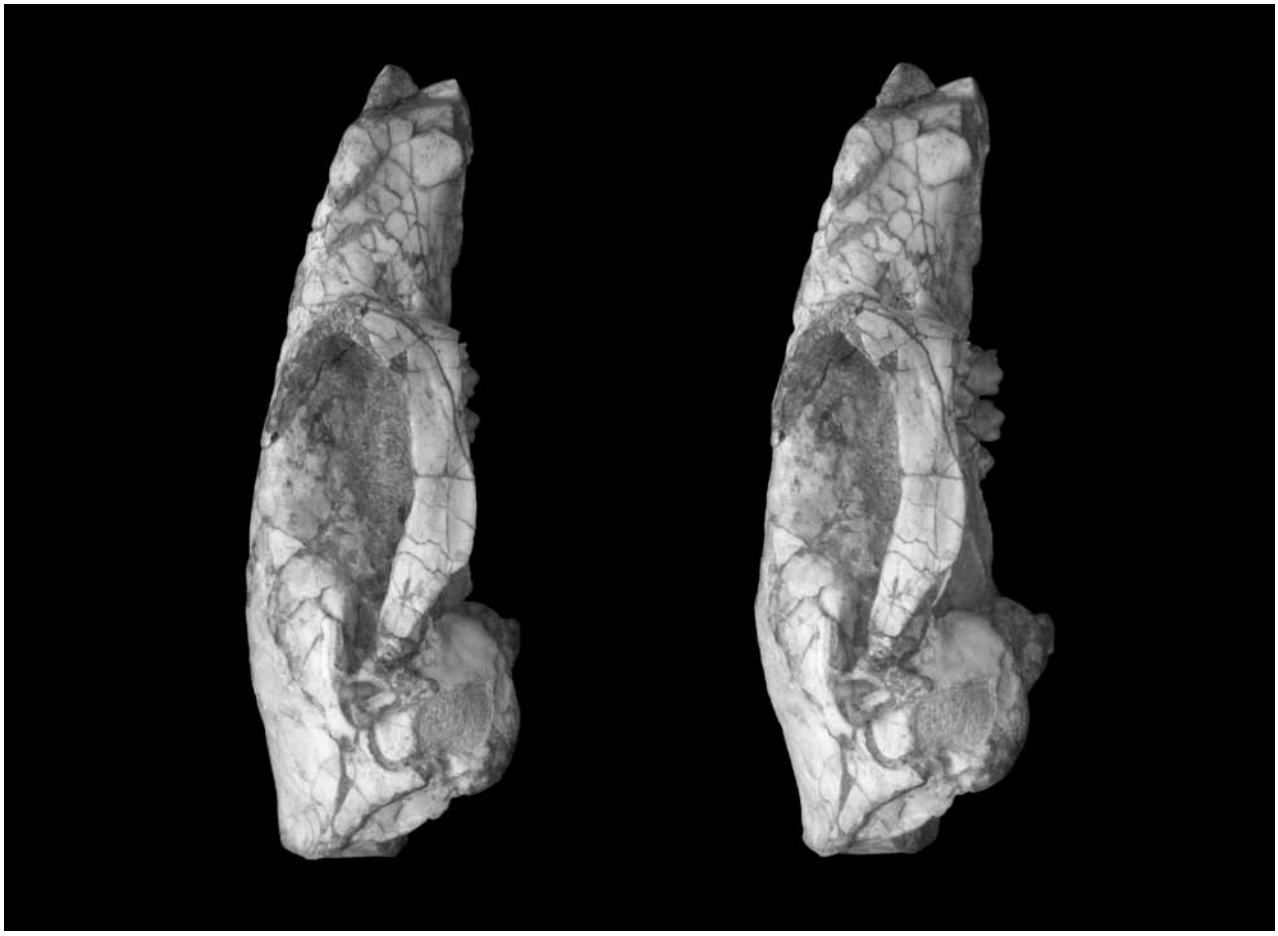

Fig. 4.—*Exmus mini* IVPP V7430, right lateral view of skull, stereophotograph and accompanying line drawing. Grey represents matrix. Scale = 5 mm. Abbreviations: **as**, alisphenoid; **dP4**, upper deciduous fourth premolar; **eam**, external acoustic meatus; **ec**, ectotympanic; **fr**, frontal; **frt**, foramen for ramus temporalis; **hy?**, possible hyoid arch element; **I2**, upper second incisor; **iof**, infraorbital foramen; **ju**, jugal; **me**, mastoid exposure; **mx**, maxilla; **na**, nasal; **pa**, parietal; **pmx**, premaxilla; **sq**, squamosal; **su**, supraoccipital; **zpsq(br)**, zygomatic process of squamosal (broken).

is almost completely preserved on the right side of V7430 (Fig. 4); missing are only the anteriormost and posteriormost ends of the bone. The anterior fourth of the jugal is preserved on the right side of V7429 (Fig. 3B). For the most part, the external surface of the jugal is gently convex, and the internal surface is gently concave. The anterior two-thirds of the jugal is uniform in height and breadth and curves gently downwards from the bone's high point on the orbital margin; the posterior one-third tapers somewhat to its damaged end and trends slightly upwards. The anterior half of the jugal overlies the zygomatic process of the maxilla and contributes to the orbital margin (Figs. 4, 5B). It reaches the facial process of the lacrimal, based on the right side of V7429 (Figs. 1A, 3B), which is most clearly seen within the orbit. The orbital margin of *Cocomys* differs in that the maxilla separates the jugal and lacrimal (Fig. 17A; Li et al. 1989: fig. 1). On the external surface of the jugal is an oval depression for the lateral deep masseter muscle (Klingener 1964) that begins just above the posterior end of the zygomatic process of the maxilla and extends to where the ventral border of the jugal bends posterodorsally. Because the posterior end of the jugal and the zygomatic process of the squamosal are damaged (Fig. 5), the nature of the contact between the two is not known. We can report that the zygomatic process of the squamosal is not a substantial part of the zygoma and that the jugal does not contribute to the glenoid fossa.

Frontal

The frontals form approximately the middle third of the length of the skull roof and are the major elements of the orbital fossae. The frontals are incompletely preserved in both specimens; the horizontal part in the skull roof is better preserved anteriorly in V7429 (Fig. 1A) and posteriorly in V7430 (Fig. 1B), and the orbital contribution is most complete on the left side of V7429 (Fig. 3A).

In dorsal view (Fig. 1), the paired frontals together are

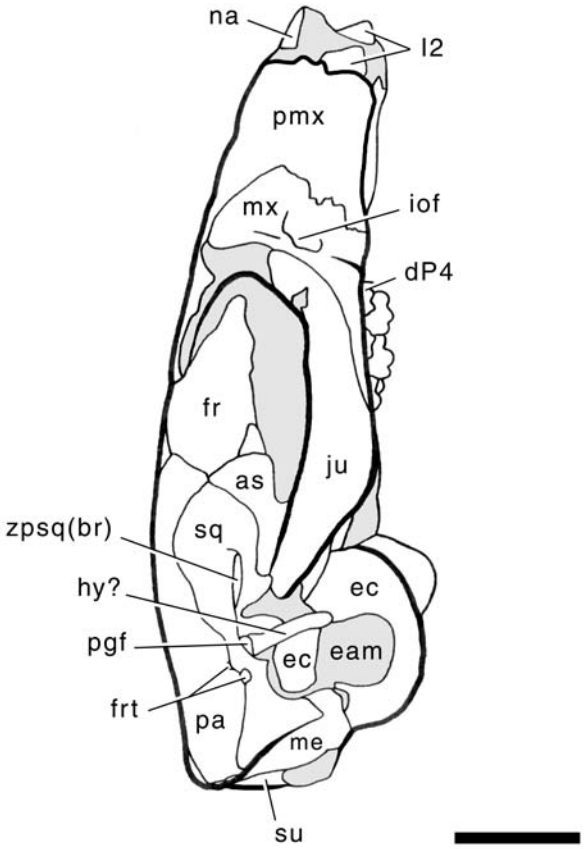

roughly triangular in outline. The base of the triangle is formed by the anterior sutures with the nasals, premaxillae, maxillae, and lacrimals, described above. The remaining two sides are the supraorbital margins anteriorly and the frontoparietal suture posteriorly. The dorsal surface of the frontal is flat medially, with some gentle convexity near the supraorbital margin and stronger convexity into the orbital fossa lateral to the temporal line (see below). The frontal forms a thickened ridge at the supraorbital margin that posteriorly includes a stout, triangular, posterolaterally directed postorbital process, preserved only on the left side of V7429 (Fig. 1A). This process is more pronounced than that reconstructed for *Cocomys* by Li et al. (1989: fig. 1), but perhaps this is a preservational artifact. Curving posteromedially from the postorbital process is a distinct temporal line, preserved only in V7430, that continues along the frontoparietal suture, but not onto the parietal (Fig. 1B). The frontoparietal suture is *U*-shaped with a tongue of the paired frontals interposed between the left and right parietals. This is best seen in V7430; even though its parietals are damaged, their positions are clearly indicated by facets on the frontals (Fig. 1B). There is a slight difference between the two specimens in the base of the *U*; in V7430 it is more or less horizontal, whereas in V7429, it is more *V*-shaped (Fig. 1A).

In lateral view (Figs. 3, 4), within the orbital fossa the frontal contacts, from front to back, the lacrimal, maxilla, palatine, orbitosphenoid, alisphenoid, and parietal. The left side of V7429 (Fig. 3A) provides the bulk of the information on the frontal's orbital sutures. The frontal sutures with the orbital processes of the lacrimal and the maxilla and the horizontal process of the palatine are described above. About halfway between the sphenopalatine foramen and optic canal (see below), the frontal encounters the orbitosphenoid. The initial part of their suture is badly damaged, but posterior to that it is broadly *S*-shaped, curving posterodorsally. Posterior to the orbitosphenoid, at the level of the back edge of the optic canal, the frontal contacts the alisphenoid; the suture between the two runs more or less horizontally, trending slightly posterodorsally, with the frontal gently concave and the alisphenoid gently convex. Posterior and dorsal to the alisphenoid, the frontal encounters the parietal at a level roughly halfway between the back of the tooth row and the front of the auditory region. The frontoparietal suture is clearly shown on the right side of V7430 (Fig. 4); it curves anterodorsally, with the frontal convex and the parietal concave, and continues onto the skull roof. Figure 3A shows a different relationship in that the frontal has a narrow contact with the squamosal, but this is an artifact resulting from displacement of the squamosal anteriorly and laterally from its natural position. Anterior to the level of the optic canal, the orbital surface of the frontal is generally concave, with an interorbital breadth that is narrower ventrally and considerably broader at the supraorbital margin. As a result, the frontal anterior to the postorbital process along with the lacrimal (see above) form a partial orbital roof, some of which is visible in ventral view (Fig. 5). Posterior to the level of the optic canal, the frontal is convex, and here contributes to the front of the braincase.

Within the orbital fossa, the frontal contributes to the borders of three foramina. As noted above, the frontal forms part of the dorsal border of the sphenopalatine foramen (Fig. 3). Based on the left side of V7429, immediately anteroventral to the tip of the postorbital process within the frontal is a small, laterally directed foramen (not visible in the figures) that resembles the foramen for the frontal diploic vein of extant placentals (Thewissen 1989; Wible and Gaudin 2004). Ventral to this foramen and posterodorsal to the sphenopalatine foramen is a narrow, elongate ethmoidal foramen that is directed anterodorsally into the frontal, most completely preserved on the left side of V7429 (Fig. 3A).

Parietal

The parietals are the principal elements of the braincase roof. Parts of the parietals are preserved in both specimens (Fig. 1), with the right parietal nearly completely preserved in V7430; missing is only its anteriormost part,

which occupies a facet on the frontal. Each parietal is somewhat ovoid, although the anterior border is more pointed and the posterior more rounded. The outer contours of the parietals reflect those of the enclosed brain. The parietals are flat along the midline and laterally are strongly convex with very prominent bulges anterolaterally over the cerebral hemispheres. Both specimens preserve only the anteriormost end of the suture between the left and right parietals; the bulk of the suture is fused (Fig. 1), which is highly unusual in that neither specimen is fully mature as shown by the retention of the dP4. We interpret the interparietal bone as missing, although V7430 has nearly symmetrical cracks forming an inverted *V* anterior to the nuchal crest.

The borders of the parietal are as follows (Fig. 1). The pointed anterior end reaches nearly to the interorbital constriction behind the postorbital process of the frontal. The medial edge of the parietal behind this is the short longitudinal suture with the frontal. This suture is raised as the temporal line and does not continue posteriorly onto the parietal proper, based on V7430 (Fig. 1B). Opposite the anterior edge of the posterior zygomatic root, the frontoparietal suture turns medially and the parietal meets its fellow of the opposite side (Fig. 1B). The posterior border of the parietal is the suture with the supraoccipital; on the midline this lies anterior to the nuchal crest, but laterally the posterior border reaches the juncture between the braincase roof and the occiput, and contributes to the anterior face of the nuchal crest, based on the right sides of both V7429 and V7430. At the posterolateral margin of the braincase, the parietal has a very narrow contact with the mastoid exposure of the petrosal (Fig. 3B; see below). In front of this lies the long suture between the parietal and the squamosal, which ends at the level of the foramen ovale in the alisphenoid (see below). The suture between the parietal and squamosal is broadly *S*-shaped, with the parietal the convex member posteriorly and the concave member anteriorly (Fig. 4). In front of the squamosal, the lateral edge of the parietal has a narrow contact with the alisphenoid, as shown on the right side of V7430 (Fig. 4), and then touches the frontal at an oblique suture that leads back to the pointed anterior end of the parietal (Figs. 3A, 4).

On the right side of V7430 (Figs. 1B, 4), there are two substantial foramina separated by a narrow bar of bone in the suture between the parietal and the squamosal, dorsal to the external acoustic meatus. The larger posteroventral foramen is laterally directed and largely within the squamosal. The smaller anterodorsal foramen is largely within the parietal and dorsally directed into a short, shallow sulcus on the parietal. Both openings are foramina for the ramus temporalis of the stapedial artery (Wible 1987; Wible and Gaudin 2004), the temporal foramina of Hill (1935). In addition to these substantial foramina, there are numerous tiny emissary foramina within the parietal on either side of the midline in V7430.

Pterygoid

The pterygoids form the nearly vertical entopterygoid crests, which serve as the lateral walls of the posterior part of the basipharyngeal canal and the medial walls of the pterygoid fossa (Fig. 5A). The pterygoids are preserved in both specimens, but are prepared to some extent only in V7429. In that specimen, only the medial surfaces can be studied; matrix was left on the lateral surfaces to buttress these delicate elements. The left pterygoid is the most complete; only its hamular region is damaged.

In medial view, the pterygoid is roughly trapezoidal with the longer, diverging sides being situated dorsally and ventrally; of these two sides, the dorsal is the longer. The anterior side is concave and contacts the palatine bone. The dorsal side is straight and the bulk of it contributes to the lateral border of the large sphenopalatine vacuity (Fig. 5A); posteriorly, it contacts a ventrolaterally directed ridge on the lateral margin of the basisphenoid (see below). The ventral and posterior sides do not contact bone; the former is straight and the latter is deeply concave. The posteriormost part of the ventral side represents the hamulus, which is damaged on both sides.

Ethmoid

In the rat (Greene 1935) and guinea pig (Cooper and Schiller 1975), the ethmoid bone is a complex midline ossification in the posterior nasal cavity and anterior cranial cavity; it includes a complex array of delicate turbinal elements and the cribriform plate for the passage of the olfactory nerves. No parts of the ethmoid are exposed in either V7429 or V7430.

Vomer

In the rat (Greene 1935) and guinea pig (Cooper and Schiller 1975), the vomer is a midline ossification underlying the nasal septum within the floor of the nasal cavity. The vomer also contributes to the roof of the nasopharyngeal meatus, the passageway connecting the nasal fossa and the choanae. No parts of the vomer are exposed in either V7429 or V7430.

Sphenoid Complex

In the rat (Greene 1935) and the guinea pig (Cooper and Schiller 1975), the sphenoid complex includes two distinct ossifications: the presphenoid in front and the basisphenoid behind. Both of these elements lie on the basicranial axis and have paired wings exposed in the orbitotemporal fossae. Following the convention usually employed in therians (Wible 2003; Wible and Gaudin 2004), we limit the terms presphenoid and basisphenoid to the parts of the

sphenoid complex on the basicranial axis and identify the wings of the presphenoid as the orbitosphenoids and the wings of the basisphenoid as the alisphenoids. In *Exmus*, the basipharyngeal canal was prepared only in V7429, in which the presphenoid and basisphenoid are well preserved (Fig. 5A). Aspects of the orbitosphenoids and the alisphenoids are preserved in both V7429 and V7430 (Figs. 3, 4).

Presphenoid

In ventral view in V7429 (Fig. 5A), the presphenoid is a very narrow midline element in the roof of the basipharyngeal canal and anterior to that in the choanae. It forms the anterior half of the medial border of the large sphenopalatine vacuity; the slightly wider basisphenoid forms the posterior half. The posteroventral surface of the presphenoid is flat. However, anteroventrally it has a rounded, longitudinal process that is interposed between the palatines and disappears into the choanae; this is the median longitudinal ridge of the presphenoid of Cooper and Schiller (1975).

The presphenoid is also visible in lateral view in V7429 (Fig. 3), more so in the left lateral view, as a rectangular element, taller than wide, but the dorsal portion has not been cleaned of matrix, except beneath the optic canal (described with the orbitosphenoid below). Covering the anterolateral surface of the presphenoid is the posteromedial part of the vertical process of the palatine (Fig. 3B).

Orbitosphenoid

Sutures do not delimit the orbitosphenoid from the presphenoid. For descriptive purposes, the orbitosphenoid arises from the dorsolateral surface of the presphenoid and arches over the optic canal. Following this usage, the floor of the optic canal is formed by the presphenoid and the remaining borders by the orbitosphenoid. Aspects of the orbitosphenoid are preserved on both sides of V7429 and on the left side of V7430, but its sutural relations in the orbit are most evident on the right side of the former specimen (Fig. 3B).

In lateral view, the orbitosphenoid roughly has the shape of a dog's head, with the snout pointing anteriorly (with the tip of the nose damaged) and the braincase arching over the optic canal (Fig. 3B). The bulk of the dorsum of the dog's head contacts the frontal, with the occiput contacting the alisphenoid. Ventrally, the orbitosphenoid has two points of contact (fusion) with the presphenoid. Anteriorly, opposite the back half of M2 and the front half of M3, the left and right orbitosphenoids have a common base on the midline; this base is the yoke or jugum sphenoidale (Evans 1993). Posteriorly and slightly laterally, dorsal to the back of the vertical process of the palatine, each orbitosphenoid has a narrow, dorsolaterally directed, columnar base on the presphenoid. Between these two bases, each orbitosphenoid arches over the optic canal. The arch and the canal are oblique to the basicranial axis, reflecting the obliquity of the two bases on the presphenoid.

Several openings are associated with the orbitosphenoid. The principal one is the optic canal (Fig. 3). It is ovoid, longer than high. Its anterior wall is formed by the narrow jugum sphenoidale and its floor by a midline crest on the presphenoid; these structures represent the only separation between the right and left optic canals. As in *Cocomys* (Li et al. 1989), the right and left optic canals in *Exmus* form a continuous opening. Between the anterior wall and the ventral midline crest is a narrow, *J*-shaped gap that is confluent between the right and left sides. The meaning of this gap is uncertain. Li et al. (1989) reported a small internal orbital foramen just in front of the optic canal in *Cocomys*; it is not present in the specimen of *Cocomys* studied by us, V7399. It is possible that a delicate bar of bone connecting the jugum sphenoidale and the midline crest was broken in *Exmus* V7429 and that a foramen was present. Such a foramen would be reminiscent of the presphenoid foramen reported by Hill (1935: 124) in extant geomyids, "transmitting a sinusoid vein between the orbits"; Wahlert (1974) identified this as the interorbital foramen. The posterolateral base of the orbitosphenoid and the adjacent presphenoid form the anterodorsomedial border of the elongate sphenorbital fissure (sphenoidal fissure of Li et al. 1989 and anterior-alar fissure of Wahlert 1983). Finally, posterodorsolateral to the optic canal there appears to be a small, anteriorly directed foramen in the damaged suture between the orbitosphenoid and alisphenoid based on the right side of V7429 (Fig. 3B). Li et al. (1989) identified a similar foramen between the alisphenoid, orbitosphenoid, and frontal in *Cocomys* as the sphenofrontal foramen of Hill (1935). A variety of terms have been coined for this aperture in mammals. We follow Wible et al. (2004) and Wible and Gaudin (2004) and call it the anterior opening of the orbitotemporal canal for the anterior division of the ramus superior of the stapedial artery.

Basisphenoid

In ventral view in V7429 (Fig. 5A), the basisphenoid is the part of the sphenoid complex flanked by the presphenoid anteriorly and the basioccipital posteriorly, between the entopterygoid crests and the auditory bullae. It has the appearance of a crude human figure, with a narrow head and neck pointing anteriorly, paired arms and legs directed ventrolaterally, and a flat trunk devoid of foramina. The basisphenoid is narrowest at its suture with the presphenoid and widest across the arms. For descriptive purposes, we designate the appendages of the basisphenoid as follows: the narrow head and neck are the rostral part of the body, the arms are the pterygoid processes, and the legs are

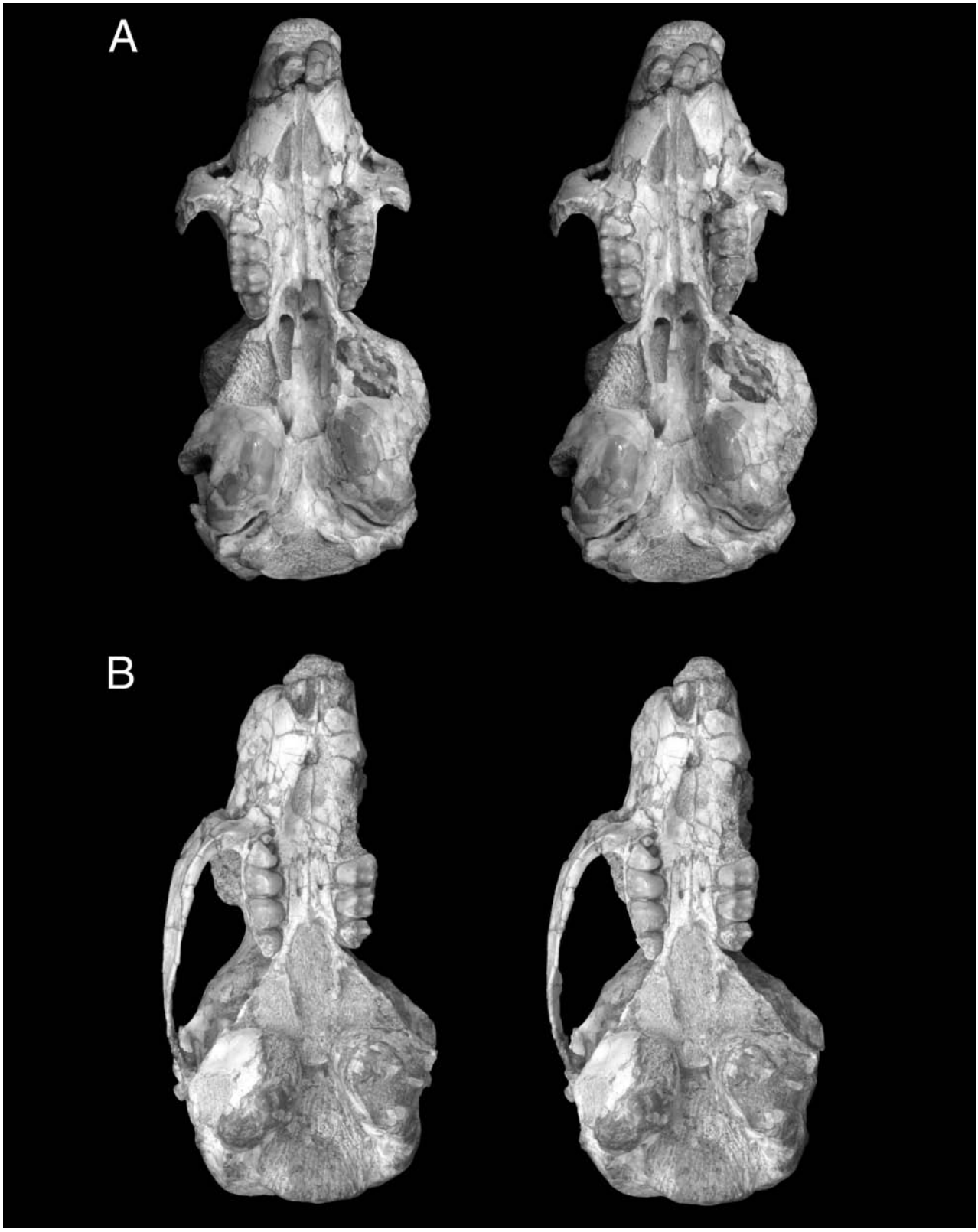
A
B

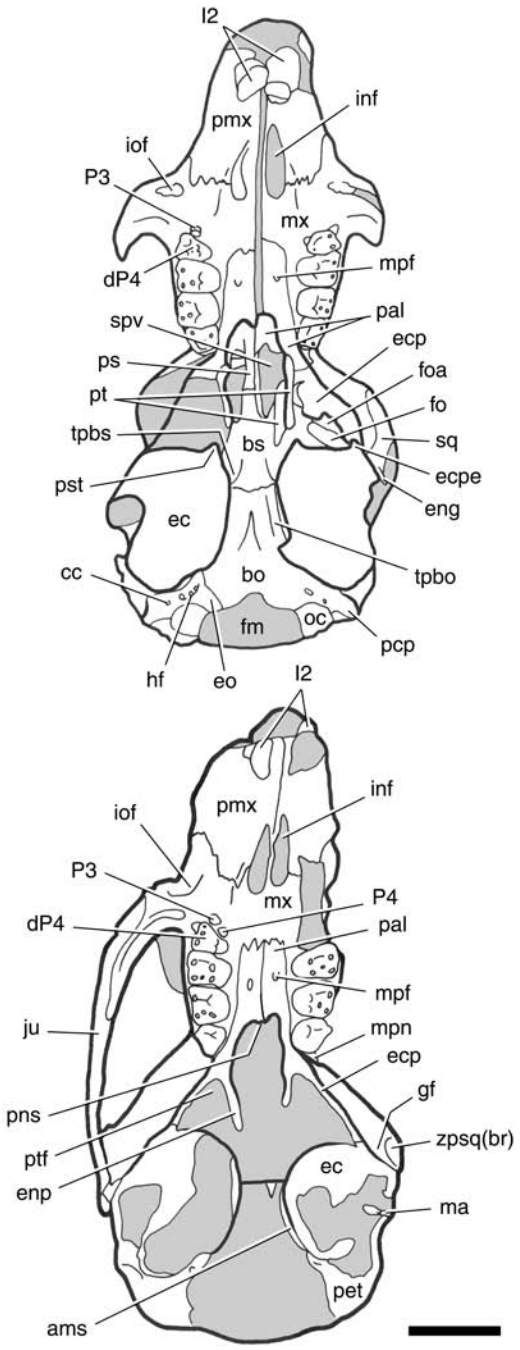

the tympanic processes, so-called because they are continuous with the prominent tympanic processes of the basioccipital. Projecting dorsolaterally from the lateral margin of the basisphenoid between the pterygoid and tympanic processes is the base of the alisphenoid; sutures do not delimit these two bones.

The rostral part of the body accounts for approximately one-third of the length of the basisphenoid. It is rectangular in ventral view, with minor tapering at its straight anterior abutment with the presphenoid; it is also rectangular in lateral view, but its endocranial surface has not been fully prepared. The rostral part of the body forms the posterior half of the medial wall of the sphenopalatine vacuity; the anterior half is formed by the presphenoid.

The pterygoid processes occupy the lateral margins of the middle third of the basisphenoid. They project slightly ventrolaterally with their distal ends abutting the posterodorsal aspect of the pterygoids. Their anterior edges form the narrow posterior borders of the sphenopalatine vacuities. We consider that the nerve of the pterygoid canal runs beneath the pterygoid process en route to the sphenopalatine vacuity from the middle ear. There is a faint indication of a groove on the right side of V7429 that appears continuous with a more substantial groove on the alisphenoid behind (see below).

The tympanic processes occupy the lateral margins of the posterior third of the basisphenoid. They are short, low longitudinal ridges that have their maximum ventral projection at their suture with the tympanic process of the basioccipital. The basisphenoid surface between the tympanic processes is slightly concave. The basisphenoid-basioccipital suture is damaged, but appears to be straight.

Alisphenoid

The alisphenoid is the largest and most complicated part of the sphenoid complex. It makes a sizeable contribution to the lateral braincase wall and forms the bulk of the ectopterygoid crest, the roof of the pterygoid fossa between the ento- and ectopterygoid crests, and the floor of the braincase in front of the ear region. Parts of the alisphenoid are preserved in both specimens, but the bone is most completely preserved on the left side of V7429 (Fig. 3A).

In ventral view on the left side of V7429 (Fig. 5A), the alisphenoid roofs the triangular space bounded by the entopterygoid crest medially, the auditory bulla posterior-

Fig. 5.—*Exmus mini* IVPP V7429, (**A**) and IVPP 7430 (**B**), ventral view of skull, stereophotograph and accompanying line drawing. Grey represents matrix. Scale = 5 mm. Abbreviations: **ams**, anteromedial shelf of petrosal; **bo**, basiooccipital; **bs**, basisphenoid; **cc**, condyloid canal; **dP4**, deciduous upper fourth premolar; **ec**, ectotympanic; **ecp**, ectopterygoid crest; **ecpe**, ectopterygoid process of ectotympanic; **eng**, entoglenoid process; **enp**, entopterygoid crest; **eo**, exoccipital; **fm**, foramen magnum; **fo**, foramen ovale; **foa**, foramen ovale accessorius; **gf**, glenoid fossa; **hf**, hypoglossal foramina; **I2**, upper second incisor; **inf**, incisive foramen; **iof**, infraorbital foramen; **ju**, jugal; **ma**, malleus; **mpf**, major palatine foramen; **mpn**, notch for minor palatine nerve; **mx**, maxilla; **oc**, occipital condyle; **P3**, upper third premolar; **P4**, upper fourth premolar; **pal**, palatine; **pcp**, paracondylar process; **pet**, petrosal; **pmx**, premaxilla; **pns**, posterior nasal spine; **ps**, presphenoid; **pst**, processus styliformis; **pt**, pterygoid; **ptf**, pterygoid fossa; **spv**, sphenopalatine vacuity; **sq**, squamosal; **tpbo**, tympanic process of basioccipital; **tpbs**, tympanic process of basisphenoid; **zpsq(br)**, zygomatic process of squamosal (broken).

ly, and the ectopterygoid crest obliquely laterad. Within this triangle, the external surface of the alisphenoid is relatively flat, except posteriorly where it is slightly concave as it disappears above the anterior wall of the auditory bulla. The anterior part of the triangle, between the ento- and ectopterygoid crests, is the pterygoid fossa, which serves for the attachment of the medial (internal) pterygoid muscle in the rat (Greene 1935) and the guinea pig (Cooper and Schiller 1975). As preserved, there is no bone in the roof of the anteriormost part of the pterygoid fossa, which results in an irregular opening comparable in size to the foramen ovale; bone is present there in *Cocomys* V7399. Given that the CT scans of V7430 appear to have bone in the pterygoid fossa roof, we think that this irregular opening in V7429 is an artifact. In the posterolateral margin of the triangle, where the part of the alisphenoid in the braincase floor meets that in the lateral wall, is the sizeable, obliquely oriented foramen ovale, some of the borders of which are damaged (Figs. 3A, 5A). On the left side of V7429, a small part of the alisphenoid anterior to the auditory bulla is preserved; it bears a narrow sulcus for the nerve of the pterygoid canal that is directed anteromedially onto the basisphenoid, medial to its pterygoid process.

The alisphenoid is the principal component of the delicate, obliquely oriented ectopterygoid crest, which begins at the level of the sphenorbital fissure and extends posterolaterally to contact the anterolateral aspect of the auditory bulla (Figs. 3A, 5A). The alisphenoid forms all but the anteriormost and posteriormost roots of the ectopterygoid crest. As seen in ventral view on the left side of V7429 (Fig. 5A), the former is formed by the palatine and the latter is buttressed medially by a short, narrow process from the auditory bulla. Posterolaterally, the ectopterygoid crest abuts the weak entoglenoid process of the squamosal (see below). The ventral aspect of the ectopterygoid crest is flared laterally; its medial (and ventral) surface is slightly convex and its lateral (and dorsal) surface, which provides attachment for the lateral pterygoid muscle in the rat (Greene 1935) and guinea pig (Cooper and Schiller 1975), is slightly concave. At the level of and contiguous with the foramen ovale is a large, oval opening in the ectopterygoid crest that lies at roughly a right angle to the foramen ovale (Figs. 3A, 5A). This represents the foramen ovale accessorius of Wahlert (1974), which transmits most of the nervous contents from the foramen ovale to peripheral structures.

The alisphenoid's contribution to the lateral braincase wall is most completely preserved on the left side of V7429 (Fig. 3A). However, the braincase wall has numerous cracks, including an extensive oblique crack above the sphenorbital fissure that is coupled with ventromedial slippage of the bone dorsal to it. Based on the right side of V7430 (Fig. 4), we think this is damage rather than a suture. In light of this interpretation, the alisphenoid's contribution to the lateral braincase wall is roughly fan-shaped, with the base of the fan between the sphenorbital fissure and the foramen ovale positioned medial to the convex dorsal margin. The anterior edge of the fan lies in roughly a frontal plane and, based on the right side of V7429, is concave (Fig. 3B). The ventral half of the anterior edge is the lateral wall of the sphenorbital fissure, and the dorsal half is the suture with the orbitosphenoid, which appears to contain the anterior opening of the orbitotemporal canal. The convex dorsal margin of the fan contacts the frontal, parietal, and squamosal, based on the right side of V7430 (Fig. 4). The suture with the squamosal is poorly preserved in both specimens, but can be reconstructed based on the right side of V7430 and the left side of V7429 (Figs. 3A, 4). In the latter (Figs. 3A, 5A), the alisphenoid approximates the anterior margin of the glenoid fossa, but some squamosal bone anterior to the glenoid has flaked off; a truer picture of the suture is preserved in V7430. The posterior edge of the fan is the root of the ectopterygoid crest. It has a large concavity in lateral view, which represents the lateral edge of the foramen ovale and the dorsal edge of the foramen ovale accessorius.

Two foramina, one substantial and the other tiny, pierce the alisphenoid's contribution to the lateral braincase wall on the left side of V7429 (Fig. 3A). The larger one is positioned just dorsal to the lateral margin of the foramen ovale; it is subcircular and directed laterally and slightly ventrally from the braincase. Because this foramen is directed toward the mandibular notch between the coronoid and condylar processes of the mandible, we interpret it to be the masticatory foramen (Wahlert 1974) transmitting the masseteric branch of the mandibular nerve. The tiny foramen lies anterior to the foramen ovale; it is subcircular and directed laterally and slightly anteriorly from the braincase. The most likely identification of this opening is the buccinator foramen (Wahlert 1974) transmitting the buccal (buccinator) branch of the mandibular nerve. Neither the masticatory or buccinator foramen is reported for *Cocomys* (Li et al. 1989); instead, anterior to the foramen ovale is the posteriorly directed alisphenoid canal. In extant rodents, this aperture transmits the ramus infraorbitalis of the stapedial artery into the cranial cavity en route to the sphenorbital fissure (Wible 1984); this vessel is frequently anastomosed to the external carotid system and identified as the internal maxillary artery (Guthrie 1963).

Although the left side of V7429 clearly lacks an alisphenoid canal, the right side of V7430 appears to have a sizeable opening anterior to the foramen ovale (not visible in the figures). Our preparation of V7430 is incomplete, but what shows of this probable aperture resembles the alisphenoid canal of *Rattus norvegicus* CM 10227. Until additional preparation is done, we are unable to offer a full interpretation.

Squamosal

The squamosal contributes to the lateral braincase wall

and houses the glenoid fossa, the cranial part of the craniomandibular joint. The squamosal is most completely preserved on the right side of V7430 (Figs. 4, 5B), which alone preserves the postglenoid region; broken is only the zygomatic process. Additional details of the squamosal are preserved on that specimen's left side and on both sides of V7429.

What is visible in lateral view of the right squamosal of V7430 resembles a fish with the head facing anteriorly (Fig. 4). Most of the sinuous dorsal border is the suture with the parietal, with the fish's head contacting the parietal and the alisphenoid. The posterodorsalmost tip of the fish's tail is broken, but appears to have a narrow contact with the supraoccipital; on the right side of V7429, this area is also damaged, but the squamosal and supraoccipital appear not to contact one another (Fig. 3B). The posterior concave surface of the fish's tail contacts the mastoid exposure of the petrosal (Fig. 4), with the lower tail fin forming all but the tip of the posttympanic process, which is completed by the petrosal (Fig. 3B). Anterior to the stout posttympanic process, the ventral margin of the squamosal has a concave surface that abuts the anterior crus of the ectotympanic (see below). Anterior to the ectotympanic is the narrow postglenoid region, which is largely hidden in lateral view by a rod-shaped osseous element that may be a displaced part of the hyoid arch (Fig. 4). The lateral margin of the postglenoid region is concave and medial to that is a ventrolaterally directed, ovoid depression that leads to the postglenoid foramen. Full preparation of the postglenoid foramen was hindered by the rod-shaped element, but we think that aperture was entirely within the squamosal. Dorsal to the back of the postglenoid foramen in the suture between the squamosal and the parietal are the two foramina for the ramus temporalis (see Parietal, above). Anterior to the postglenoid region is the glenoid region, which is largely hidden in lateral view by the posterior end of the jugal (Fig. 4). The posterolateral margin of the glenoid region is marked by the small, ventrally directed zygomatic process of the squamosal, all but the posteriormost part of which is broken from the right side of V7430. The left side of this specimen preserves more of a stump here, which includes a damaged, laterally directed, triangular surface that may have contacted the posterior end of the jugal (Fig. 5B).

The glenoid fossa, best preserved on the left side of V7430 (Fig. 5B), is not well delimited from its surroundings. It is represented by a narrow concavity, longer than wide, between the zygomatic process laterally and a broad shelf of the squamosal medially that buttresses the anterolateral base of the ectotympanic's anterior crus and contributes to the formation of the auditory bulla. We identify this anteroventromedially directed shelf as an entoglenoid process of the squamosal (see Wible et al. 2004), the anterior end of which abuts the ectopterygoid crest (Figs. 3A, 5A, 9). There is no postglenoid process.

Bilaterally in V7429, the part of the anterior crus of the ectotympanic contacting the squamosal in front of the posttympanic process is missing (Fig. 3). This allows a view inside the auditory bulla at the point where the lateral braincase meets the horizontal epitympanic recess over the mallear-incudal articulation. Sutures delimiting the squamosal and the petrosal are incomplete in this region, but both sides show that the squamosal is excluded from the posterolateral rim of the epitympanic recess (Figs. 3B, 9). On the left side of V7430, a part of the squamosal-petrosal suture is preserved, and it also shows that the squamosal forms only a narrow, lateral rim. In *Cocomys* V7399, a clear suture between the squamosal and the petrosal is preserved on the right side (Fig. 7A, B); it shows that the squamosal contributes a narrow, dorsolateral rim, but is excluded from the epitympanic recess, as in *Paramys* (Wahlert 2000), *Reithroparamys* (Meng 1990), and *Cocomys* V7399 (Fig. 7A, B).

Petrosal

The petrosal encases the inner ear, forms the roof of the middle ear, and contributes to the sidewall of the braincase and the occiput. Two divisions of the petrosal are generally recognized and named for the included parts of the inner ear: the pars cochlearis, enclosing the cochlear duct and the saccule, and the pars canalicularis, enclosing the utricle and the semicircular canals. The pars cochlearis is positioned anteroventromedially and the pars canalicularis, posterodorsolaterally. In *Exmus*, much of the ventral or tympanic surface of the petrosal is hidden by the extensive, underlying auditory bulla, formed by the ectotympanic (Fig. 5; see Ectotympanic below). Both bullae are well preserved in V7429 and are present, but broken, in V7430. In V7429, the right middle ear, the space between the ventral surface of the petrosal and the underlying bulla, was cleaned of matrix to the extent possible by access through the damaged external acoustic meatus (Fig. 6). This provides a reasonable view of much, but not all, of the ventral surfaces of the pars cochlearis and the pars canalicularis. The external braincase surfaces of the petrosal, which are formed by the pars canalicularis, are preserved on both sides of V7429 and on the right side of V7430 (Figs. 3, 4). Finally, the medial aspect of the intracranial surface of both petrosals is visible in V7430 (not visible in the figures), in which the basioccipital and the exoccipitals are missing. We describe the petrosal in four views: ventral, lateral, posterior, and dorsal. With regard to the first and the last, our descriptions are not based on direct ventral and dorsal views, but on the oblique views available to us. Following this is a separate treatment of the vascular reconstruction associated with the petrosal.

Ventral view.—The most prominent feature of the petrosal in ventral view (Fig. 6) is the globose promontorium, the principal part of the pars cochlearis. The shape of the promonto-

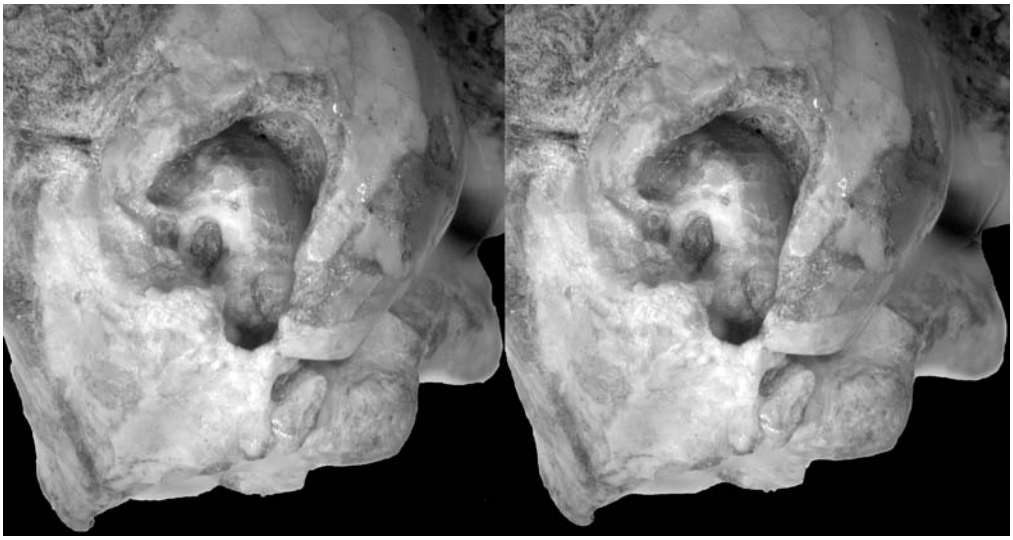

Fig. 6.—*Exmus mini* IVPP V7429, oblique view of right ear region, stereophotograph and accompanying line drawing. Scale = 5 mm. Abbreviations: **ac**, anterior crus of ectotympanic; **bo**, basioccipital; **cp**, crista parotica; **ctpp**, caudal tympanic process of petrosal; **ec**, ectotympanic; **eo**, exoccipital; **er**, epitympanic recess; **fc**, fenestra cochleae; **fv**, fenestra vestibuli; **gsa**, groove for stapedial artery; **me**, mastoid exposure; **oc**, occipital condyle; **pa**, parietal; **pc**, posterior crus of ectotympanic; **pcp**, paracondylar process; **pp**, paroccipital process; **sf**, stapedius fossa; **sff**, secondary facial foramen; **smn**, stylomastoid notch; **sq**, squamosal; **th**, tympanohyal; **tt**, tegmen tympani; **ttf**, tensor tympani fossa.

rium, which reflects the encased coils of the cochlear duct, is roughly two-thirds of a sphere, although it is not a perfect sphere because the promontorium is longer than wide. The long axis of the sphere is directed anteromedially.

Two sizeable, subequal openings are found in the posterior and posterolateral aspects of the promontorium, the fenestra cochleae and the fenestra vestibuli, respectively (Fig. 6). In life, the former opening is covered by the secondary tympanic membrane and the latter contains the footplate of the stapes. The fenestra cochleae (round window) is teardrop-shaped with the wider end positioned ventrally; the aperture is directed posteriorly and slightly ventrally and laterally. It is likely that the fenestra cochleae is recessed slightly from the promontorial surface with a space, the cochlear fossula (sensu MacPhee 1981), between the secondary tympanic membrane and the promontorium, as described in *Paramys* (Wahlert 2000) and present in *Rattus norvegicus* CM 10227. The fenestra vestibuli (oval window) is oval, longer than high, with a stapedial ratio (of Segall 1970, length/width) of 2.05; it is directed laterally and slightly ventrally. The fenestra vestibuli is not at the same horizontal plane as the fenestra cochleae, but is more dorsally placed. Its long axis is not horizontal, but tilted anteroventrally at roughly 30°. The fenestra vestibuli is recessed slightly from the promontorial surface, leaving a narrow vestibular fossula (sensu MacPhee 1981).

The remaining visible promontorial surface is smooth with one noteworthy exception. There is a well-developed vascular groove that runs obliquely across the posteroventral promontorial surface (Fig. 6). It begins posteromedially at a circular foramen between the auditory bulla and the promontorium immediately anterior to the jugular foramen (Fig. 9), passes just anterior to the ventral edge of the fenestra cochleae, and ends at the fenestra vestibuli, where it notches the center of the ventral edge (Fig. 6). We believe the occupant of this foramen and groove to be the stapedial artery (see Vascular Reconstruction), the primary extracranial branch of the internal carotid artery, which in extant placentals passes through the intercrural foramen of the stapes (Wible 1987).

The petrosal bone extends in all directions from the promontorium. The anterior and medial extensions are the epitympanic wings of the petrosal (only the medialmost aspect of which is visible on the right side of V7429 in Figure 5A and of V7430 in Figure 5B), part of the pars cochlearis; the posterior and lateral extensions are the ventral surfaces of the pars canalicularis. We treat these two elements separately. The promontorium does not lie in the middle of these extensions, but is nearer to the posterior and medial ones.

To aid in the description of the epitympanic wing of *Exmus*, we first consider the corresponding, fully exposed element in *Cocomys* V7399 (Fig. 7A, B; see also Li et al. 1989: figs. 3, 4, 7). In V7399, the epitympanic wing can be divided into two parts: an anteromedial shelf and an anterior depression, with the former lying ventral and medial to the latter. The anteromedial shelf is a broad, flat platform that extends from the posteromedial aspect of the promontorium forward to the level of the basisphenoid-basioccipital suture. It is tapered somewhat at its anterior and posterior ends. As noted by Li et al. (1989), the anteromedial shelf provides support for the auditory bulla. Anterior to the promontorium is an expansive depression

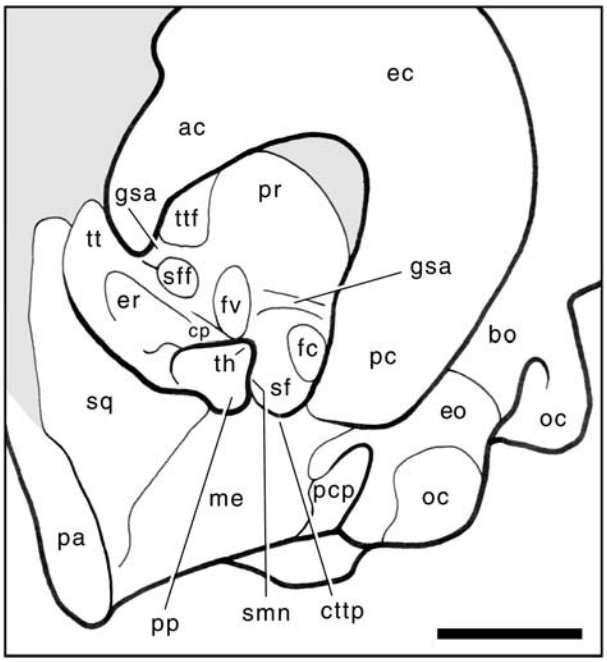

that is broader mediolaterally than anteroposteriorly. The medial border of this anterior depression is the more ventrally lying anteromedial shelf; the anterolateral border is the downturned posteromedial rim of the piriform fenestra, a sizeable gap in the braincase floor between the petrosal and alisphenoid. As noted by Li et al. (1989), occupying the lateral part of the anterior depression is the tensor tympani muscle, although a distinct fossa is not present. Based on our observations, within the area of the tensor tympani origin on the right side is a small depression close to the promontorium that may be a hiatus Fallopii for the greater petrosal nerve. Furthermore, occupying a groove in the medialmost part of the anterior depression is the internal carotid artery. The internal carotid comes off a very faint groove on the anteromedial aspect of the promontorium that continues forward onto the depression just dorsolateral to the anteromedial shelf and enters the braincase at the carotid foramen between the basisphenoid and the petrosal (identified as transverse canal by Li et al. 1989). An additional small opening occurs in the seam between the petrosal and alisphenoid, halfway between the piriform fenestra and carotid foramen. Li et al. (1989: fig. 4) labeled this opening as the middle lacerate foramen. We consider it to be a disjunct part of the piriform fenestra. As noted by MacPhee (1981), the piriform fenestra is the large gap seen in all fetal mammals and in a few adults anterior to the auditory capsule, usually between that element, the sphenoid (basi- and alisphenoid), and the squamosal. *Cocomys* is unusual in that rather than having one piriform fenestra, it has two.

The two principal components of the epitympanic wing of *Cocomys*, the anteromedial shelf and the anterior depression, are present in *Exmus*. Unfortunately, on the right side of V7429, the anteromedial shelf is covered by the auditory bulla and only the part of the anterior depression adjacent to the anterolateral promontorium can be accessed for preparation. An anteromedial shelf resembling that in *Cocomys* is exposed bilaterally in V7430 (Fig. 5B) in which the basioccipital and exoccipitals are missing. Based on V7429, the medial edge of this shelf abuts the ventrolateral surface of the prominent tympanic process of the basioccipital (Fig. 5A; see Basioccipital, below). Posteriorly, the anteromedial shelf begins in front of the foramen for the inferior petrosal sinus (see below), and anteriorly, it extends to the level of the basisphenoid-basioccipital suture (Fig. 8). This shelf provides broad attachment for the expanded, flat dorsomedial surface of the ectotympanic (see Ectotympanic, below). However, between the tympanic process of the basioccipital and the ectotympanic is a narrow gap roofed by the anteromedial shelf, best seen on the left side of V7430, which may have accommodated soft tissues. Preserved bilaterally in V7429, the narrow posterior aperture into this gap lies at the back of the basioccipital's tympanic process and is quarter moon-shaped (Fig. 8). The position of the anterior aperture is unknown. Whatever occupied this gap was not a substantial structure (see Vascular Reconstruction).

As noted above, only the part of the anterior depression of the epitympanic wing adjacent to the anterolateral promontorium is visible on the right side of V7429 (Fig. 6). This is essentially the area of attachment for the tensor tympani muscle. This area is reminiscent of that in *Cocomys* (Fig. 7A, B), but the downturned anterolateral border of the depression is at a steeper angle in V7429, which constricts the tensor tympani attachment (Fig. 6). As in *Cocomys*, the ventral edge of the downturned anterolateral border forms the posteromedial border of a piriform fenestra in V7429, for which the other borders and size are unknown. Other features of the anterior depression of the epitympanic wing of *Cocomys*, such as the groove for the internal carotid artery, the carotid foramen, and the hiatus Fallopii, cannot be confirmed or denied in V7429.

The ventral surface of the pars canalicularis in V7429 is roughly *L*-shaped with the short arm posterior to and the long arm lateral to the promontorium (Fig. 6). Although these arms are continuous, we consider them separately below. The short arm of the *L* behind the promontorium consists of a depression, wider than long, bordered by a high posterior wall. The posterior part of this depression cannot be fully cleaned of matrix. The exposed part of the depression, adjacent to the promontorium, appears to be flat but is tilted such that it is more ventral medially, immediately posterior to the opening by which the stapedial artery reaches the middle ear. This depression is the post-promontorial tympanic sinus (sensu Wible 1990), housing part of the cavum tympani, the air-filled chamber of the middle-ear space. The high posterior wall can be divided into medial and lateral sections, with the medial section

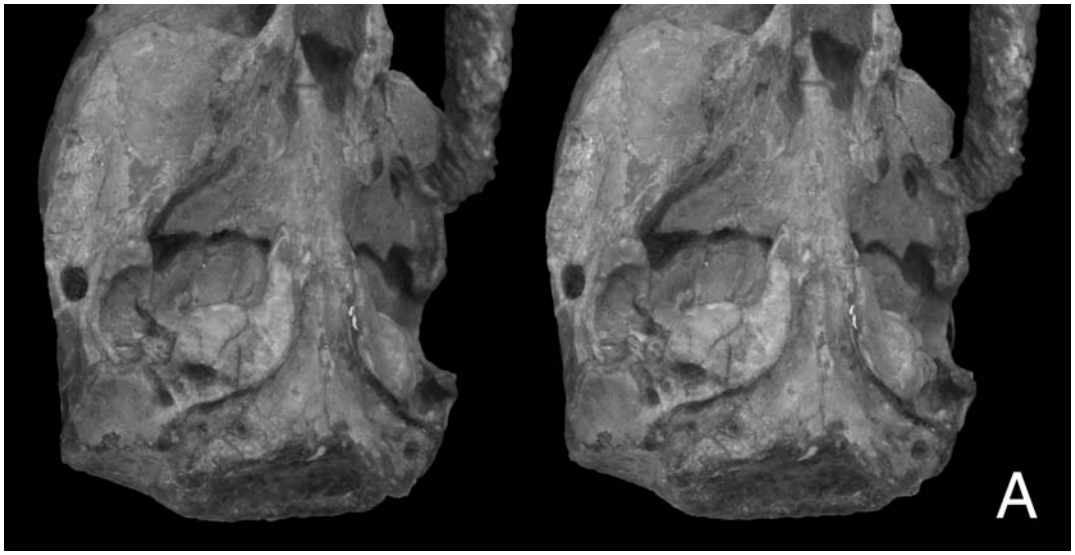

Fig. 7.—*Cocomys lingchaensis* IVPP V7399, oblique view of basicranium, stereophotograph (**A**), accompanying line drawing (**B**), and arterial reconstruction (C). Scale = 2 mm. Abbreviations: **ad**, anterior depression; **ams**, anteromedial shelf; **as**, alsiphenoid; **bo**, basioccipital; **bs**, basisphenoid; **cf**, carotid foramen; **cc**, condyloid canal; **ctpp**, caudal tympanic process of petrosal; **ecp**, ectopterygoid crest; **enp**, entopterygoid crest; **eo**, exoccipital; **er**, epitympanic recess; **fc**, fenestra cochleae; **fm**, foramen magnum; **fo**, foramen ovale; **foa**, foramen ovale accessorius; **fr**, frontal; **fsa**, foramen for stapedial artery; **fv**, fenestra vestibuli; **gica**, groove for internal carotid artery; **gri**, groove for ramus inferior; **gsa**, groove for stapedial artery; **hF**, hiatus Fallopii; **ica**, internal carotid artery; **jf**, jugular foramen; **me**, mastoid exposure; **oc**, occipital condyle; **os**, orbitosphenoid; **pa**, parietal; **pcp**, paracondylar process; **pf**, piriform fenestra; **pgf**, postglenoid foramen; **pp**, paroccipital process; **pr**, promontorium; **ps**, presphenoid; **ri**, ramus inferior; **rio**, ramus infraorbitalis; **rm**, ramus mandibularis; **sa**, stapedial artery; **sff**, secondary facial foramen; **sq**, squamosal; **sof**, sphenorbital fissure; **spv**, sphenopalatine vauity; **tt**, tegmen tympani.

higher and 1.5 times wider than the lateral. The medial section is flat, on the same plane as the anteromedial shelf of the epitympanic wing, and in contact with the back of the auditory bulla. Within the medial section, lateral to the jugular foramen, is a small foramen that is directed anterolaterally into the middle ear (Fig. 8). In light of its position, this may have transmitted the tympanic nerve, a branch of the glossopharyngeal nerve, and/or the auricular branch of the vagus nerve, which joins the facial nerve at the stylomastoid notch (see MacPhee 1981: fig. 4). The lateral section is uncovered, at the ventral edge of the part of the petrosal exposed on the side wall of the braincase (Fig. 6), and is visible in lateral view as an inverted *U* (Fig. 3B); the lateral part of the inverted *U* forms the posterodorsal border of the stylomastoid notch, by which the facial nerve exits the middle ear (see below). Both the medial and lateral sections of the posterior wall represent the caudal tympanic process of the petrosal (sensu MacPhee 1981). We refer to the stout lateral section as the paroccipital process (see below).

The long arm of the *L* is more complex than the short arm, with medial and lateral longitudinal spaces partially separated posteriorly by a crest, the crista parotica (sensu DeBeer 1937; Fig. 6). The principal occupant of the medial space is the facial nerve, whereas the wider lateral space is the epitympanic recess (sensu Klaauw 1931) over the mallear-incudal articulation. The crista parotica is a ubiquitous feature of the mammalian pars canalicularis to which Reichert's (or hyoid) cartilage attaches embryonically (DeBeer 1937). Anteriorly, in V7429, the crista parotica starts opposite the front of the fenestra vestibuli, and it rises posterolaterally to its juncture with the paroccipital process, near the stylomastoid notch. At that juncture is a short, triangular, medially directed process on the crista parotica that represents the tympanohyal, the ossified remnant of Reichert's cartilage. Posteromedial to the tympanohyal is the stylomastoid notch on the petrosal, which is closed ventrally by the posterior crus of the ectotympanic to form a stylomastoid notch. Lateral to the tympanohyal and connected to it by a low ridge is a prominent process that in ventral view is oblong and oriented obliquely, in an anterolateral direction. In lateral view, this process represents the tip of the well-developed posttympanic process on the squamosal that forms the back of the external acoustic meatus (Figs. 3B, 9). Various names have been applied to the process on the petrosal at the juncture of the crista parotica and the caudal tympanic process. Li et al. (1989) referred to that in *Cocomys* as the mastoid process; Wahlert (2000) referred to that in *Paramys* as the mastoid eminence. Following Wible et al. (2004) and Wible and Gaudin (2004), we employ the term paroccipital process, because it reflects the broad homology of this element with that in Mesozoic mammaliaforms. We realize that a potential source of confusion with the term paroccipital process is that some authors (e.g., Gregory 1910) have applied it to a large process of the exoccipital

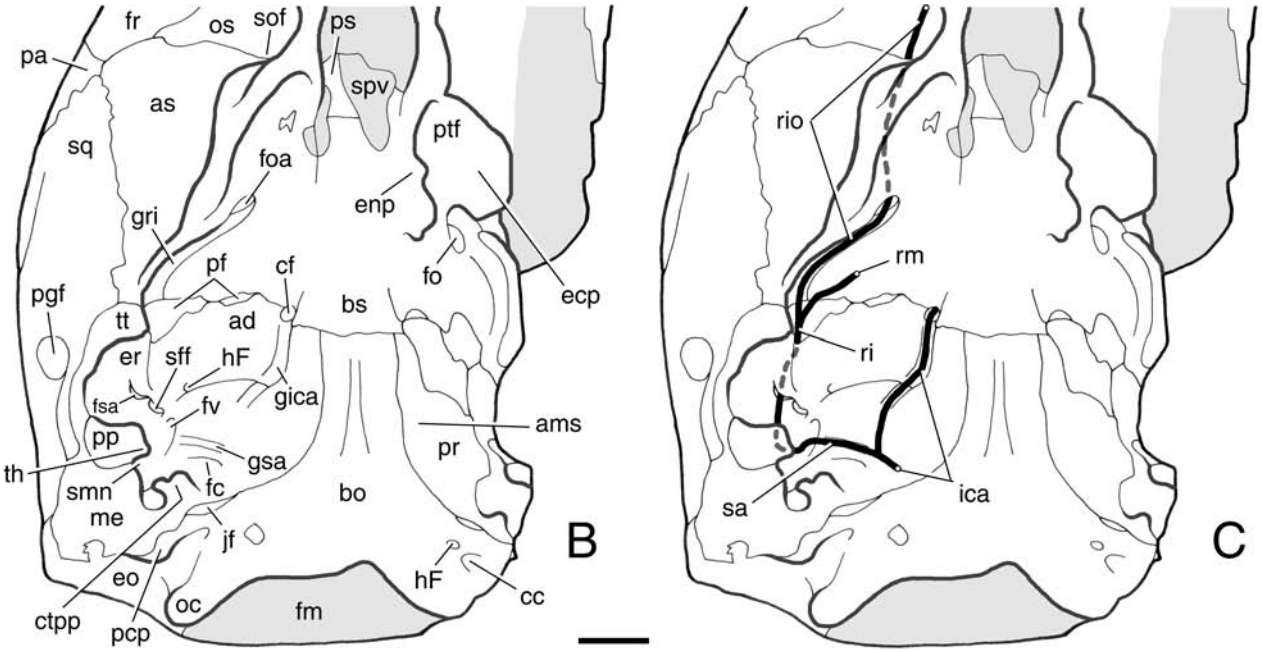

bone. However, the base and tip of that process are respectively the jugular process and paracondylar process of the Nomina Anatomica Veterinaria (1994); the latter is sometimes referred to as the paramastoid process (Sisson 1910; Greene 1935).

In the narrow space between the crista parotica and the promontorium lies the facial nerve. The facial nerve enters the middle ear via an oval, posterolaterally directed foramen, situated anterodorsal to the fenestra vestibuli (Fig. 6). This is the secondary facial foramen; the primary facial foramen transmits the facial nerve into a space, the cavum supracochleare (sensu Gaupp 1908), hidden within the substance of the petrosal. Within the middle ear, the facial nerve runs posteriorly in a groove between the fenestra vestibuli and the crista parotica. It continues undercover of the crista parotica and ultimately leaves the middle ear at the stylomastoid notch.

The spaces occupied by the facial sulcus and the postpromontorial tympanic sinus are continuous in V7429; the crista interfenestralis (sensu Wible et al. 1995) does not continue posteriorly connecting the promontorium and the caudal tympanic process as in some Cretaceous eutherians (Wible et al. 2004). At the juncture of these two spaces in V7429 is a small, shallow pit that represents the fossa for the stapedius muscle (Fig. 6).

Lateral and anterolateral to the crista parotica is a wedge-shaped shelf of bone, narrow posteriorly (Fig. 6). This shelf is best preserved on the right side of V7429, in which it extends forward to the level of the posterior border of the piriform fenestra, but its anterior tip appears to be missing, based on the left side of V7430. Only the lateralmost margin of this shelf is visible on the left side of V7430, and it reaches forward opposite the back of the glenoid fossa where it contacts the entoglenoid process. A suture delimits this shelf posteriorly from the squamosal in V7429 (Figs. 3B, 9). This shelf is broadly concave, with the anterior end reaching as far ventrally as the paroccipital process. The bulk of this shelf represents the tegmen tympani (Fig. 6; DeBeer 1937), a part of the embryonic auditory capsule that grows forward from the crista parotica. The major feature on this shelf in V7429 is the epitympanic recess, the egg-shaped depression, narrower posteriorly, which forms the roof over the mallear-incudal articulation. The anterior border of the epitympanic recess is marked by a low, curved ridge at the level of the front of the secondary facial foramen. In the back of the epitympanic recess is a shallow pit at the level of the posterior rim of the fenestra vestibuli. On the left side of V7429 (Fig. 9), the short arm or crus breve of the incus rests in this pit, which, therefore, is the fossa incudis. Within the shelf anterior to the epitympanic recess is a small, oval foramen that is directed anterodorsally into the skull; it transmits the stapedial artery. Curving posteromedially from this foramen is a well-developed groove for the stapedial artery that ends lateral to the secondary facial foramen (Fig. 6).

In ventral view, outside of the confines of the middle ear, the posteromedial aspect of the petrosal contributes to the anterolateral borders of two large, obliquely oriented openings: the jugular foramen and the foramen for the inferior petrosal sinus (Figs. 5, 8). The jugular foramen is a narrow, oblong opening with pointed ends; its posteromedial border is formed by the exoccipital. The jugular foramen transmits the glossopharyngeal, vagus, and accessory nerves along with the sigmoid sinus; the presence of

the last is marked by a groove on the intracranial surface of the petrosal described below. Anteromedial to the jugular foramen is a similar shaped, smaller aperture that is directed anteriorly into the skull; its posteromedial border is formed by the exoccipital and basioccipital. This aperture transmits the inferior petrosal sinus, the presence of which is marked by another groove on the intracranial surface of the petrosal described below. The foramen for the inferior petrosal sinus and the jugular foramen are separated by small bony projections from the basioccipital and petrosal.

Lateral view.—A triangular wedge of the pars canalicularis is visible on the sidewall of the braincase posterior to the squamosal, with the apex pointing dorsally (Figs. 3B, 4). Its narrow, concave inferior border is formed by the caudal tympanic process of the petrosal. Its anterior border buttresses the posttympanic process of the squamosal, and below that process, the paroccipital process of the petrosal is partially visible in lateral view (Fig. 3B). The posterior border of the wedge is raised as the nuchal crest (Fig. 10), which ends inferiorly at the paracondylar process of the exoccipital (see below). Along the inferior half of the posterior border, the petrosal abuts the exoccipital, with both bones raised to form the nuchal crest. Along the superior half of the posterior border, the petrosal extends onto the occiput (see below) and the nuchal crest is formed solely by that bone. We term the parts of the petrosal visible on the sidewall and occiput the mastoid exposure.

Posterior view.—A smaller triangular wedge of the pars canalicularis is visible on the occiput, with the apex pointing medially (Fig. 10). Its curved lateral border is the nuchal crest. Its oblique ventral and dorsal borders abut the exoccipital and supraoccipital, respectively. On the right side of V7429, a small foramen directed anterodorsomedially into the skull appears near the middle of the side contacting the supraoccipital, with the foramen three-quarters within the petrosal. The left side of this specimen is damaged in this particular spot, and the two sides of V7430 have no such foramen. In light of its position, this is a mastoid foramen, which transmits a small vein to the transverse sinus from the deep muscles of the neck in extant rodents (Hill 1935).

Dorsal view.—A narrow exposure of the dorsomedial aspects of the pars cochlearis in front and the pars canalicularis behind is visible bilaterally in V7430 (not shown in the figures), because the basioccipital and exoccipitals are missing. The most conspicuous feature on the pars cochlearis is the broad, longitudinal vascular sulcus for the inferior petrosal sinus. This sulcus is most defined posteriorly and barely discernible anteriorly. It is positioned near the ventromedial margin of the pars cochlearis, such that in life it would have transmitted an endocranial inferior petrosal sinus from the cavernous sinus to the internal jugular vein. The most conspicuous feature on the pars canalicularis is the broad sulcus for the sigmoid sinus, which lies at roughly 90º to the sulcus for the inferior petrosal sinus. The ventral terminus of the sulcus for the sigmoid sinus is posterolateral to the posterior terminus of the sulcus for the inferior petrosal sinus, which reflects the arrangement of their foramina of exit from the braincase, the jugular foreman and the foramen for the inferior petrosal sinus, respectively. These two sulci are subequal, suggesting that the included vessels were also subequal contributors to the internal jugular vein. Dorsal to the termini of these sulci is a subcircular foramen that is directed anterolaterally into the pars cochlearis. Running posteroventrally from the ventral margin of this foramen is a narrow sulcus that joins the sulcus for the sigmoid sinus at its terminus. This foramen is the cochlear canaliculus (cochlear aqueduct) for the perilymphatic duct and the sulcus connecting it to the sigmoid sinus is likely for the vein accompanying the perilymphatic duct.

Vascular reconstruction.—Before discussing the petrosal vasculature of *Exmus*, we reconstruct the arteries on the basicranium of *Cocomys* V7399 (Fig. 7C). Reconstructing arteries in the latter form is more straightforward than with *Exmus*, because the entire middle ear is exposed in V7399. Although Li et al. (1989) described most of the features associated with the basicranial arteries, they did not attempt an overall arterial reconstruction. The basis for our reconstruction is the sizeable literature on the basicranial arteries in extant rodents and other placentals (see Tandler 1899, 1901; Guthrie 1963, 1969; Bugge 1974, 1985; Wahlert 1974; Wible 1984, 1987).

Grooves on the right promontorium of *Cocomys* V7399 (Fig. 7A, B) reveal an arterial pattern (Fig. 7C) essentially the same as that reconstructed in *Paramys copei* and *Sciuravus nitidus* by Wahlert (2000). A faint groove for the internal carotid artery begins at the posteromedial corner of the promontorium, at the back of the anteromedial shelf, and runs obliquely toward the fenestra vestibuli. Opposite the medial edge of the fenestra cochleae, the internal carotid groove bifurcates into a much fainter groove (with only a very low medial rim) that curves anteromedially toward the anterior pole of the promontorium and another groove that continues to the fenestra vestibuli. The former very faint groove leads to a more well-defined internal carotid groove in the medialmost part of the anterior depression, dorsolateral to the anteromedial shelf, that ends at the carotid foramen between the basisphenoid and the petrosal (identified as the transverse canal by Li et al. 1989). The latter, the groove for the stapedial artery, ends at the fenestra vestibuli. Based on the sizes of the grooves at the carotid foramen and the fenestra vestibuli, it appears that the internal carotid and stapedial arteries were subequal at their bifurcation. At the fenestra vestibuli, the stapedial artery probably ran through the intercrural foramen in the stapes, the pattern that exists in all extant placentals (Wible 1987). However, the groove on the promontorium for the stapedial artery is not centrally placed with

regard to the long axis of the fenestra vestibuli; it is positioned slightly posteriorly. Beyond the stapes, the stapedial artery crossed the facial nerve ventrally and entered a foramen situated anterolateral to the secondary facial foramen. This anteriorly directed foramen for the stapedial artery lies between the anteromedial aspect of the epitympanic recess and the posterolateral aspect of the anterior depression. The foramen is oval and subequal to the secondary facial foramen.

We are not certain of all the details in the course of the stapedial artery beyond the foramen for the stapedial artery (stapedial foramen of Wahlert 2000). A crest runs forward from the foramen for the stapedial artery, between the epitympanic recess and the anterior depression, and ends at the posterolateral margin of the piriform fenestra (foramen lacerum medium of Hill 1935) on the right side of V7399; the left side is damaged here. We believe that this crest indicates the presence of an arterial canal; the damaged left side appears to preserve the roof of this canal. Within the posterolateral margin of the piriform fenestra, there appears to be a foramen that could have been the anterior opening of this canal, but this region is not readily accessible to preparation or investigation. There are two possible reconstructions here, both of which include the ramus superior and the ramus inferior, the primary branches of the stapedial artery, but which differ in the position of the ramus superior-inferior bifurcation. First, the bifurcation may have occurred within the canal, with the ramus superior running dorsally into the braincase through what appears to be a foramen in the roof of the canal on the damaged left side of V7399 and the ramus inferior running forward into the posterolateral margin of the piriform fenestra. Second, the bifurcation may have occurred within the posterolateral margin of the piriform fenestra, with the ramus superior entering the cranial cavity via the piriform fenestra. A choice between the two ultimately hinges on whether the apparent foramen in the roof of the canal on the damaged left side is real or artifact. For now, we accept it as real and favor the first reconstruction.

Anterior to its origin, the ramus inferior entered a well-developed groove in the alisphenoid, preserved bilaterally in V7399, that bends anteromedially through the foramen ovale accessorius (Fig. 7C) and then into the alisphenoid canal (visible in lateral view in Fig. 18A). As in the rat (the palatine portion of the pterygopalatine artery of Greene 1935), the ramus inferior entered the alisphenoid canal, ran through the cavum epiptericum, and then entered the orbit via the sphenorbital fissure (Fig. 7C). Beyond its origin, the further course of the ramus superior is indicated by three or four foramina in the braincase wall: the anterior opening of the orbitotemporal canal between the frontal, alisphenoid, and orbitosphenoid (sphenofrontal foramen of Hill 1935) transmitted the anterior division of the ramus superior into the orbit; and the foramina for ramus temporalis within the squamosal and within the parietal (plus a second between the parietal and squamosal on the right side) transmitted temporal branches of the posterior division of the ramus superior. The foramina for ramus temporalis are referred to as temporal foramina by Wahlert (1974).

The stapedial artery and some of its branches marked in *Cocomys* V7399 are also indicated in *Exmus*. On the right side of V7429 (Fig. 6), a well-marked groove for the stapedial artery crosses the back of the promontorium and notches the middle of the ventral rim of the fenestra vestibuli. Anterolateral to the secondary facial foramen is a well-defined, anterolaterally directed groove between the epitympanic recess and the anterior depression (Fig. 6). This groove ends at an anterodorsally directed foramen for the stapedial artery; this differs from the condition in *Cocomys* V7399 in that it is not so close to the secondary facial foramen. Based on the CT scans of V7430, the foramen for the stapedial artery leads to a short canal, whose rostral opening is in the back of the piriform fenestra. We are uncertain of the details of the further course of the stapedial artery in *Exmus*. The ramus superior is indicated indirectly by several foramina of exit from the cranial cavity. The foramina for ramus temporalis in the parietosquamous suture on the right side of V7430 (Fig. 4) transmitted the temporal branches of the posterior division of the ramus superior. There appears to be a small anterior opening of the orbitotemporal canal in the damaged suture between the orbitosphenoid and alisphenoid on the right side of *Exmus* V7429 (Fig. 3B), which would have transmitted the orbital branches of the anterior division of the ramus superior. However, there is no real indication of the further course of the ramus inferior in V7429. Not present are the large groove in the alisphenoid connecting the piriform fenestra and the foramen ovale, and the alisphenoid canal visible on the lateral braincase anterior to the foramen ovale in *Cocomys* V7399. Moreover, based on the left side of V7429, there is no conduit for a sizeable artery in the narrow seam between the anterior auditory bulla and the alisphenoid. If the ramus inferior was present as a sizeable structure in *Exmus*, it may have followed an entirely endocranial course between its origin at the piriform fenestra and the sphenorbital fissure; a similar course for the ramus inferior is illustrated for the dipodid *Sicista betulina* by Bugge (1971: fig. 4D).

The presence and course of the internal carotid artery in *Exmus* is a mystery. Wible (1986) recognized three principal extracranial courses for the mammalian internal carotid artery and accompanying nerve: transpromontorial or within the middle ear on the promontorium; perbullar or in a canal through the substance of the auditory bulla; and extrabullar or medial to the auditory bulla. According to Wible (1986), all three conditions are known to occur in extant rodents (the first condition occurs only in scuiroids and gliroids, in which the transpromontorial portion of the artery is absent and the transpromontorial course is marked by the internal carotid nerve [Wible 1984]). A fourth condition that occurs in aplodontids, caviomorphs,

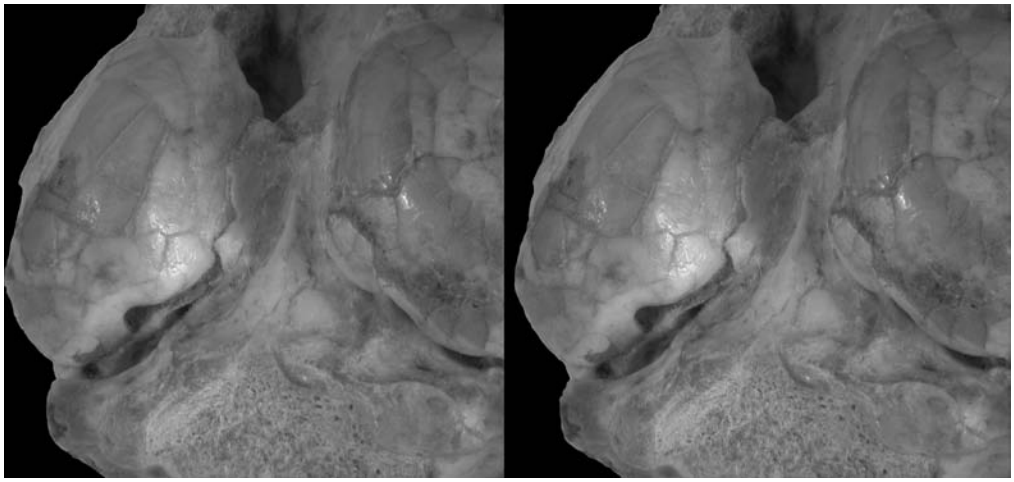

Fig. 8.—*Exmus mini* IVPP V7429, oblique view of basicranium, stereophotograph and accompanying line drawing. Scale = 2 mm. Abbreviations: **abv**, foramen for auricular branch of vagus nerve; **bo**, basioccipital; **bs**, basisphenoid; **cc**, condyloid canal; **ec**, ectotympanic; **eo**, exoccipital; **fm**, foramen magnum; **fsa**, foramen for stapedial artery; **hf**, hypoglossal foramen; **ica**, foramen for internal carotid artery; **ips**, foramen for inferior petrosal sinus; **jf**, jugular foramen; **oc**, occipital condyle; **pcp**, paracondylar process; **pst**, processus styliformis; **tpbo**, tympanic process of basioccipital; **tpbs**, tympanic process of basisphenoid.

hystricids, thryonomyids, bathyergids, and ctenodactylids is the total absence of the extracranial portion of the internal carotid artery (Bugge 1985).

Exmus V7429 has no evidence of an internal carotid groove on the promontorium (Fig. 6) as occurs in *Cocomys* V7399 (Fig. 7A, B). Moreover, the CT scans of V7430 show that there is no carotid foramen in the suture between the petrosal and basisphenoid as occurs in *Cocomys* V7399. Together, the absence of a groove and foramen for the internal carotid within the confines of the middle ear in *Exmus* argue strongly against the occurrence of a transpromontorial artery like that occurring in *Cocomys* V7399, *Paramys copei* and *Sciuravis nitidus* (Wahlert 2000). The absence of a carotid foramen in the suture between the petrosal and basisphenoid also argues strongly against the occurrence of an extrabullar artery, because that vessel has no appropriate point of entry into the cranial cavity. We believe the most viable option for the artery in *Exmus* is a perbullar course. V7429 has a small opening between the tympanic process of the basioccipital, the anteromedial shelf of the petrosal, and the ectotympanic, anteromedial to the foramen for the inferior petrosal sinus (Fig. 8). V7430, in which the basioccipital is missing, reveals that this opening leads to a narrow, longitudinal canal (Fig. 5B). It is possible that this foramen and canal lead to a narrow seam between the petrosal and basioccipital, by which the internal carotid reaches the cranial cavity. *Rattus norvegicus* CM 10227 has a small, short perbullar carotid canal that does just this; the posterior foramen of entrance is between the basioccipital, petrosal, and ectotympanic, and the endocranial aperture is between the basioccipital and petrosal. Another possibility is that the internal carotid artery beyond the origin of the stapedial artery is lacking in *Exmus*, but we do not endorse this option because it leaves no viable occupant for the small foramen between the basioccipital, petrosal, and ectotympanic. If our reconstruction of the perbullar course for the internal carotid artery in *Exmus* is correct, then the large foramen between the ectotympanic and petrosal, lateral to the foramen for the inferior petrosal sinus, visible on both sides of V7429 (Fig. 8) and on the right side of V7430, transmitted only the stapedial artery into the middle ear; this is the opening for the stapedial artery of Hill (1935) and the stapedial foramen of Wahlert (1974).

Ectotympanic

In *Exmus,* a single osseous element is the principal component of the moderately inflated auditory bulla, the floor of the middle ear. This single element must be the ectotympanic, the bone forming the auditory bulla in extant rodents (Klaauw 1931; Novacek 1977). In ventral view, the ectotympanic in V7429 completely covers the petrosal and is shaped like an irregular dome, deeper medially than laterally (Fig. 5A). In the lateral aspect of the ectotympanic, there is a laterally directed opening, the external acoustic meatus. Forming the anterolateral margin of the external acoustic meatus is the ectotympanic's anterior crus or leg and forming the caudolateral margin is the posterior crus or leg (Fig. 6). The ectotympanic is best preserved on the right side of V7429 (Figs. 3B, 5A, 6); missing are only the tips of both the anterior and posterior crura, but these are fully preserved on the right side of V7430 (Fig. 4).

Dorsally, the ectotympanic is tightly appressed to the skull base, with only a very narrow gap between the ante-

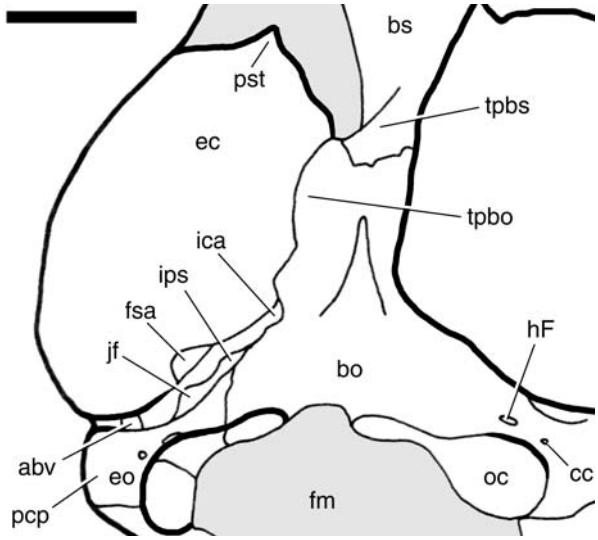

rior and posterior crura, based on the right side of V7430 (Fig. 4). This means that the external acoustic meatus is almost entirely within the ectotympanic; filling the narrow gap between the anterior and posterior crura, the tympanic incisure, is the base of the tympanohyal. The shape of the laterally directed external acoustic meatus is not well preserved, but it appears to be oval, longer than high (Figs. 3, 4). Based on the right side of V7430, the broad end of the anterior crus forms the stout lateral wall of the epitympanic recess and contacts the anterior face of the posttympanic process of the squamosal (Fig. 4). Anterior to the epitympanic recess, the anterior crus contacts successively the entoglenoid process of the squamosal, the ectopterygoid crest of the alisphenoid, and the alisphenoid behind the foramen ovale, best shown on the left side of V7429 (Fig. 3A). The next clear abutment of the ectotympanic is with the tympanic process of the basioccipital (Fig. 8). Between the alisphenoid and basioccipital contacts, the dorsal margin of the ectotympanic is concave, based on the left side of V7429, marking the passageway for the auditory (Eustachian) tube. Dorsal and posterior to the contact with the basioccipital, the ectotympanic has a longitudinal contact with the anteromedial shelf of the petrosal's epitympanic wing (Fig. 5B). At the back of the contact with the basioccipital, the ectotympanic forms the medial wall of the narrow opening into the perbullar carotid canal described above (Fig. 8). Posterior to the abutment with the anteromedial shelf is the opening for the stapedial artery and behind that, the contact of the posterior crus with the caudal tympanic process of the petrosal (Fig. 8). This contact curves posterolaterally, contacting the paroccipital process (Fig. 9), and then anterolaterally, ending with the narrow tip of the posterior crus abutting the base of the tympanohyal, based on the right side of V7430. Posteromedial to the tympanohyal is the stylomastoid notch between the posterior crus and caudal tympanic process of the petrosal, preserved on the right side of V7429 (Fig. 6) and the right side of V7430. On the left side of V7429, anterior to the tympanohyal, the tip of the posterior crus has a small process that projects anteriorly and appears to contact the posterior aspect of the ventral end of the lateral process of the malleus (Fig. 9; see below). This contact is most likely artifactual.

The external surface of the ectotympanic is smooth with the exception of two small processes on the anterior aspect of the anterior crus. Projecting anteriorly from the anteromedial corner of the ectotympanic on both sides of V7429 is a processus styliformis (sensu Klaauw 1931; Fig. 5A) that underlay the auditory tube. This process is a flattened triangle that is tilted obliquely with its lateral edge higher than its medial edge. It approximates but does not contact the pterygoid hamulus. Projecting anteromedially from the anterolateral corner of the ectotympanic on the left side of V7429 and both sides of V7430 (Fig. 5) is another short triangular process that is tilted obliquely with its medial edge higher than the lateral. Because the dorsolateral surface of this process contacts the back of the ectopterygoid crest, we identify it as an ectopterygoid process of the ectotympanic. Continuing onto the ectotympanic behind the ectopterygoid process is a low ridge, the lateral surface of which contacts the entoglenoid process of the squamosal (Fig. 9). Dorsomedial to the ectopterygoid process is a narrow gap in the suture between the ectotympanic and alisphenoid that represents the Glaserian fissure (canal of Huguier of Wahlert 1974), which transmitted the chorda tympani nerve from the middle ear.

The internal surface of the right ectotympanic of V7430 is visible in the CT scans. Lateral to the deepest point of the tympanic floor is a low semicircular ridge, the crista tympanica, marking the medial margin of the sulcus tympanicus, to which the tympanum (tympanic membrane) is attached. We reconstruct the right tympanum as oblique, at approximately 35º to the vertical.

Middle-Ear Ossicles

The left side of V7429 preserves the incus and part of the malleus (Fig. 9). Damage to the anterior crus of the left ectotympanic allowed room for preparation of the lateral and dorsal surfaces of both bones; to buttress these delicate elements, matrix was left on their medial surfaces. The malleus is also preserved on the left side of V7430. Less preparation was done on this specimen because the anterior crus of the ectotympanic is in place. However, because the incus is missing, we have a glimpse of the posteromedial surface of the malleus. In both specimens, the ossicles appear to be in or near their life positions.

Auditory ossicles have been figured for only a small percentage of the vast diversity of rodents (see Doran 1878; Cockerell et al. 1914a, 1914b; Wassif 1948; Fleischer 1973). Of those figured elsewhere or investigat-

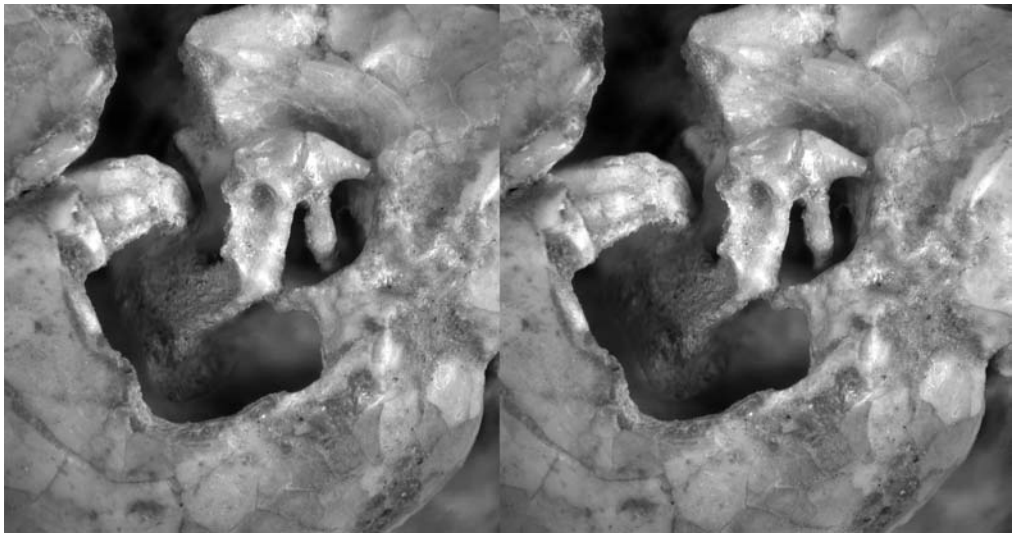

Fig. 9.—*Exmus mini* IVPP V7429, lateral view of left ear region, stereophotograph and accompanying line drawing. Scale = 2 mm. Abbreviations: **ap(br)**, anterior process of malleus (broken); **cb**, crus breve; **cl**, crus longum; **eam**, external acoustic meatus; **ec**, ectotympanic; **egp**, entoglenoid process; **er**, epitympanic recess; **fi**, fossa incudis; **h**, head of malleus; **i**, incus; **lp**, lateral process of malleus; **ma**, malleus; **mn**, manubrium; **n**, neck of malleus; **pet**, petrosal; **pp**, paroccipital process; **ptp**, posttympanic process of squamosal; **sq**, squamosal.

ed by us, the malleus of V7429 and V7430 is reminiscent of that in *Rattus norvegicus* CM 10227. Terminology of the auditory ossicles seems nearly as diverse as the bones themselves. In describing the malleus and incus here, we follow Henson (1961).

Malleus

Our descriptions are based on the left malleus of V7429 (Fig. 9), except where noted. The four basic parts of the malleus recognized by Henson (1961) are the head, neck, manubrium, and anterior process. The first two are well preserved and the last two broken in V7429.

The malleus sits beneath, but not in contact with, the epitympanic recess in the petrosal bone. It is oriented more or less vertically, with its head, neck, and manubrial base (the area of confluence of the neck, manubrium, lateral process, and lower part of the anterior process) essentially on a straight line. The posterior surface of the small, smooth, globular head articulates with the incus. Although the malleus and incus are in articulation, the contact shows that the malleus has two distinct articular surfaces for the incus: a larger superior one that is nearly vertical and a smaller inferior one at slightly more than a right angle to the superior one. The anterior end of the head is not fully prepared, but it seems to end in a slight capitular spine that separates it from the top of the anterior process. Extending ventrally from beneath the inferior incudal facet is the narrow, straight, rod-shaped neck. At approximately the same level as the ventral extent of the crus longum of the incus, the neck, merging with the manubrial base, bends ventrolaterally as the prominent lateral process, which projects into the tympanum (Henson 1961). Projecting anteroventromedially from the ventral base of the lateral process is the delicate manubrium, which is embedded in the tympanum and vibrates with it (Henson 1961). Roughly, only the proximal half of the manubrium is preserved. Projecting anteriorly from between the head and the lateral process is the broad, flange-like anterior process, the distal part of which is missing. The superior and inferior margins of the anterior process, the outer lamella, and the pars processus anterioris of the anterior process respectively are curved towards each other and raised over the intervening basin-like bone, the lamina.

What is preserved of the malleus in V7430 conforms to the above, but one additional feature is evident. Along the posteromedial border, where the neck merges with the manubrial base, a low, medially directed process is visible. This is the posterior end of the muscular process for the tensor tympani insertion.

Incus

The basic parts of the incus are the body, short process (crus breve), long process (crus longum), and lenticular process. The left incus of V7429 (Fig. 9) preserves all but the last.

The body of the incus articulates with the head of the malleus at two facets mirroring those described above on the malleus. There is little to the body beyond these articular surfaces. Extending posteriorly from the body is the crus breve, which is conical but with a blunt posterior end;

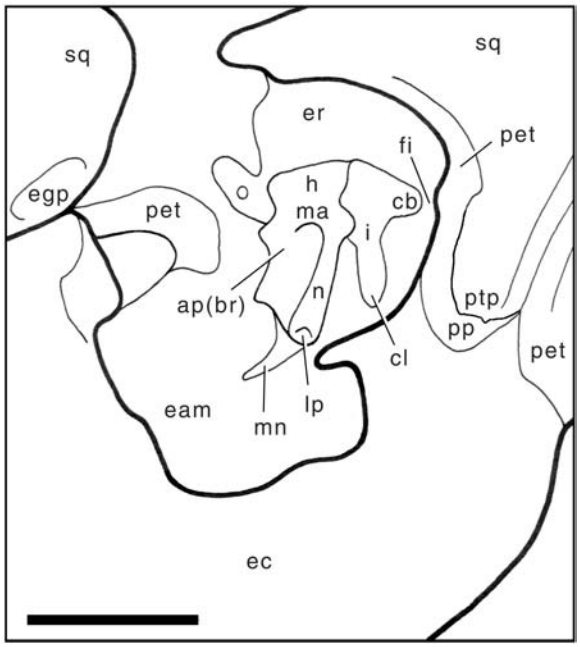

it projects into the fossa incudis of the petrosal and is held in place by the posterior incudal ligament (Henson 1961). As its name implies, the crus breve is shorter than the crus longum, but it is also stouter. The more delicate crus longum projects ventrally and slightly posteriorly from the body. It is rod-shaped, although tapered at its proximal end, with a rounded distal end. Though not visible, presumably a narrow pedicle extends medially from the distal end as the base for the lenticular process, which articulates with the stapes (Henson 1961).

Stapes

The basic parts of the stapes are the head, anterior and posterior crura for a bicrurate stapes or a single crus for a columellar stapes, and the footplate. Stapes are not preserved for V7429 or V7430. However, two features of the stapes can be inferred based on the morphology of the right petrosal of V7429. First, the shape of the footplate mirrors that of the fenestra vestibuli; consequently, the footplate of V7429 is oval with a stapedial ratio (of Segall 1970, length/width) of 2.05. Second, the position of the groove for the stapedial artery on the promontorium shows that the stapedial artery crosses the middle of the fenestra vestibuli (Fig. 6); consequently, the stapes of V7429 is bicrurate with an intercrural fenestra for the stapedial artery.

Occipital Complex

In the guinea pig *Cavia* (Cooper and Schiller 1975) and the gundi *Ctenodactylus* (Schrenk 1989), a single occipital bone occurs in the adult, but is formed from unpaired basioccipital and supraoccipital ossifications (the latter initially paired in the guinea pig; Dierbach 1985) and paired exoccipital ossifications. In both rodents, the basioccipital forms the anteroventral border of the foramen magnum, the exoccipitals the lateral borders, and the supraoccipital the posterodorsal border. The entire occipital complex is well preserved in V7429; in fact, sutures delineate its four constituent elements: basioccipital, supraoccipital, and paired exoccipitals (Figs. 5A, 10). Only the supraoccipital is preserved in V7430. As in the guinea pig and gundi, all four elements contribute to the borders of the foramen magnum in V7429, which is ovoid, wider than high (6.8 × 4.4 mm).

Basioccipital

The basioccipital forms the skull base between the left and right ear regions and the anteroventral margin of the foramen magnum. Well preserved in V7429 (missing from V7430), it is roughly hexagonal with unpaired anterior and posterior sides and paired anterolateral and posterolateral sides (Fig. 5A). The anterior and the paired posterolateral sides are subequal and are shorter than the posterior and the paired anterolateral sides, which are also subequal.

The anterior side is the transverse suture with the basisphenoid. The middle half of this suture is essentially flat, but the right and left lateral quarters are turned down at sharp angles, slightly more than 90°, representing the anterior ends of the prominent tympanic processes of the basioccipital (Fig. 8). Anteriorly, these contact the much lower tympanic processes of the basisphenoid.

The anterolateral sides are concave, with the basioccipital widest at the posterior ends of these sides (Fig. 5A). The anterior two-thirds of the anterolateral side is the well-developed tympanic process of the basioccipital (Fig. 8), which overlies the ectotympanic ventrally and the medial edge of the pars cochlearis of the petrosal dorsally, based on V7430 in which the basioccipital is wholly absent. In the posterior one-third of the anterolateral side, the basioccipital contacts only the pars cochlearis of the petrosal. It is in this part of the basioccipital-petrosal contact that the front of the foramen of the inferior petrosal sinus mentioned above occurs (Fig. 8). Also mentioned above, anterior to this foramen is the narrow perbullar carotid canal between the tympanic process of the basioccipital, the ectotympanic, and the medial edge of the petrosal. The posterior aperture into this narrow gap at the back of the basioccipital's tympanic process in V7429 is quarter moon-shaped (Fig. 8).

From the opening for the inferior petrosal sinus, the posterolateral sides trend posteromedially and end at the anteroventral margin of the foramen magnum (Fig. 5A). The posterior side forms the middle two-thirds of the

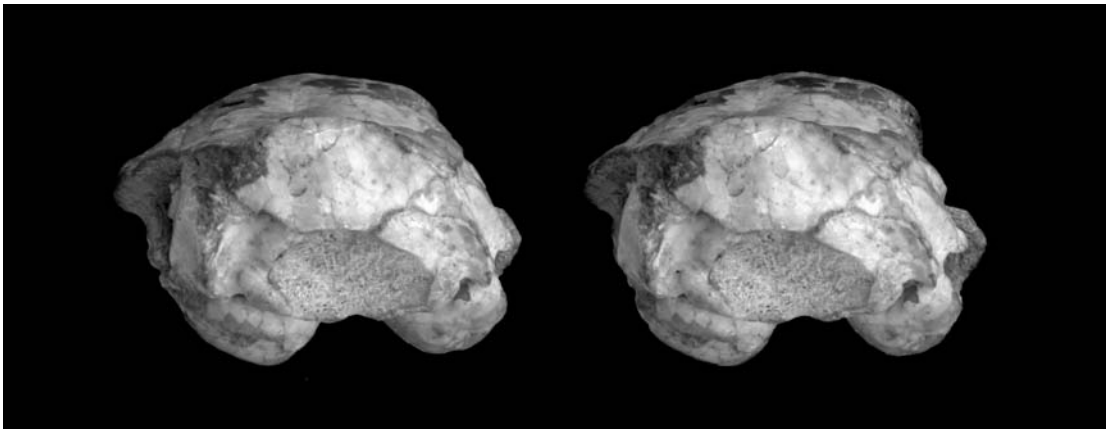

Fig. 10.—*Exmus mini* IVPP V7429, occiput, stereophotograph and accompanying line drawing. Grey represents matrix. Scale = 5 mm. Abbreviations: **ctpp**, caudal tympanic process of petrosal; **ec**, ectotympanic; **eo**, exoccipital; **fm**, foramen magnum; **masf**, mastoid foramen; **me**, mastoid exposure; **nc**, nuchal crest; **oc**, occipital condyle; **pa**, parietal; **pcp**, paracondylar process; **pp**, paroccipital process; **su**, supraoccipital.

anteroventral margin of the foramen magnum. This margin includes a distinct midline notch, the odontoid notch, accommodating the dens of the axis.

The ventral surface of the basioccipital is not flat but includes an inverted funnel-shaped part, with the wide cone at the foramen magnum and the tapered base forming a midline keel that nearly reaches to the basisphenoid (Figs. 5A, 8). On either side of the keel is a muscular depression, longer than wide, presumably for the longus capitis and the rectus capitis ventralis muscles, as in the guinea pig (Cooper and Schiller 1975) and wood rat (Wahlert and Sawitzke 1988). The tympanic process of the basioccipital forms the lateral aspect of this depression.

Exoccipital

Well preserved in V7429 (missing from V7430), the exoccipitals form the lateral margins of the foramen magnum and have roughly quadrangular horizontal and vertical parts, in the skull base (Figs. 5A, 8) and occiput (Fig. 10), respectively.

The anteromedial side of the horizontal part is the oblique suture with the basioccipital (Figs. 5A, 8). The concave posteromedial side forms the ventrolateral margin of the foramen magnum. The posterolateral side is the back of the skull base; it is convex medially, with the convexity being the occipital condyle, and concave laterally, presumably with the occipital artery occupying that notch as in extant rodents (Bugge 1974; Cooper and Schiller 1975). The concave anterolateral side is the longest and abuts the pars canalicularis of the petrosal; situated in this abutment is the foramen for the inferior petrosal sinus and the jugular foramen (see Petrosal, above).

The principal features on the horizontal part are the hypoglossal foramina, the occipital condyle, and the paracondylar process (Fig. 5A). The hypoglossal foramina are situated immediately posteromedial to the jugular foramen. On the right side, three foramina occupy a kidney bean-shaped depression; on the left side, there is only one foramen in a smaller oval depression. Posterior to the hypoglossal depression is the occipital condyle, which is visible in both ventral and occipital views. In ventral view (Fig. 5A), the right and left condyles are slightly different, with the left side larger and more oval and the smaller right side subcircular. This appears to be a natural difference and not the result of postmortem damage. The low paracondylar process (paramastoid or paroccipital process of Greene 1935) occupies the extreme lateral aspect of the horizontal part; it is well preserved on the left side, but broken on the right. It has the shape of an inverted pyramid, which is most easily seen in occipital view; it is also visible in lateral view, which shows how its ventral end is tilted forward and nearly touches the back of the auditory bulla. Muscles attaching to the paracondylar process vary in rodents: in the wood rat (Howell 1926), arising are the posterior digastric and stylohyoid muscles; in the rat (Greene 1935) and guinea pig (Cooper and Schiller 1975), sternomastoid and posterior digastric muscles, along with jugulohyoideus in the guinea pig; and in *Zapus* (Klingener 1964), posterior digastric and jugulohyoideus. In the interval between the hypoglossal foramina, occipital condyle, and paracondylar process, a small foramen is present bilaterally in V7429 (Fig. 5A). Following Wible (2003), we identify this opening as a condyloid canal (Fig. 8).

Best preserved on the right side of V7429, the vertical part of the exoccipital is an obliquely oriented quadrangle with short ventral and lateral sides and long dorsal and medial sides (Fig. 10). Medially, the dorsal side contacts the supraoccipital and laterally, the part of the mastoid exposure of the petrosal on the occiput; the suture at the former is weakly sinuous and at the latter, the exoccipital is convex. The concave medial side forms the lateral margin of the foramen magnum. The convex lateral

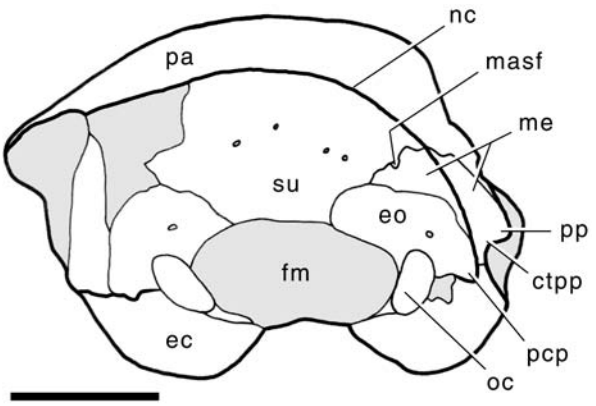

side contacts the part of the mastoid exposure of the petrosal on the sidewall of the braincase, and together these elements form the ventrolateral part of the nuchal crest, which ends inferiorly as the paracondylar process. The ventral side is convex medially, reflecting the shape of the occipital condyle, and concave laterally, with the paracondylar process at the ventrolateral edge of the concavity.

The principal features on the vertical part are the occipital condyle, the paracondylar process, and several small foramina (Fig. 10). In posterior view, the condyle is roughly egg-shaped with the wider end directed dorsolaterally; the condyle's lateral edge is convex and its medial edge is concave. The asymmetry between the right and left condyles reported from the ventral view is also evident in posterior view, with the axis of rotation of the right condyle at a higher angle than the left. As noted above, the undamaged right paracondylar process is best seen in occipital view; the tip of the left process is missing. Small foramina are present on both sides, with the number differing between the two; these are probably venous in function, related to the underlying sigmoid sinus, whose groove in the intracranial surface of the petrosal is shown in V7430. On the left side, there is a foramen immediately lateral to the condyle and a second subequal one halfway between the top of the condyle and the suture with the supraoccipital. On the right side, in addition to these two, there is a third subequal foramen immediately dorsolateral to the top of the condyle.

Supraoccipital

The supraoccipital is present, but damaged, in both specimens with slightly better preservation in V7430. It forms roughly the dorsal half of the occiput and the middle of the dorsal margin of the foramen magnum (Fig. 10); it also has a small, triangular exposure on the dorsal surface of the braincase behind the parietals (Fig. 1).

The dorsal edge of the supraoccipital is convex (Fig. 1). The middle third of the dorsal edge has a triangular wedge that extends forward between the parietals, representing the supraoccipital's contribution to the braincase roof mentioned above. The transition here from occiput to skull roof is fairly smooth. The lateral thirds of the dorsal edge meet the parietals at an acute angle, marking the transition from occiput to skull roof. This part of the supraoccipital-parietal juncture is raised as a low, but distinct, posteriorly directed nuchal crest. The supraoccipital-parietal suture is visible on the skull roof on the right side of both V7429 and V7430 (Fig. 1) and the supraoccipital is the major component of the nuchal crest. The extreme ventrolateral aspect of the dorsal edge of the supraoccipital appears to have a very narrow contact with the squamosal on the right side of V7430 (Fig. 4); there appears to be no such contact on the right side of V7429 (Fig. 3B), but this area is damaged.

Medially, the ventral edge of the supraoccipital forms the concave dorsal border of the foramen magnum (Fig. 10). Lateral to that, the ventral edge of the supraoccipital has two more concavities; the medial one is the contact with the exoccipital and the lateral one is the contact with the part of the mastoid exposure of the petrosal on the occiput.

In V7430, there is a low, raised vertical ridge on the supraoccipital's midline, the external occipital crest, which extends from just above the foramen magnum nearly to the top of the occiput. This ridge is present, but less distinct in V7429 (Fig. 10). At the base of the external occipital crest is a small, presumed venous foramen in V7430, but not V7429. In both specimens, on either side of the external occipital crest are a half-dozen or so small foramina per side, asymmetrically arranged, also presumably of venous function.

Mandible

Right and left mandibles are preserved for both V7429 and V7430, but all four have some damage. The left mandible of V7429 is the most complete; missing are only the condylar process and condyle and some bone around the incisor alveolus (Fig. 11). Fortunately, the next most complete mandible, the right one of V7430, preserves the condylar process, although the condyle is damaged (Fig. 12). The mandible has a short, narrow, tooth-bearing horizontal part, the body, and a high, broad, vertical part, the ramus.

The body of the mandible, from the front of the coronoid process to the tip of the alveolus for the enlarged lower incisor, is less than half the antero-posterior length of the ramus from the same point to the tip of the angular process (Figs.11A, 12A). The body is sturdy, deepest beneath dp4 or p4 (5.4 mm measured on the labial side of the left mandible of V7429), where there is a rounded,

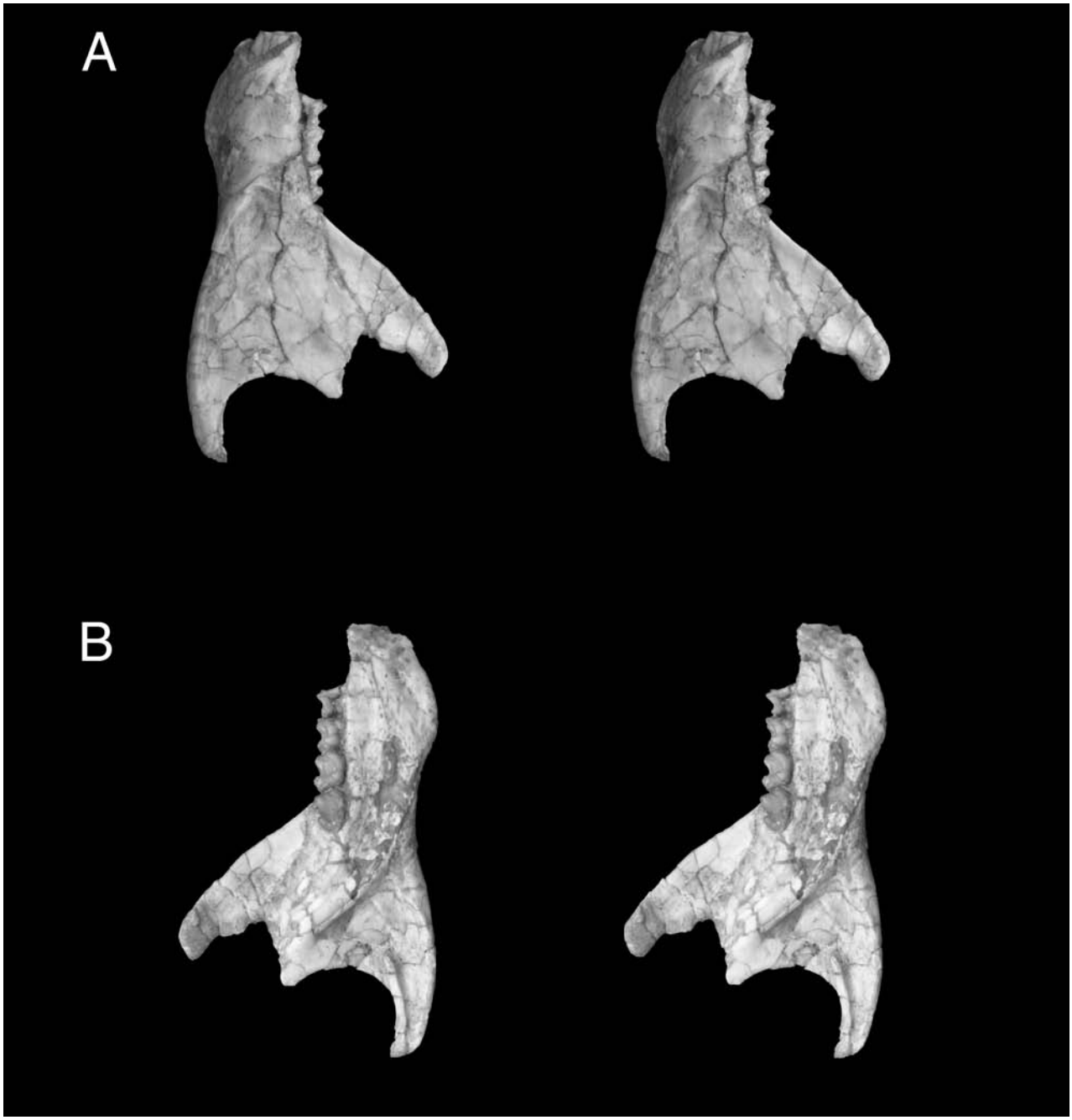

Fig. 11.—*Exmus mini* IVPP V7429, left mandible, stereophotograph and accompanying line drawing, lateral (**A**) and medial (**B**) views. Grey represents matrix. Scale = 2 mm. Abbreviations: **an**, angle; **coc**, coronoid crest; **cop**, condyloid (condylar) process (broken); **cor**, coronoid process; **dp4**, deciduous lower fourth premolar; **i2**, lower incisor (broken); **maf**, masseteric fossa; **mal**, masseteric line; **manf**, mandibular foramen; **mf**, mental foramina; **mpt**, medial pterygoid muscle attachment; **ss**, symphyseal surface.

ventral prominence (Fig. 11A). Anterior to the deepest point, the ventral border of the body is convex, whereas it is concave posteriorly. There is a distinct diastema between the incisor and premolar, but its dorsal border is only slightly depressed compared to the alveolar border of the premolar (Figs. 11A, 12A). A low, sharp ridge runs along the diastema from the lingual side of the premolar to the incisor alveolus; it likely marks the upper margin of the pars mandibularis anterior of the buccinator muscle (Rinker 1954). This ridge is continuous posteriorly with a

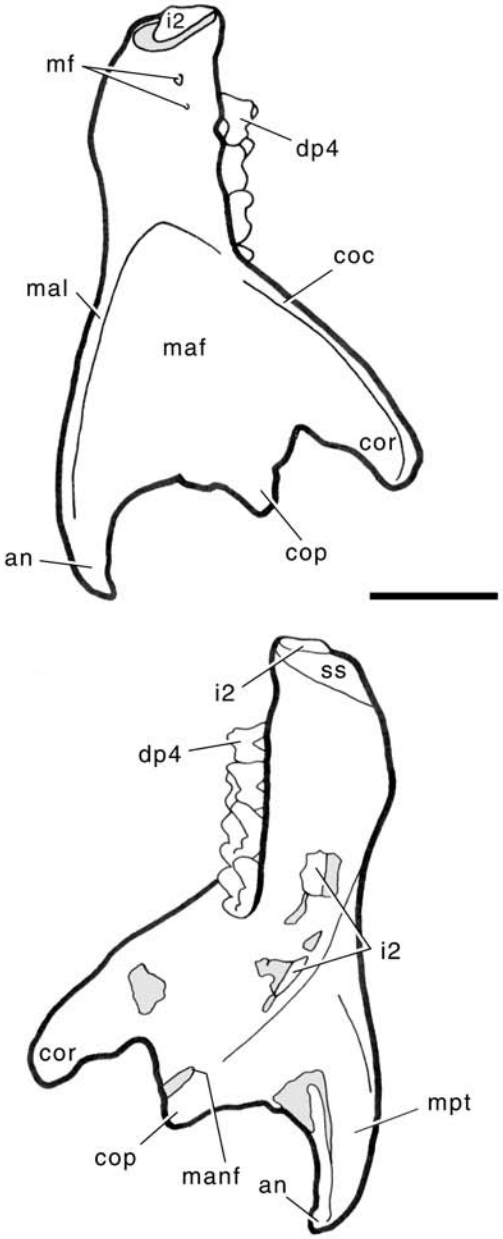

ridge along the lingual alveolar margin of the cheek teeth.

On the labial surface are anterior and posterior mental foramina (Figs. 11A, 12A). The large anterior mental foramen lies below the anterior root of the premolar, nearer the alveolar border of the mandibular body than the ventral; a well-developed sulcus leads anteriorly from this anteriorly directed foramen in V7430, but this sulcus is weak in V7429. The tiny posterior mental foramen, which is laterally directed, lies just posterodorsal to the anterior one. The masseteric fossa (see below) extends onto the mandibular body, to below the middle of m2.

In lingual view, the symphyseal surface is not completely preserved in any specimen (Fig. 11B); the most shows on the left mandible of V7429. What is preserved is keel-shaped, with the bottom of the keel facing anteroventrally, but much of the anterior surface is damaged. It is clear that the symphysis was short anteroposteriorly and broad dorsoventrally. It extended from the dorsomedial aspect of the incisor alveolus all the way to the ventral border, at a level just in front of the anterior root of the premolar. Immediately posterior to the symphysis is the rounded prominence on the ventral margin described above (Fig. 11B). The medial aspect of this prominence is subtly raised, providing attachment for the anterior digastric muscle (Klingener 1964; Woods 1972). On the left side of V7429, this raised edge continues posteriorly as a line that diverges from the ventral margin below the posterior part of m1. It curves posterodorsally, continues as a rounded prominence onto the mandibular ramus, and ends well above the occlusal plane, anteroventral to the condylar process. Bone damage on the left sides of V7429 (Fig. 11B) and V7430 exposes parts of the extensive lower incisor and reveals that this line on the body and the rounded prominence on the ramus, at least to a level some 3.5 mm behind m3, marks the lower border of the incisor. The part of this line below the molars likely marks the attachment of the mylohyoid muscle (Klingener 1964; Woods 1972). Also, in this same area, the bone between this line and the alveolar margin is riddled with dozens of small foramina on the right side of V7429 and V7430. The significance of these foramina is not known, but may reflect the immature age of the specimens.

The ramus of the mandible has three salient processes: coronoid, condylar (articular), and angular (Figs. 11, 12A). The first two are well above the occlusal surface of the cheek teeth and the last forms the posteroventral border of the ramus. The prominent coronoid process is essentially fully preserved on the left side of V7429 (Fig. 11); it is shark fin-shaped, with a convex anterior margin and a more or less concave posterior one. With the molar occlusal surface horizontal, the coronoid process extends some 3 mm more dorsally than the condylar process, which is incomplete in V7429 but preserved on the right side of V7430 (Fig. 12). The lateral edge of the anterior border of the coronoid process, the coronoid crest, is thickened dorsally in both specimens, but it is more developed and extends further ventrally in V7429 (Figs. 11A, 12A). The coronoid process rises at an angle of about 45º to the body; in lateral view its base hides the talonid of m3. Between the coronoid and condylar processes is the narrow, *U*-shaped mandibular notch. The condylar process is preserved only on the right side of V7430, where a small amount of bone has flaked off the posterolateral surface (Fig. 12). The process is short, rising only a little over the mandibular notch, and erect with the articular surface of the condyle dorsally directed. In dorsal view, the condyle is quadrangular: almost twice as long as wide and about

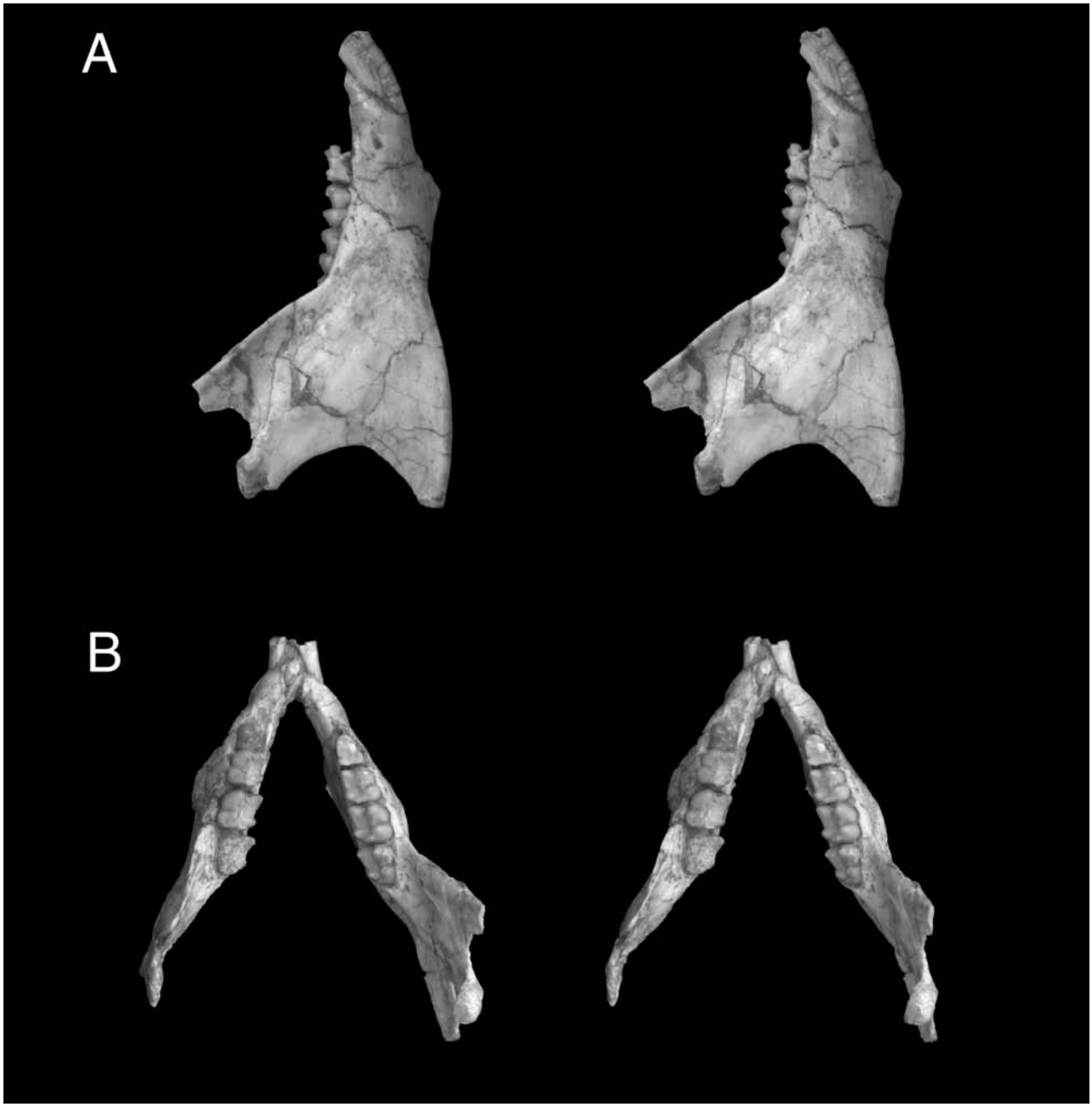

Fig. 12.—*Exmus mini* IVPP V7430, lateral view of right mandible (**A**) and occlusal view of left and right mandibles (**B**), stereophotographs and accompanying line drawings. Grey represents matrix. Scale = 5 mm. Abbreviations: **an(br)**, angular process (broken); **con**, condyle; **cor(br)**, coronoid process (broken); **dp4**, lower deciduous fourth premolar; **i2**, lower second incisor; **maf**, masseteric fossa; **manf**, mandibular foramen; **mf**, mental foramina; **p4**, lower fourth premolar.

equal in width for its entire length, not tapering in either direction (Fig. 12B). It lies oblique to the occlusal surface, so that its posterior side is more medial than its anterior one, and the bulk of the condyle lies medial to the plane of the mandibular notch. Its articular surface is not flat, but is gently convex. The prominent angular process is a near mirror image of the coronoid process in shape and size, except that it tapers more to a point at its posterodorsal end (Fig. 11). In dorsal view of V7429, it is apparent that the angular process is slightly inflected from the plane of the coronoid and condylar processes, with the ventral border of the angular process medial to its dorsal border. On the medial surface, the dorsal and ventral edges of the angular process are marked by raised, medially directed crests (Fig. 11B), which

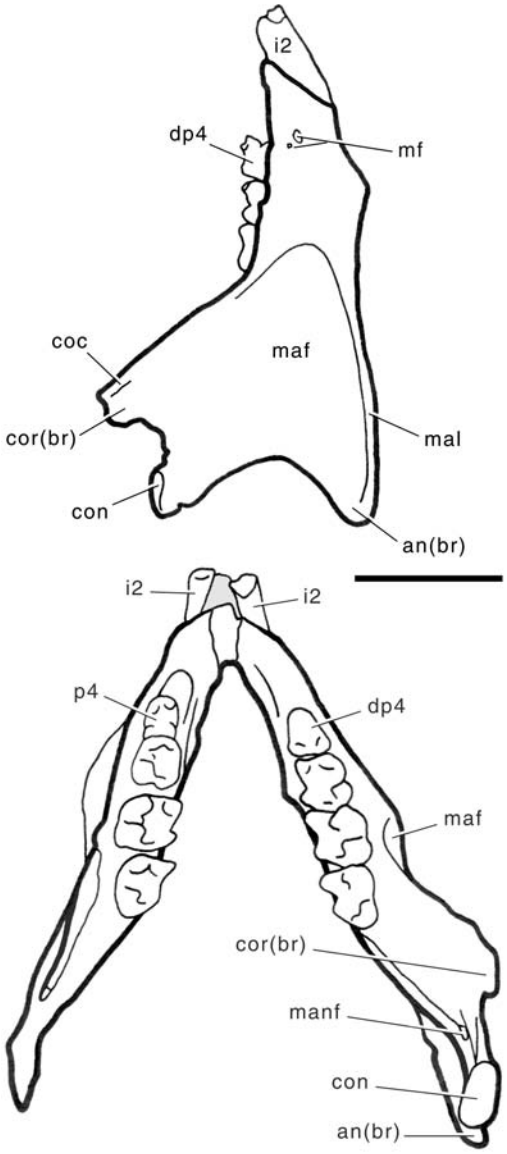

define the back of the pterygoid fossa (see below).

The principal feature on the lateral surface of the ramus is the extensive insertion area for the masseter muscle (Figs. 11A, 12A). The masseteric fossa is wide and high but shallow and extends forward beneath the middle of m2. The fossa is bordered by anterodorsal and ventral crests that meet anteriorly below the trigonid of m2. The anterodorsal edge of the fossa continues as the coronoid crest and the ventral crest or masseteric line reaches posteriorly almost to the tip of the angle. On the medial surface of the ramus, the fossa for the attachment of the medial pterygoid muscle (Fig. 11B; Rinker 1954; Klingener 1964; Woods 1972) is shallow but distinct. This triangular depression is bordered by the rounded prominence over the incisor end anterodorsally and the crests on the dorsal and ventral edges of the angular process described above. As mentioned above, the rounded prominence over the incisor end extends nearly to the condylar process. Anterodorsal to the posteriormost point of the incisor is the small mandibular foramen (Figs. 11B, 12B). It lies closer to the level of the occlusal surface than the condyle, below the anterior part of the mandibular notch. Anterodorsal to the mandibular foramen, the attachment of the temporalis muscle to the medial surface of the coronoid process (Rinker 1954; Klingener 1964; Woods 1972) is not marked. Posterodorsal to the mandibular foramen, however, is a shallow, ovoid pterygoid fovea for the attachment of the lateral pterygoid muscle (Rinker 1954; Klingener 1964; Woods 1972).

Dentition

The upper incisors are best preserved in V7429, although well worn (Fig. 5A); they are broken off at or above the alveolus in V7430 (Fig. 5B). The upper incisor is narrow transversely and flattened anteriorly and medially. Enamel covers its anterior side,and overlaps a short way medially and less than halfway up the lateral side. Enamel is more restricted anteriorly on the lateral side in *Cocomys* (Li et al. 1989: fig. 5c). As in *Cocomys*, the enamel surface in *Exmus* is smooth. The pulp cavity is long and narrow. The incisor is nearly vertical in its orientation at the front of the skull, and its alveolus appears to be confined to the premaxilla. Based on the CT scans of V7430, the open incisor end extends posteriorly to the level of the back of the incisive foramen, with the enamel covered portion of the tooth extending farther posteriorly than the dentine covered portion.

P3 is well preserved on the right side of V7429 and broken at the alveolus on the left side (Figs. 5A, 13). In V7430, the crown of the right P3 is broken, and on the left side both the tooth and its alveolus are missing (Fig. 5B). P3 is a small, single-rooted peg (Fig. 13); its connate surface has a central, posteroventrally facing wear facet; the only other pattern is a very small posterior cingular shelf. A pit about the size of P3 occurs on both specimens in the bone anteromedial to P3. Perhaps this is the remnant of an alveolus of dP3.

DP4 is preserved bilaterally in V7429 and on the right side of V7430 (Figs. 5, 13). It has a long buccal wall and is tapered lingually (Fig. 13). The relatively straight buccal wall is formed of a large anteriorly projecting parastyle (broken on the right side of V7429), subequal rounded paracone and metacone, and a small mesostyle between them. There is a loph between the paracone and protocone and in V7429 a tiny protoconule, but in V7430 the protoconule is not visible because of wear. The metaconule, preserved in both specimens between the metacone and the protocone, is significantly larger than the protoconule. The metaconule is not joined to the protocone by a loph. The protocone and hypocone are considerably worn and in this

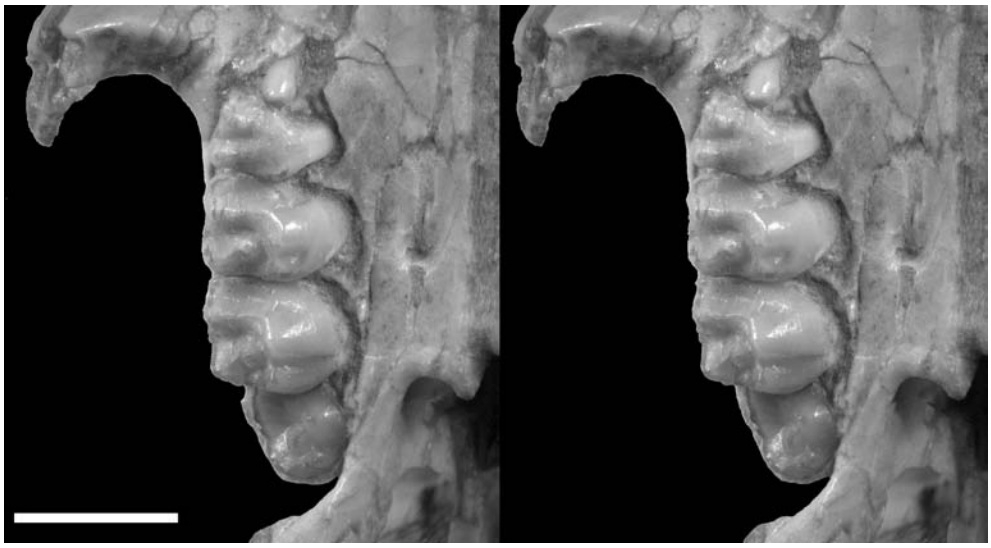

Fig. 13.—*Exmus mini* IVPP V7429, right maxillary dentition, stereophotograph. Scale = 2 mm.

state of wear are subequal. The hypocone projects farther linguad than the protocone. From the parastyle a well-developed anterior cingulum crosses nearly the entire anterior surface. The posterior cingulum is a ridge extending buccally from the hypocone nearly the entire width. P4 is covered by the deciduous tooth in both V7429 and V7430, but CT scanning revealed remarkable details of the structure of that tooth in the latter specimen (Fig. 14). The unworn crown of P4 is slightly longer lingually than buccally, so there is a slight unilateral hypsodonty. There is a single buccal cusp, the paracone, with a slight swelling (metacone) on its posterior side. The paracone is connected to the protocone, centrally situated on the lingual side, by two transverse crests that lack conules. Anterior and posterior cingula are well developed, extending nearly the width of the tooth. The posterior cingulum ends lingually in a small hypocone.

The bunodont, roughly quadrate upper molars, preserved bilaterally in both specimens (Fig. 5), also are slightly unilaterally hypsodont. M1 has a prominent parastyle connected to an anterior cingulum that crosses about three-quarters of the anterior side (Fig. 13). The rounded paracone connects by a narrow protoloph to the large protocone, which fills more than half the lingual side. The mesostyle is small and obliquely oriented. The metacone, subequal to the paracone, connects to the large metaconule by a very narrow loph; at the early stage of wear shown by V7429 and V7430 there is no loph from metaconule to protocone. The hypocone is smaller than the protocone and continues buccally into a posterior cingulum, extending the entire width. The posterior cingulum is narrower than the anterior. The lingual groove between the protocone and hypocone is short and shallow. M2 is larger than M1 and more quadrate in shape with a straighter buccal wall (Fig. 13). Cusps and lophs are similar to those of M1, except that the anterior cingulum extends farther linguad and the parastyle is reduced. M3 is not fully erupted in either specimen, but it is more so in V7430, and it is subequal to M1. M3 is rounded posteriorly and resembles M1 and M2 in its trigon, except for the metacone and hypocone (Fig. 13). The former is reduced to a slightly swollen crest forming the posterobuccal wall of the tooth, and the hypocone is a very small cuspule at the lingual end of the posterior cingulum. The parastyle and anterior cingulum are as in M2. M3 retains a large, rounded metaconule. The lingual groove between the protocone and hypocone is very small.

The right side of V7429 has the most complete lower incisor; the others are broken near their alveoli (Figs. 11, 12). The lower incisor is narrow transversely and has a slightly flattened anterior surface. Enamel covers the anterior side, extends about halfway up the lateral side, and has a short overlap onto the medial surface (see below for analysis of incisor enamel). The enamel surface is smooth. The pulp cavity as seen in cross section is long and narrow.

The deciduous premolars are both in place in V7429 (Fig. 11, 15A), but p4 is exposed on the left side in V7430 (Figs. 12, 15B). The least worn dp4 occurs on the right side of V7429 (Fig. 15A). It has an elongate trigonid compared with p4 that is narrower than the talonid. The trigonid has an isolated anterior cuspid, presumably the paraconid, centrally located at the anterior side. The metaconid is the highest cusp. The protoconid and metaconid are connected by a narrow transverse lophid, and an ectolophid joins protoconid and hypoconid. The hypoconid continues to the posterior wall, and the entoconid connects separately to the posterior wall where there is a small hypoconulid swelling.

The left p4 in V7430 (Fig. 15B) is erupting, unworn, and is shorter anteroposteriorly than dp4. The cusps, of

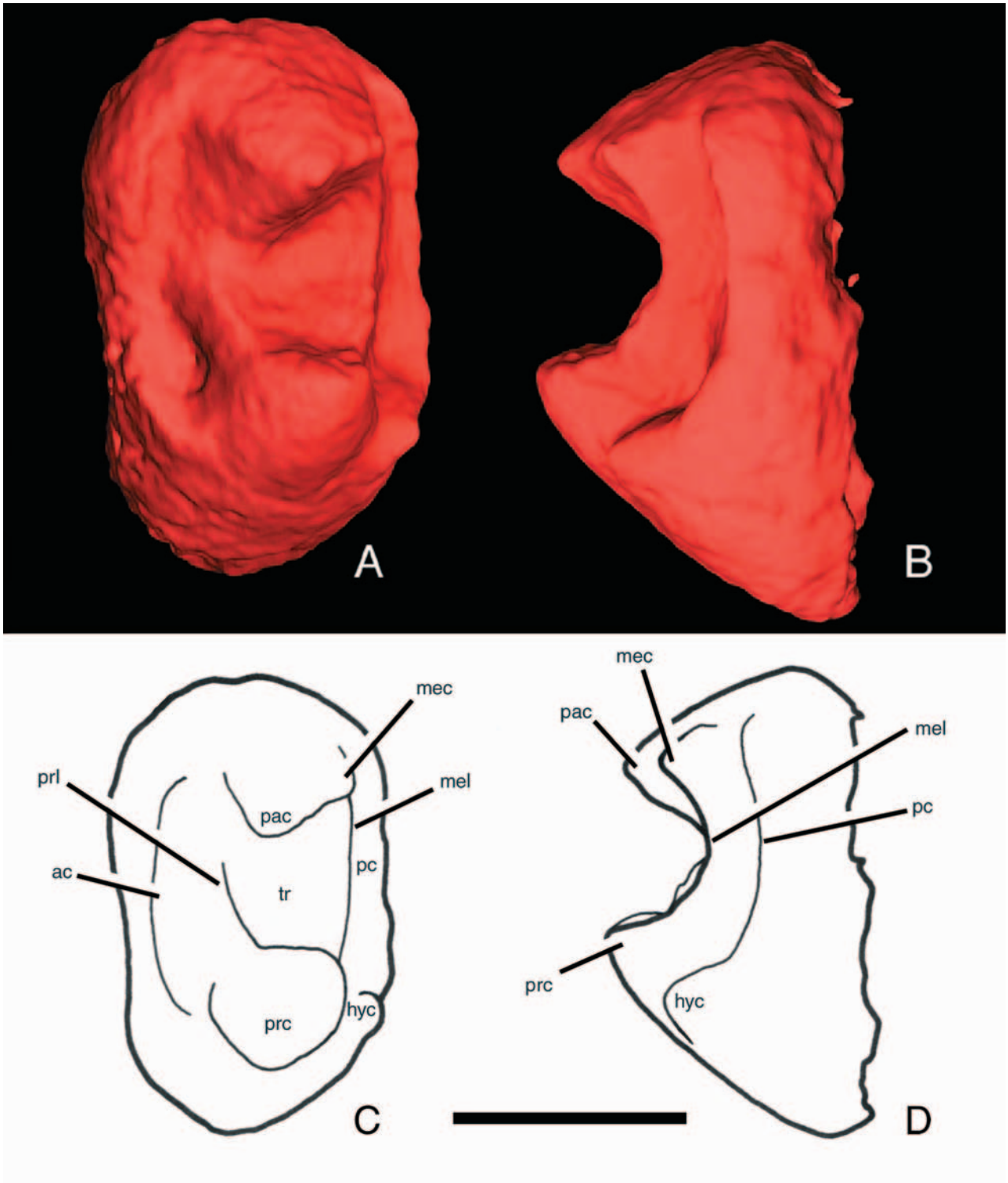

Fig. 14.—*Exmus mini* IVPP V7430, occlusal (**A**) and posterior (**B**) view of right P4 from high-resolution CT scans with accompanying line drawings in (**C**) and (**D**). Scale = 1 mm. Abbreviations: **ac**, anterior cingulum; **hyc**, hypocone; **mec**, metacone; **mel**, metaloph; **pac**, paracone; **pc**, posterior cingulum; **prc**, protocone; **prl**, protoloph; **tr**, trigon.

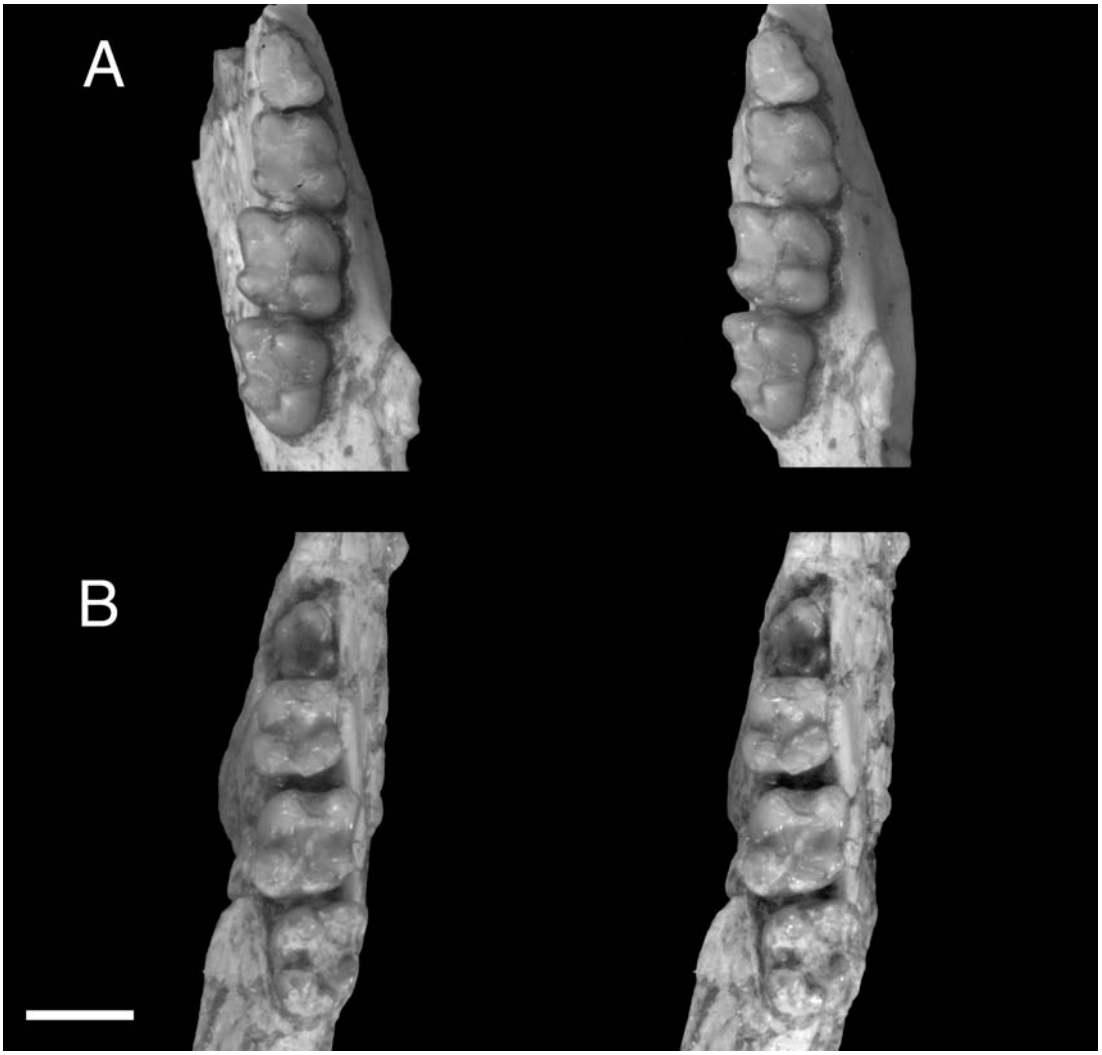

Fig. 15.—*Exmus mini* IVPP V7430, occlusal views of right (A) and left (B) mandibular dentitions, stereophotograph. Scale = 2 mm.

which the metaconid is highest, are bunodont. On the trigonid, the metaconid is in a line slightly anterior to the protoconid; the two cusps are separated by an oblique valley. The isolated anterior cuspid present on the dp4 is absent from the p4. The talonid is only slightly wider transversely than the trigonid and is formed of a low hypoconid and larger entoconid and hypoconulid. These three talonid cusps are joined along the posterior edge of the tooth.

The lower molars are bunodont and subrectangular, increasing in size posteriorly (Fig. 15). The metaconid is the highest cusp on m1 and m2, with the protoconid highest on m3. The m1 and m2 are similar in morphology except that the posterior arm of the protoconid (=metalophid II) is slightly longer on m1, although still not complete. Both molars lack a hypolophid and have a well-developed hypoconulid and a weak ectolophid between the protoconid and hypoconid. A small, rounded mesoconid is present on the ectolophid. Anterior and posterior cingula are very poorly developed. The m3 is similar to m1 and m2 in the trigonid but has a narrower talonid, more posteriorly protruding hypoconulid, and a slight trace of a mesoconid on the weak ectolophid.

Measurements of the cheek teeth of both specimens are included in Table 2.

The microstructure of the incisor enamel was studied by Professor Wighart von Koenigswald, who provided the following report, dated November 25, 2003. "The incisor enamel [of V7430] was investigated as KOE 3686 from a longitudinal and a transverse section [for explanation of the technical terms employed below see Koenigswald and Sander, 1997, and refer to Fig. 16]. Both sections show the two-layered schmelzmuster with an inner layer formed by Hunter Schreger bands (HSB) and an

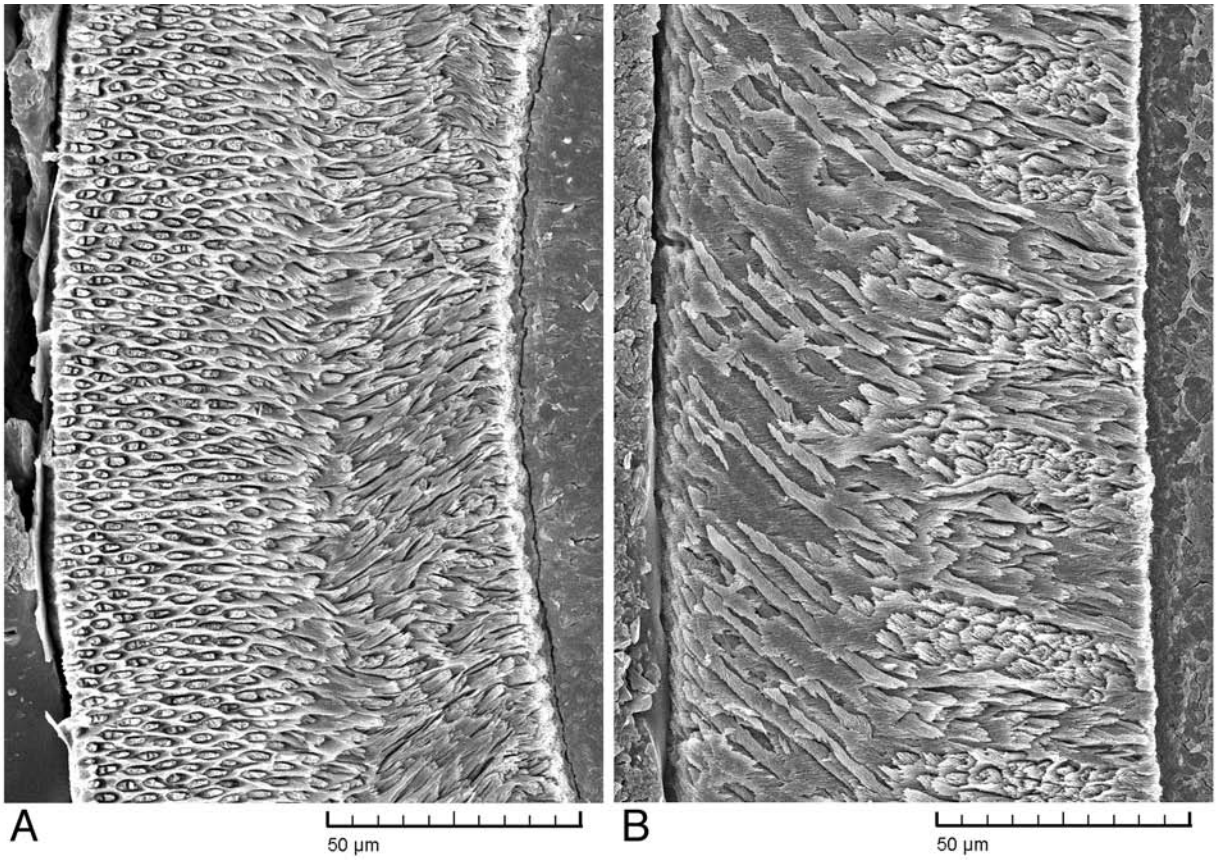

Fig. 16.—*Exmus mini* IVPP V7430, scanning electron micrographs of lower incisor enamel. The enamel-dentine junction is to the left. Longitudinal (**A**) and transverse (**B**) sections.

outer layer with radial enamel. Both layers are of almost equal thickness. This is typical schmelzmuster for rodent incisors.

"The thickness of the HSB forms a character to distinguish the various classical rodents groups (Korvenkontio 1934; Wahlert 1968; Martin 1992; Kalthoff 2000). In addition several other characters were used for better discrimination (Martin 1993, 1997).

"In the portio interna the prisms of adjacent HSB decussate with about 60° as seen in transverse sections. The interprismatic matrix (IPM) is parallel to the prisms. Each band is about 3–4 prisms thick. As seen in the longitudinal section, the bands are slightly inclined, about 20°. Only single prisms change from one band to the next. No transition zone is present.

"In the portio externa the prisms of the radial enamel are mostly rounded, sometimes a bit irregular, or slightly flattened. They rise toward the outer surface at about 45°. The IPM surrounds the prisms and is fairly thick. Its crystallites are almost perpendicular to the outer enamel surface (OES) and thus in a distinct angle to the prisms. The prisms reach the OES. A distinct external layer lacking prisms (PLEX) is not developed.

"According to Martin (1993, 1997), all these characters but one fall into the range of pauciserial enamel. The inclination of the prisms in the radial enamel is steeper than normally expected with 45° instead of 20–30°. But in a typical multiserial enamel the inclination would be expected to reach 80°. Nevertheless, the incisor enamel of *Exmus* has to be classified as pauciserial.

"Already Korvenkontio (1934) derived multiserial enamel from pauciserial enamel, therefore transitional stages should be present in the fossil record. If it is postulated because of other morphological reasons that *Exmus* may have given rise to rodents with multiserial enamel, the slight inclination of the HSB, the few transitional prisms between bands, and the stronger inclination of the prisms in the portio externa might be regarded as slight hints that in *Exmus* an early transitional stage toward multiserial enamel is preserved."

COMPARISONS

In the following, we first compare the two specimens of *Exmus* to each other and then to other well-known Eocene

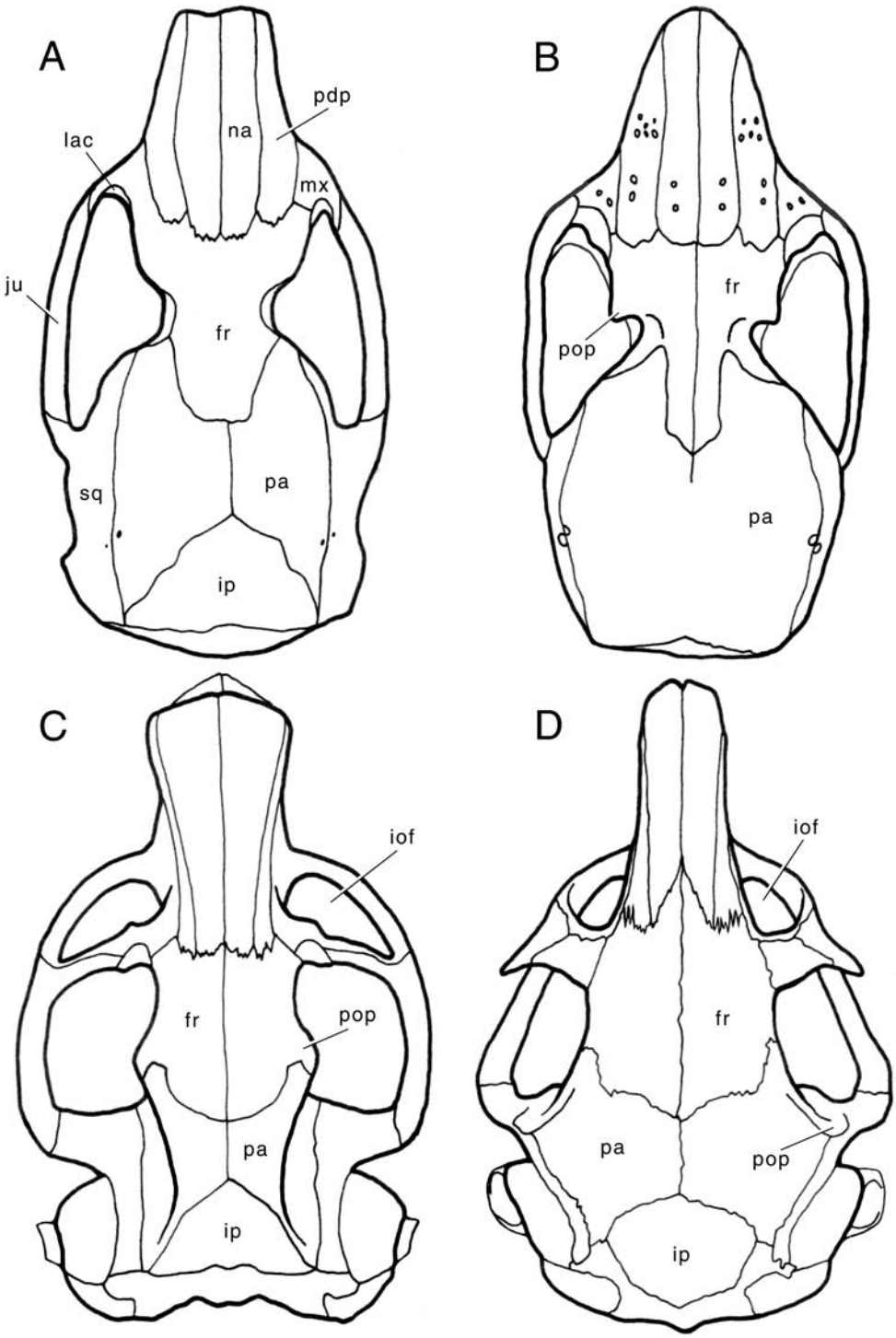

Fig. 17.—Ctenodactyloid skulls in dorsal view. (**A**) *Cocomys lingchaensis* (redrawn from Li et al. 1989: fig. 1); (**B**) *Exmus mini*; (**C**) *Tataromys* sp. (based on Wang 1997: fig 1; MAE S6-94-6438 and S6-97-5307; IVPP 91-12788a&b); (**D**) *Ctenodactylus gundi* (redrawn from Schrenk 1989: fig. 23). Abbreviations: **fr**, frontal; **iof**, infraorbital foramen; **ip**, interparietal; **ju**, jugal; **lac**, lacrimal; **mx**, maxilla; **na**, nasal; **pa**, parietal; **pdp**, posterodorsal process of premaxilla; **pop**, postorbital process; **sq**, squamosal.

rodents, including the slightly older ctenodactyloid *Cocomys*. In light of the many features that *Exmus* shares with *Cocomys* (see also Phylogenetic Analysis below), we considered *Exmus* also to be a basal ctenodactyloid. Given that, we include comparisons with an extinct and an extant ctenodactylid, *Tataromys* and *Ctenodactylus*, respectively. Also included are line drawings of the skulls of *Exmus*, *Cocomys*, *Tataromys*, and *Ctenodactylus* is dorsal, lateral, and ventral views and of their mandibles in lateral view (Figs. 17–20).

Within *Exmus mini*

V7429 and V7430 are remarkably similar and, therefore, we interpret them to be the same taxon. Nevertheless, we did uncover some differences between the two, which we list here. In V7429, the lingual roots of M2-3 are exposed in the orbital floor, and in V7430, it is the lingual roots of M1-3. The back of the *U*-shaped frontoparietal suture is straight in V7429 (Fig. 1A), but *V*-shaped in V7430 (Fig. 1B). The alisphenoid canal is not present in V7429, but appears to be present anterior to the foramen ovale in V7430. The supraoccipital appears to have a narrow contact with the squamosal in V7430 (Fig. 4), but not in V7429 (Fig. 3). V7429 has a mastoid foramen between the mastoid exposure and supraoccipital (Fig. 10), and V7430 does not. V7430 has a small foramen at the base of the external occipital crest in the supraoccipital, but V7429 does not (Fig. 10). Finally, the coronoid crest is more developed in V7429 (Fig. 11A) than in V7430 (Fig. 12A)

With *Cocomys* and Some North American Eocene Rodents

Of other Eocene rodents known by nearly complete crania, *Exmus* most closely resembles *Cocomys* from the early Eocene of Hunan. Below, we compare *Exmus* and *Cocomys* with three North American rodents chosen because they are known from fairly complete, well-described crania: *Paramys* (Wood 1962; Wahlert 1974, 1985, 2000), *Reithroparamys* (Wood 1962; Wahlert 1974; Meng 1990), and *Sciuravus* (Dawson 1961; Wahlert 1974, 2000). *Paramys copei* is from the late early Eocene Wind River Formation, and *P. delicatus*, *Reithroparamys delicatissimus*, and *Sciuravus nitidus* are from the middle Eocene Bridger Formation. For these comparisons, we had the opportunity to study *R. delicatissimus* AMNH 12561 and *S. nitidus* USNM 18100 and 22477. Unless noted below, information is taken from Li et al. (1989) for *Cocomys*, from Wood (1962) for *Paramys* and *Reithroparamys*, and from Dawson (1961) for *Sciuravus.*

Characters distinguishing *Exmus* and *Cocomys* from *Paramys*, *Reithroparamys*, and *Sciuravus* are the following: overall skull form and proportions; short, robust rostrum that tapers anteriorly; large orbit (greater than 20% skull length); sagittal crest absent (Fig. 17A, B); incisive foramina more posteriorly positioned; horizontal process of palatine extends more anteriorly, to P4 (Fig. 19A, B); orbital process of palatine extends more anteriorly, to M1 (Fig. 18A, B); sphenopalatine foramen merged with dorsal palatine foramen and not within maxilla (Fig. 18A, B); frontoparietal suture with broad *U*-shaped process of frontals between parietals (Fig. 17A, B); large optic canal, confluent between orbits (Fig. 18A, B); deep pterygoid fossa (Fig. 19A, B); sphenopalatine vacuity present (Fig. 19A, B); stout ectopterygoid crest contacts auditory bulla and floors foramen ovale accessorius (Figs. 18, A, B, 19A, B); piriform fenestra restricted, does not occupy nearly entire anterior face of petrosal epitympanic wing (Fig. 19A, B); caudal tympanic process of petrosal forms the back of the skull base, no petrosal shelf posterior to caudal tympanic process (Figs. 7A, B, 19A, B); condyloid canal present (Figs. 7A, B, 8); cheek teeth with some unilateral hypsodonty and increasing in size posteriorly; P4 not molariform; upper molar mure (or endoloph, which connects the protocone and hypocone) absent; lower molar ectolophid weak or absent; and lower molar hypoconulid distinct with that on m3 enlarged. *Exmus* and *Cocomys* also share the following features that only occur in *Reithroparamys* AMNH 12561 among the North American taxa: narrow contact between alisphenoid and parietal (Fig. 18A, B); alisphenoid tympanic process (on ectopterygoid crest) behind foramen ovale; anterior tip of tegmen tympani extends level with paroccipital process; epitympanic recess extends anterior to level of promontorium (Fig. 19A, B); and post-promontorial tympanic sinus extends posteriorly level with stapedius fossa.

Despite the remarkable craniodental similarities between *Exmus* and *Cocomys*, there are a number of striking differences. For example, compared to *Cocomys*, *Exmus* has: a shallower braincase; a larger incisive foramen and diastemata (Fig. 19A, B); a larger, more superiorly positioned infraorbital foramen (Fig. 2); a posterodorsal process of premaxilla extending more posteriorly than the nasal (Fig. 17A, B); a more vertical zygomatic root; a postglenoid foramen positioned anterior to the foramen for ramus temporalis rather than level with it (Fig. 18A, B); a more inflated auditory bulla tightly attached to the skull base; a more prominent paracondylar process of the exoccipital (Fig. 19A, B); pauciserial incisor enamel that may be a transitional stage toward multiserial enamel; upper incisor enamel covering more of the lateral side of the tooth; a metacone, albeit small, on P4; a hypocone on P4; no conules on P4; absence of protoconule on the upper molars; and a tricuspate talonid on p4. *Exmus* is also distinguished from *Cocomys* by the following features that also occur in some North American forms: interpremaxillary foramen absent in *Exmus*, present in *Cocomys* IVPP V7399 and *Paramys*; accessory palatine foramen absent in *Exmus* (Fig. 19B) and *Reithroparamys* (Wahlert 1974),

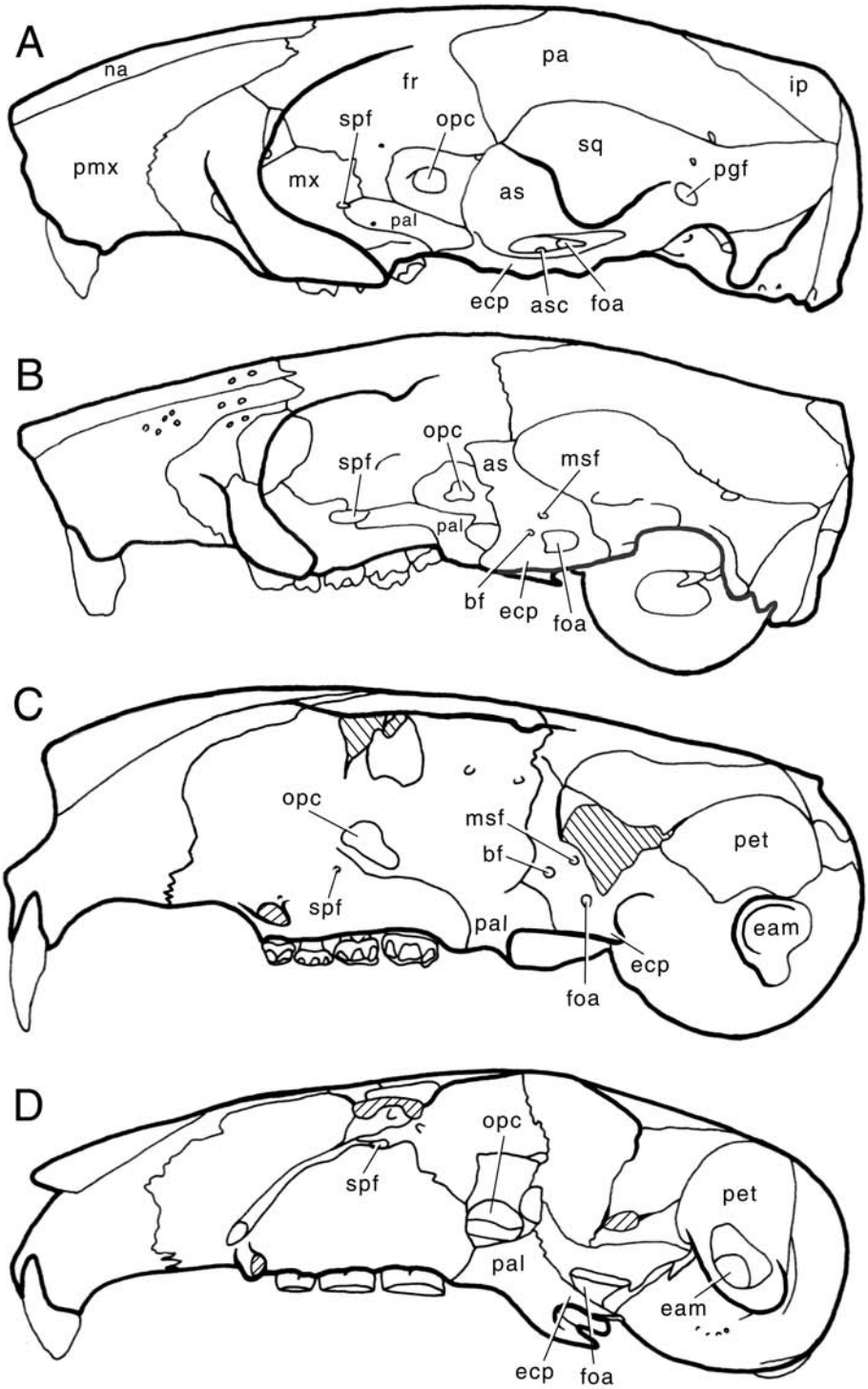

Fig. 18.—Ctenodactyloid skulls in lateral view with zygoma removed; parallel lines represent cut edges. (**A**) *Cocomys lingchaensis* (reversed and redrawn from Li et al. 1989: fig. 2, with minor adjustments to parietal-alisphenoid contact based on IVPP V7399); (**B**) *Exmus mini*; (**C**) *Tataromys* sp. (based on Wang 1997: fig. 6; MAE S6-94-6438 and S6-97-5307; IVPP 91-12788a&b); (**D**) *Ctenodactylus gundi* (modified from Schrenk 1989: fig. 24 based on CM 45490 and 74249). Abbreviations: **as**, alisphenoid; **asc**, alisphenoid canal; **bf**, buccinator foramen; **eam**, external acoustic meatus; **ecp**, ectopterygoid crest; **foa**, foramen ovale accessorius; **fr**, frontal; **ip**, interparietal; **msf**, masticatory foramen; **mx**, maxilla; **na**, nasal; **opc**, optic canal; **pa**, parietal; **pal**, palatine; **pet**, petrosal; **pgf**, postglenoid foramen; **pmx**, premaxilla; **spf**, sphenopalatine foramen.

present in *Cocomys* (Fig. 19A) and *Paramys*; interparietal absent in *Exmus* (Fig. 17B), *Paramys*, and *Reithroparamys* AMNH 12561, present in *Cocomys* (Fig. 17A) and *Sciuravus* USNM 22477; tympanic process of the basisphenoid present in *Exmus* (Fig. 8) and *Reithroparamys* AMNH 12561, absent in *Cocomys* IVPP V7399 (Fig. 7A, B), *Paramys*, and *Sciuravus* USNM 22477; groove for ramus inferior on alisphenoid behind foramen ovale absent in *Exmus* (Fig. 5A), *Reithroparamys* AMNH 12561, and *Sciuravus* USNM 22477, present in *Cocomys* IVPP V7399 (Fig. 7A, B) and perhaps in *Paramys* (see Wahlert, 2000: fig. 2); carotid foramen between basisphenoid and petrosal absent in *Exmus* and *Reithroparamys* AMNH 12561, present in *Cocomys* IVPP V7399 (Fig. 7A, B), *Paramys* and *Sciuravus* (Wahlert 1974); auditory bulla tightly attached in *Exmus* (Fig. 8) and *Reithroparamys* AMNH 12561, loosely attached in *Cocomys*, *Paramys*, and *Sciuravus*; auditory bulla with ectopterygoid process in *Exmus* (Fig. 8) and perhaps *Reithroparamys* AMNH 12561, absent in *Cocomys*, *Paramys*, and *Sciuravus* USNM 22477; prominent tympanic process of the basioccipital present in *Exmus* (Fig. 8) and *Reithroparamys* AMNH 12561, absent in *Cocomys* IVPP V7399 (Fig. 7A, B), *Paramys*, and *Sciuravus* USNM 22477; and mandibular symphysis extends below anterior root of p4 in *Exmus* (Fig. 11B), *Sciuravus* USNM 18100, and *Reithroparamys* AMNH 12561, behind level of m1 in *Cocomys* and *Paramys*.

The following features are unique to *Exmus* among the other Eocene taxa: multiple nutritive foramina in nasal, posterodorsal process of premaxilla, and facial process of maxilla (*Paramys copei* has them in the premaxilla, Wood 1962: fig. 13B, C) (Figs. 1, 17B); larger facial process of lacrimal (Figs. 1, 17B); substantial orbital roof formed by lacrimal and frontal (Fig. 5); sphenopalatine foramen with frontal contribution (Figs. 3, 18B) rather than just maxilla and palatine (*Cocomys* based on Meng et al. 2003; Fig. 18A); prominent postorbital process (Figs. 1A, 17B); frontal diploic vein foramen present; a suture between the parietals that is nearly completely fused (Figs. 1, 17B); large sphenopalatine vacuity (small in *Cocomys* IVPP V7399 and absent elsewhere where known Fig. 17A, B); perbullar carotid canal (Fig. 8; transpromontorial carotid groove in *Cocomys* IVPP V7399 [Fig. 7A, B], *Paramys* and *Sciuravus*, Wahlert 1974; carotid lacking in *Reithroparamys*, Meng et al. 2003); foramen for stapedial artery separated from secondary facial foramen; and foramen for tympanic nerve and/or auricular branch of vagus in medial section of caudal tympanic process of petrosal (Fig. 8).

The following features are unique to *Cocomys* among the other Eocene taxa: postpalatine torus absent in *Cocomys* IVPP V7399 (Fig. 19A), present in *Exmus* (Fig. 5A), *Paramys*, *Reithroparamys* AMNH 12561, and *Sciuravus* USNM 22477; maxilla separates lacrimal and jugal in the anterior orbital rim in *Cocomys* (Fig. 17A), but not in *Exmus* (Fig. 17B), *Paramys*, *Reithroparamys* AMNH 12561, and *Sciuravus* USNM 22477; anterior zygomatic root over P3/P4 in *Cocomys* (Fig. 19A), over P3 in *Exmus* (Fig. 19B), *Paramys*, *Reithroparamys* AMNH 12561, and *Sciuravus* USNM 22477; no subdivision of sphenorbital fissure in *Cocomys* IVPP V7399, bar on alisphenoid partially subdivides sphenorbital fissure in *Exmus* and *Paramys*; masticatory and buccinator foramina absent in *Cocomys* (Fig. 18A), present in *Exmus* (Figs. 3A, 18B), *Paramys* and *Sciuravus* (Wahlert 1974); anterior opening of orbitotemporal canal with frontal contribution in *Cocomys* (Fig. 18A), between alisphenoid and orbitosphenoid in *Exmus* (Figs. 3B, 18B), *Paramys* and *Sciuravus* (Wahlert 1974); groove for internal carotid artery and carotid foramen are medially placed, above anteromedial shelf, in *Cocomys* IVPP V7399 (Fig. 7A, B), more laterally placed in *Paramys* (Wahlert 2000: fig. 3) and *Sciuravus* USNM 18100 and 22477, and absent in *Exmus* and *Reithroparamys* (Meng 1990); a deep notch separates the paroccipital process and caudal tympanic process of petrosal in *Cocomys* IVPP V7399 (Fig. 7A, B), but not in *Exmus* (Figs. 3B, 6), *Paramys* (Wahlert 2000: fig. 2), *Reithroparamys* AMNH 12561, and *Sciuravus* USNM 18100 and 22477; and masseteric fossa extends below m3 in *Cocomys* (Fig. 20A), below m2 in *Exmus* (Fig. 20B), *Paramys*, *Reithroparamys*, and *Sciuravus* (Meng et al. 2003).

Two reviewers of our original submission suggested that we make comparisons with the paramyid *Franimys amherstensis* from the early Eocene of Wyoming and New Mexico. Below we offer a few comparisons, but we choose not to include *Franimys* in our phylogenetic analysis (see below), because it is not as completely preserved as *Paramys* and *Reithroparamys* and because we did not have the opportunity to study the original specimens. Our observations on *Franimys* are based on Wood (1962) and Korth (1984). *Franimys* differs from *Paramys* and *Reithroparamys* and resembles *Exmus* and *Cocomys* in that it has a short, robust rostrum with incisive foramina at mid-rostrum, a restricted piriform fenestra, and an absent/weak lower molar ectolophid and hypolophid. However, the other features distinguishing *Exmus* and *Cocomys* from *Paramys* and *Reithroparamys* are either absent or unknown in *Franimys*, which has a small orbit, a sagittal crest, a *V*-shaped frontoparietal suture, and a petrosal shelf behind the ear region. Interestingly, *Franimys* shares several features with *Exmus* not found in *Cocomys*, including multiple nutritive foramina in the premaxilla (also in *Paramys copei*), a large facial process of the lacrimal, a postorbital process, and absence of upper molar protoconules. The meaning of these comparisons awaits restudy of the original material.

With Some European Eocene Rodents

Possible relationships between primitive ctenodactyloids

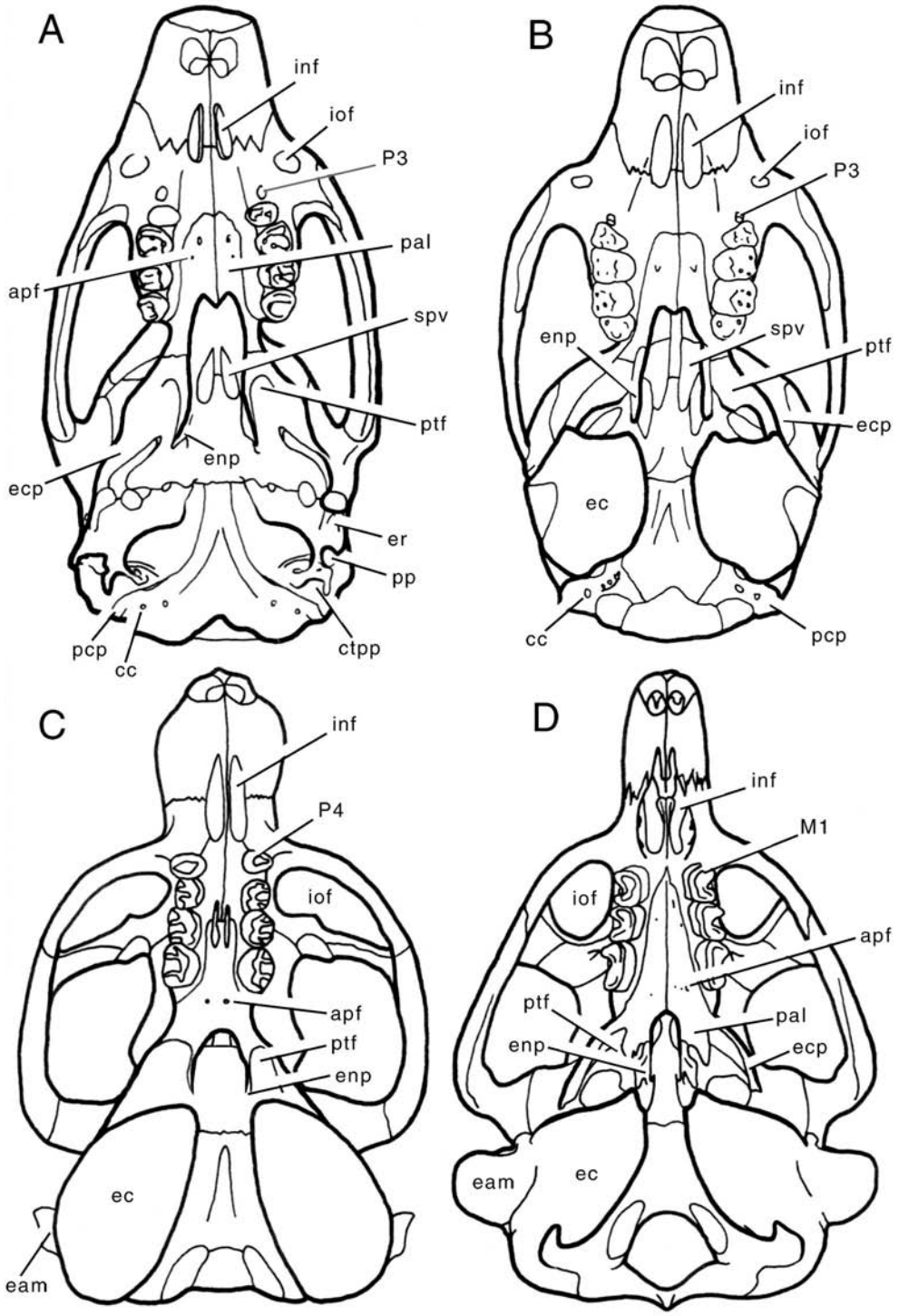

Fig. 19.—Ctenodactyloid skulls in ventral view. (**A**) *Cocomys lingchaensis* (modified from Li et al. 1989: fig. 3 based on IVPP V7399); (**B**) *Exmus mini*; (**C**) *Tataromys* sp. (based on Wang 1997: fig. 5; MAE S6-94-6438 and S6-97-5307; IVPP 91-12788a&b); (**D**) *Ctenodactylus gundi* (redrawn from Schrenk 1989: fig. 22). Abbreviations: **apf**, accessory palatine foramen; **cc**, condyloid canal; **ctpp**, caudal tympanic process of petrosal; **eam**, external acoustic meatus; **ec**, ectotympanic; **ecp**, ectopterygoid crest; **enp**, entopterygoid crest; **inf**, incisive foramen; **iof**, infraorbital foramen; **M1**, upper first molar; **P3**, upper third premolar; **P4**, upper fourth premolar; **pal**, palatine; **pcp**, paracondylar process; **ptf**, pterygoid fossa; **pp**, paroccipital process; **spv**, sphenopalatine vacuity.

and European theridomyids have been discussed (Vianey-Liaud 1985). In fact, Wahlert (2000: 13) recently wrote "knowledge of the ear region in early ctenodactyloids may help solve the problem of theridomyids origins." Therefore, we make comparisons between the ear regions of *Exmus*, *Cocomys*, and those attributed to the theridomyid (or theridomorph) *Adelomys* (or "*Adelomys*") (Lavocat 1967; Parent 1980, 1983; Lavocat and Parent 1985). For these comparisons, we rely entirely on illustrations and descriptions in the above articles.

Adelomys does not exhibit either of the two unique auditory features listed above that distinguish *Exmus* and *Cocomys* from *Paramys*, *Reithroparamys*, and *Sciuravus*. The piriform fenestra of *Adelomys* does not appear to be restricted and the caudal tympanic process of petrosal does not form the back of the skull (Lavocat 1967: pl. 1, fig. 3; pl. 2, fig. 2). Interestingly enough, Lavocat and Parent (1985: 336) stated "in *Sciuravus* and Theridomorpha, the auditory region is located at the very posterior part of the skull, and the stapedius muscle, according to the shape of its insertion, was extending out of the tympanic cavity onto the posterior region of the skull." We disagree with this statement for both *Sciuravus* and *Adelomys*. Posterior to the caudal tympanic process of petrosal, *Sciuravus* USNM 22477 (see also AMNH 12531 in Wahlert, 2000: fig. 4) and *Adelomys* (Lavocat 1967: pl. 1, fig. 3; pl. 2, fig. 2) have a horizontal petrosal shelf that represents the back of the skull, unlike the condition in *Exmus* and *Cocomys* where this shelf is absent. This shelf is even more pronounced in *Paramys* ("m" in Wahlert 2000: fig. 1) and *Reithroparamys* ("mp" in Meng 1990: fig. 1). Additionally, the stapedius muscle in all these Eocene rodents was bordered posteriorly by the lateral section of the caudal tympanic process of petrosal and included within the middle ear. There are instances among placentals (e.g., *Erinaceus*) where the stapedius muscle origin extends outside the middle ear, but these forms essentially lack the lateral section of the caudal tympanic process of petrosal (MacPhee 1981). One feature that may be shared by *Adelomys*, *Exmus*, and *Cocomys* is a condyloid canal. However, this opening appears in one of the figured *Adelomys* (Lavocat 1967: pl. 3, fig. 2), but not the other (Lavocat 1967: pl. 1, fig. 3).

Of the three auditory region features that *Exmus* and *Cocomys* share exclusively with *Reithroparamys*, *Adelomys* clearly lacks two. Its epitympanic recess does not extend anteriorly beyond the promontorium; and its post-promontorial tympanic sinus does not extend posteriorly level with the stapedius fossa and the caudal tympanic process of petrosal is immediately behind the fenestra cochleae (Lavocat 1967: pl. 1, fig. 3). Based on the available photographs of *Adelomys*, it is inconclusive if it has the third feature that *Exmus* and *Cocomys* share with *Reithroparamys*: the anterior tip of the tegmen tympani extending level with the paroccipital process.

Does *Adelomys* share auditory features with any North American taxa? Lavocat and Parent (1985: 338) claimed that "the most primitive rodent auditory region presently known by us is that of the Theridomorpha." Wahlert (2000) critically evaluated their claim with a careful character analysis and concluded, correctly in our opinion, that *Paramys* and *Sciuravus* present the structurally most primitive rodent ears, assuming the primitive condition to be little inflation of the middle ear. Wahlert noted two features to distinguish between *Paramys* and *Sciuravus*: the latter has a less developed anteromedial shelf and a common aperture for the secondary facial foramen and stapedial artery. We see even less distinction between the ear regions of these two taxa, because one of the *Sciuravus* studied by us, USNM 18100, has separate foramina for the facial nerve and stapedial artery, and the other one, USNM 22477, has a more developed anteromedial shelf reminiscent of that in *Paramys*. One difference between *Paramys* and *Sciuravus* noted by us is the smaller petrosal shelf behind the caudal tympanic process of petrosal in *Sciuravus*, a feature that is also repeated in *Adelomys*. The overall form of the ear region of *Adelomys* is more like that of *Paramys* and *Sciuravus* than it is like *Exmus* and *Cocomys*: for example, the course of the internal carotid artery anterior to the promontorium and the extent of the epitympanic recess and the post-promontorial tympanic sinus. However, *Adelomys* is distinguished from *Paramys* and *Sciuravus* in several features. First, it has a more extensive anteromedial shelf that reaches nearly to the level of the fenestra cochleae (Lavocat 1967: pl. 1, fig. 3); in *Paramys* (Wahlert 2000: fig. 2) and *Sciuravus* USNM 18100 and 22477, the shelf extends posteriorly only to the groove for the internal carotid, well anterior to the fenestra cochleae. Second, its crista parotica and the crest below the canal for the stapedial artery form a continuous wall medial to the epitympanic recess (Lavocat 1967: pl. 1, fig. 3); in *Paramys* (Wahlert 2000: fig. 2) and *Sciuravus* USNM 18100 and 22477, these crests are separated by a broad gap. *Reithroparamys* AMNH 12561 also has a wall medial to its epitympanic recess, but it abuts the promontorium and contains the facial nerve canal; in *Adelomys*, the groove for the facial nerve separates the wall from the promontorium. Another supposed unique feature of theridomyids was reported by Wahlert (2000: 13): "a partition anterior to the foramen [fenestra] vestibuli extends from the promontorium to the medial side of the lateral petrosal flange [tegmen tympani]; the partition marks the head of the fossa for the origin of the tensor tympani." We disagree with his claim because *Exmus*, *Cocomys*, and *Sciuravus* USNM 18100 and 22477 have the same partition, formed by the floor of the secondary facial foramen bridging the gap between the promontorium and tegmen tympani (Fig. 6).

In summary, comparisons of the ear regions of *Exmus*, *Cocomys*, and *Adelomys* do not support a special relationship between ctenodactyloids and theridomyids. In fact,

the ear region of *Adelomys* is more reminiscent of that of North American Eocene rodents, although distinguished from them by several unique features. We note that there are well-preserved skulls of Eocene theridomyids (see Hartenberger 1969, 1973) that are clearly deserving of restudy in light of the recent advances in our base knowledge of the skulls of Eocene rodents. Such restudy should help pinpoint the broader relationships of theridomyids.

With the Ctenodactylid *Tataromys*

The best known of the earliest ctenodactylids is *Tataromys* from the early Oligocene to early Miocene of Mongolia, North China, and Kazakhstan (Bohlin 1946; Wang 1997, 2001a). The cranial anatomy of *Tataromys* has been summarized recently by Wang (1997) based on two specimens, both of which are damaged in the auditory and jugal region. We have access to three specimens of *Tataromys* sp. not studied by Wang: MAE S6-94-6438, a damaged braincase preserving part of the left ear region; MAE S6-97-5307, a right half of a skull missing much of the rostrum; and IVPP 91-12788a&b, a partial skull and jaws missing the orbits, occiput, and right braincase. The first two are from the Tatal member of the Hsanda Gol Formation.

Some characters distinguishing *Exmus* and *Cocomys* from *Paramys*, *Reithroparamys*, and *Sciuravus* also occur in *Tataromys:* large orbit (greater than 20% skull length); sagittal crest absent (Fig. 17A–C); frontoparietal suture with broad *U*-shaped process of frontals between parietals (Fig. 17A–C); large optic canal, confluent between orbits (Fig. 18A–C); deep pterygoid fossa (Fig. 19A–C); sphenopalatine vacuity present; stout ectopterygoid crest contacts auditory bulla and floors foramen ovale accessorius (Fig. 19A–C); caudal tympanic process of petrosal forms the back of the skull base, no petrosal shelf posterior to caudal tympanic process; cheek teeth with some unilateral hypsodonty and increasing in size posteriorly; upper molar mure absent; and distinct hypoconulid on lower molars with that on m3 enlarged.

Tataromys shares the following characters with *Exmus* that do not occur in *Cocomys*: posterodorsal process of premaxilla extends farther posteriorly than nasals (Fig. 17B, C); larger facial process of lacrimal (Fig. 17B, C); substantial orbital roof formed by lacrimal and frontal; prominent postorbital process (Fig. 17B, C); separate masticatory and buccinator foramina (Fig. 18B, C); prominent tympanic process of the basioccipital; P4 without conules; and upper molars without protoconules.

Although *Tataromys* shares a number of features with *Exmus* and *Cocomys*, it is a much more specialized form with numerous differences, including: larger upper and lower diastema (Figs. 19C, 20C); orbit more posteriorly positioned (Fig. 18C); optic canal more anterior positioned (Fig. 18C); enlarged incisive foramen (Fig. 19C); an enormous infraorbital foramen (Fig. 17C); posterior margin of palate well posterior to m3 (Fig. 19C); tiny palatine orbital wing (Fig. 18C); internal carotid artery absent; inflated mastoid including an extensive lateral exposure dorsal to the external acoustic meatus (Fig. 18C); an osseous external acoustic meatus (Figs. 18C, 19C); single mental foramen (Fig. 20C); coronoid process at level of condylar process (Fig. 20C); incisors with multiserial enamel; P3 absent; cheek teeth with stronger lophs and main cusps lophed; lower molar hypoflexid deep; and lower molar hypolophid complete.

With *Ctenodactylus*

Living ctenodactylids, the gundis of northern Africa, include five species in four genera: *Ctenodactylus*, *Felovia*, *Massoutiera*, and *Pectinator* (George 1985a; Dieterlen 1993). A cluster analysis of 28 morphological characters by George (1985a) supported: the monophyly of the two species of *Ctenodactylus*; *Felovia* and *Massoutiera* as sister genera; and *Pectinator* as isolated from the others. We make comparisons with *C. gundi*, the best-known taxon from the standpoint of general cranial morphology, whose skull development has been treated in monographic form (Schrenk 1989).

Some characters shared by *Exmus*, *Cocomys*, and *Tataromys* also occur in *Ctenodactylus*: large orbit (greater than 20% skull length); sagittal crest absent (Fig. 17); large optic canal, confluent between orbits (Fig. 18); deep pterygoid fossa (Fig. 19); sphenopalatine vacuity present (Fig. 19); stout ectopterygoid crest flooring foramen ovale accessorius (Fig. 19); caudal tympanic process of petrosal forms the back of the skull base, no petrosal shelf posterior to caudal tympanic process; cheek teeth increasing in size posteriorly; upper molar mure absent; and large hypoconulid on m3. In addition, some characters shared by *Exmus* and *Tataromys* also occur in *Ctenodactylus*: posterodorsal process of premaxilla extends farther posteriorly than nasal (Fig. 17B-D); larger facial process of lacrimal (Fig. 17B-D); substantial orbital roof formed by lacrimal and frontal; and upper molars without protoconules. *Ctenodactylus* exhibits all the specializations of *Tataromys* listed above, except the more anterior position of the optic canal. Finally, *Ctenodactylus* is highly specialized with numerous differences from *Exmus*, *Cocomys*, and *Tataromys*, including: lacrimal foramen within lacrimal; sphenopalatine foramen positioned more dorsally (Fig. 18D); postorbital process on parietal (Fig. 17D); ectopterygoid crest composed largely of palatine (Fig. 18D); no alisphenoid-frontal contact (Fig. 18D); separate masticatory and buccinator foramina absent (as in *Cocomys*; Fig. 18D); postglenoid foramen between squamosal and petrosal; fenestra cochleae turned laterally; malleus and incus fused; mental foramen in diastema (Fig. 20A); coronoid process absent (Fig. 20D); mandibular foramen lower than tooth row; dorsal margin of masseteric

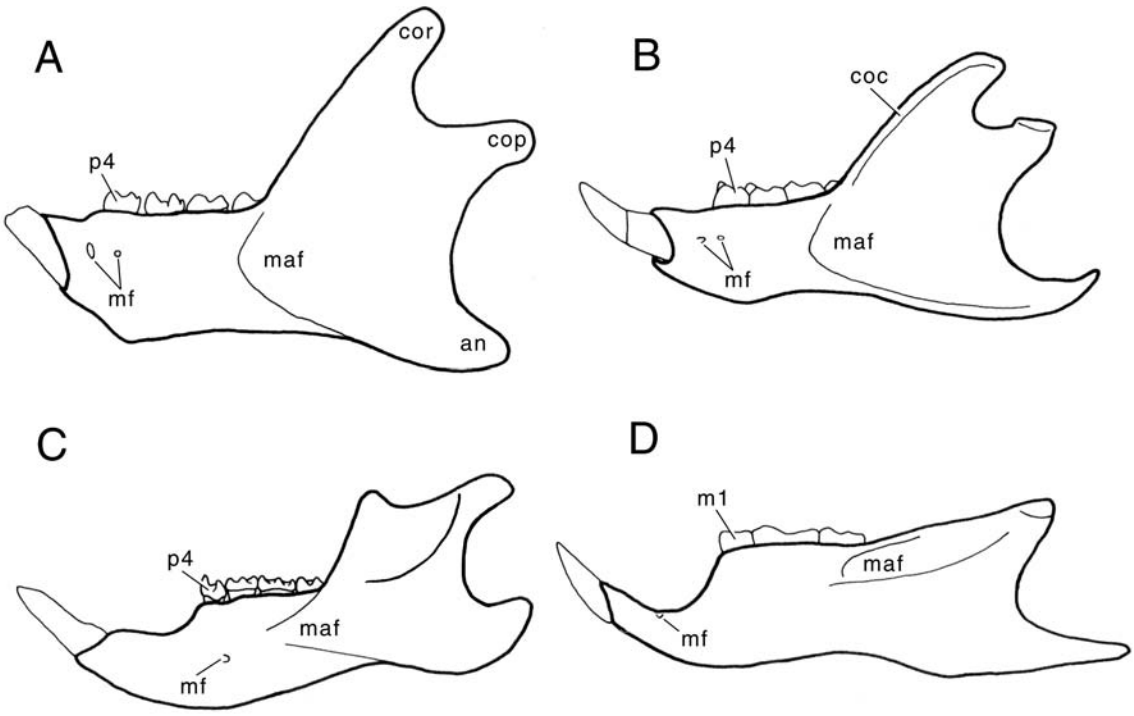

Fig. 20.—Ctenodactyloid mandibles in lateral view. (**A**) *Cocomys lingchaensis* (based on IVPP V7457 and V7458); (B) *Exmus mini*; (C) *Tataromys* sp. (based on Bohlin 1946: pl. III, fig. 3; Wang 1997: figs. 13, 14); (**D**) *Ctenodactylus gundi* (modified from Schrenk 1989: fig. 24 based on CM 45490 and 74249). Abbreviations: **an**, angle; **coc**, coronoid crest; **cop**, condylar process; **cor**, coronoid process; **maf**, masseteric fossa; **mf**, mental foramina; **p4**, lower fourth premolar; **m1**, lower first molar.

fossa horizontal (Fig. 20D); hypsodont cheek teeth; and P4/p4 absent.

PHYLOGENETIC ANALYSIS

Cocomys and some other ctenodactyloids have been included in several recent phylogenetic analyses (e.g., Averianov 1996; Dashzeveg and Meng 1998; Meng et al. 2003; Marivaux et al. 2004; Meng 2004). In order to test the relationships of *Exmus* to other ctenodactyloids and of ctenodactyloids to other Eocene rodents, we first scored *Exmus* for the large data matrix in Meng et al. (2003). Their original analysis was conducted primarily to test the relationships of *Rhombomylus*, which like *Exmus* is from the Yuhuangding Formation, to other basal gliroids. Meng et al. (2003) compiled a matrix of 83 dental, 90 craniomandibular, and 54 postcranial characters across 50 taxa (33 gliroid and 17 non-gliroid). Our Appendix 1 includes the scores for *Exmus* in the Meng et al. (2003) matrix; the reader is referred to Meng et al. (2003) for the full character list, data matrix, and analyses. Although we did not agree with all the characters and scores in Meng et al. (2003), we accepted them for the purposes of this preliminary test, with the exception of seven scores for *Cocomys* (noted in Appendix 1). We ran our amended version of the Meng et al. (2003) matrix with PAUP* 4.0b10 (Swofford 2002) following the parameters originally employed by those authors, with characters (1) all unordered, (2) all ordered, and (3) 19 characters of presence/absence of teeth and digits ordered as irreversible-up. In our first two analyses, the only change to the topologies of the consensus trees reported by Meng et al. (2003: figs. 74, 75) was the addition of *Exmus* at an unresolved multichotomy with *Cocomys* (Fig. 21). Regarding the third analysis, the only change was the addition of *Exmus* as the sister taxon of *Cocomys* (see Meng et al. 2003: fig, 76). Because the preferred tree of Meng et al. (2003: fig. 75) resulted from their second analysis (all characters ordered), we illustrate here the consensus tree resulting from our second amended analysis (Fig. 21). In that tree, *Cocomys* and *Exmus* fall at a trichotomy with the remaining rodents in the analysis, with the next clade off in Rodentia being *Paramys* and *Sciuravus* from the North American Eocene and the immediate outgroup being *Tribosphenomys* and *Sinomylus* from the Chinese Paleocene. *Cocomys* and *Exmus* are widely separated from the only other ctenodactyloid included in the Meng et al. (2003) matrix, *Tataromys,* which is the sister taxon to the hystricognaths.

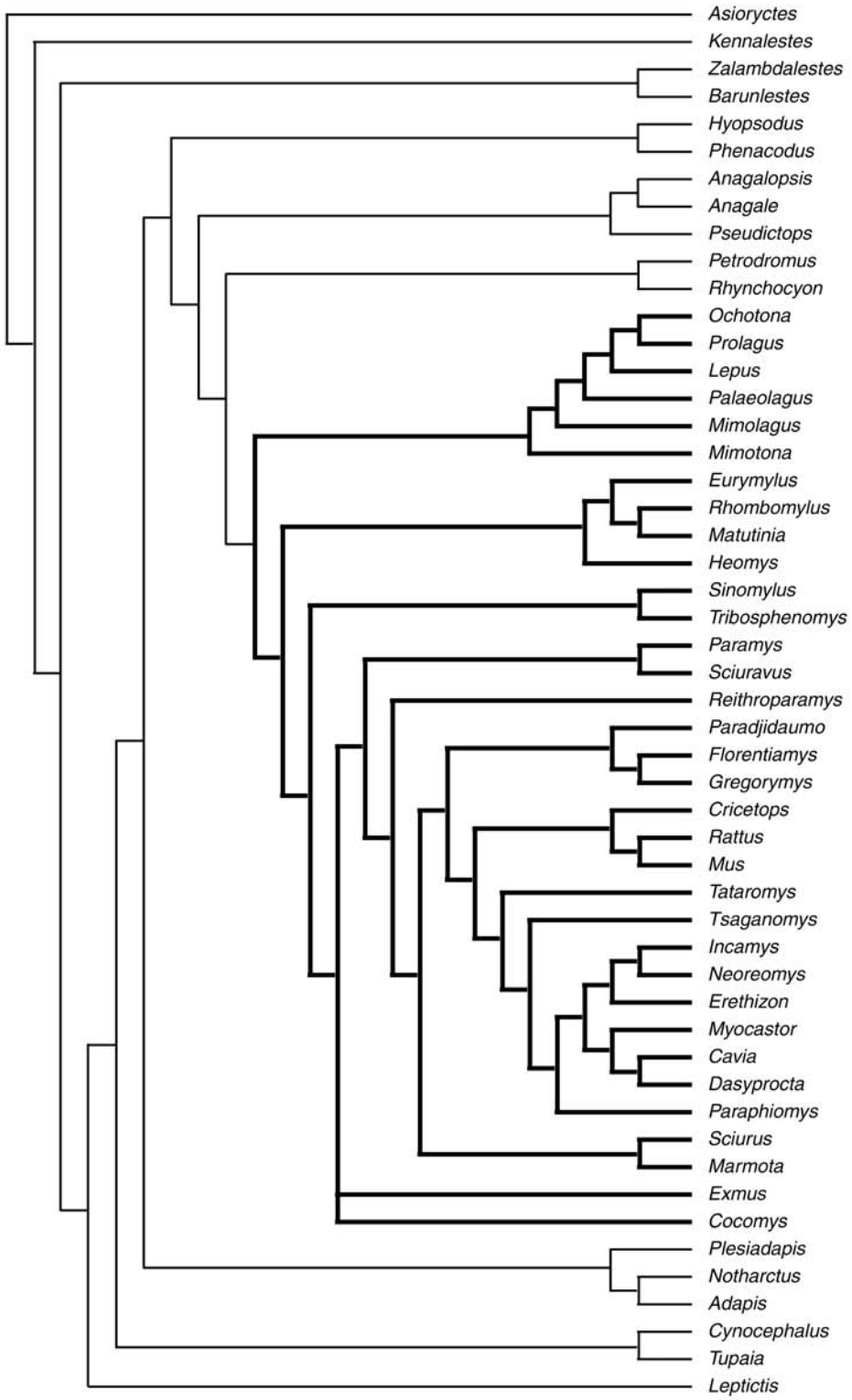

Fig. 21.—Strict consensus tree based on four most parsimonious trees derived from PAUP analysis of the modified Meng et al. (2003) matrix in Appendix 1, with all characters ordered. Darkened lines are Glires taxa. Individual trees are at 1038 steps, CI = 0.3642, RI = 0.7890/ Strict consensus is at 1040 steps, CI = 0.3635, RI = 0.7884.

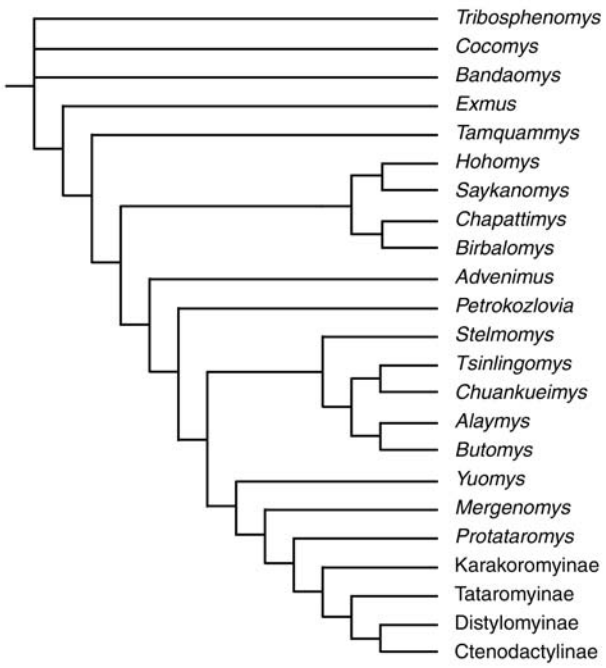

Fig. 22.—Strict consensus tree based on 43 most parsimonious trees derived from PAUP analysis of the modified Dashzeveg and Meng (1998) matrix in Appendix 2. Individual trees and strict consensus trees are at 75 steps, CI = 0.6267, RI = 0.7971.

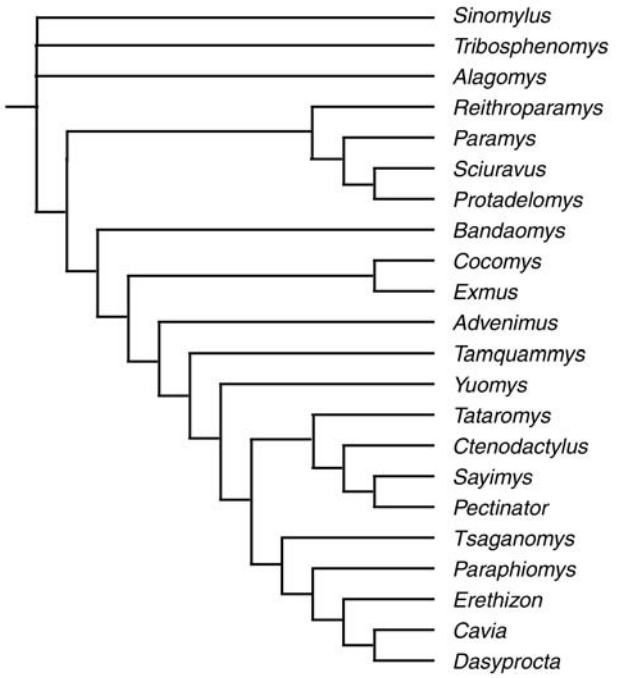

Fig. 23.—Strict consensus tree based on two most parsimonious trees derived from PAUP analysis of taxon-character matrix in Appendix 5 with selected multistate characters ordered. Individual trees are at 262 steps, CI = 0.4924, RI = 0.7134; strict consensus tree is at 264 steps, CI = 0.4886, RI = 0.7091.

We then scored *Exmus* for the matrix published in Dashzeveg and Meng (1998). The original analysis by these authors was intended to test relationships within ctenodactyloids using dental characters only, given that most of the fossil taxa are known primarily from their teeth. They compiled a matrix of 26 dental characters across 21 ctenodactyloid ingroups and the outgroup *Tribosphenomys*. The majority of the ingroups are fossil genera, but four are subfamilies, including Ctenodactylinae, which includes the four Recent genera. Our Appendix 2 includes the scores for *Exmus* in the Dashzeveg and Meng (1998) matrix; the reader is referred to the original publication for the full character list, data matrix, and analysis. Although we did not agree with all the characters and scores in the original, we accepted them for the purposes of this preliminary test. We ran our amended version of the Dashzeveg and Meng (1998) matrix with PAUP* 4.0b10 (Swofford 2002) following the parameters originally employed by those authors. In the strict consensus of two most parsimonious trees (Fig. 22), *Exmus* fell at the next node up from a basal multichotomy of *Tribosphenomys*, *Cocomys*, and *Bandaomys* from the early Eocene Wutu Formation. In the original consensus tree of Dashzeveg and Meng (1998: fig. 5), the first three taxa were identified as successive outgroups with *Tribosphenomys* at the base and *Bandaomys* the most derived. However, the most profound effect of the addition of *Exmus* concerns the position of *Tamquammys* from the middle Eocene of eastern and central Asia. In our analysis (Fig. 22), *Tamquammys* is at the next node up from *Exmus*, but in the original (Dashzeveg and Meng 1998: fig. 5) it is more derived, placed on the opposite side of *Hohomys*, *Saykanomys*, *Chapattimys*, and *Birbalomys*. In addition, the last four taxa form a monophyletic clade in our analysis, whereas in the original *Hohomys* and *Saykanomys* fall at a multichotomy at the next node out from the *Chapattimys-Birbalomys* clade. These dramatic changes are not surprising in light of the very weak support for these nodes in the original (Dashzeveg and Meng 1998: appendix 1b). Wang (2001a) reran the Dashzeveg and Meng (1998) matrix with the addition of two new taxa that fell just outside the Ctenodactylidae in her consensus tree. The addition of these two taxa by Wang (2001a) also pulled *Tamquammys* down to the next node up from *Cocomys*.

We were not entirely satisfied with either of these two tests. The first did not include enough ctenodactyloids and the second did not sample enough morphology and non-ctenodactyloid forms. In addition, we had objections to certain characters and scorings in both tests as originally completed. Therefore, we decided to conduct our own phylogenetic analysis. For our choice of taxa (see Appendix 3), we included the well-known North American Eocene rodents *Paramys, Reithroparamys,* and *Sciuravus,*

and European Eocene theridomyid *Protadelomys,* selected Eocene, Oligocene, Miocene, and Recent ctenodactyloids, and selected hystricognathiforms (sensu Bryant and McKenna 1995), resulting in 19 ingroup taxa. For the outgroups, we used Paleocene *Tribosphenomys* and *Sinomylus*, and late Paleocene to early Eocene *Alagomys*. For our character list, we used Meng et al. (2003) as our starting point, removing or modifying those characters or character states irrelevant to our more limited morphological and taxonomic coverage; in addition to rodents, Meng et al. (2003) sampled lagomorphs, elephant shrews, primates, tree shrews, dermopterans, and various Late Cretaceous and early Tertiary taxa. We also removed or modified those characters whose scores we could not duplicate. Our character list (see Appendix 4) includes 104 characters (41 dental and 63 cranial), of which 23 are multistate.

We ran one analysis with PAUP* 4.0b10 (Swofford 2002), with selected multistate characters ordered (13 of 23, see Appendix 4). Heuristic searches (1000 repetitions, stepwise-addition) resulted in two most parsimonious trees, the strict consensus of which is shown in figure 23. The two trees differed only in the placement of the outgroup *Tribosphenomys*: either with *Sinomylus* or *Alagomys*. The ingroups are divided into a clade of North American-European Eocene forms (paramyids, sciuravids, and theridomyids) and a clade composed of *Bandaomys* and "ctenodactyloids," including Ctenodactylidae (*Tataromys*, *Sayimys*, *Pectinator*, and *Ctenodactylus*), Hystricognathiformes (*Tsaganomys* + Hystricognathi [*Paraphiomys*, *Erethizon*, *Cavia*, and *Dasyprocta*]), and stem taxa (*Exmus* + *Cocomys*, *Advenimus*, *Tamquammys*, and *Yuomys*). Our clade of Ctenodactylidae + Hystricognathiformes is equivalent to the Ctenohystrica of Huchon et al. (2000). Diagnoses for the nodes in the consensus trees from the PAUP analysis are included in Appendix 6.

DISCUSSIONS

One of the fastest growing segments of the Eocene mammalian record during the past thirty years has been that of rodents in eastern and central Asia, and within this sphere the ctenodactyloid rodents have perhaps the most extraordinary record. In 1945, Simpson included no extinct taxa within Ctenodactyloidea, although reported in his classification were three extinct Oligocene and/or Miocene genera, *Tataromys*, *Karakoromys*, and *Sayimys*, shown convincingly by Bohlin (1946) to be ctenodactylids. Simpson (1945) questionably allied the last with the family Thryonomyidae and the others with the Theridomyidae. Currently, the Eocene record in central and eastern Asia of taxa identified as ctenodactyloids includes as many as 29 genera, some of which are probably not valid, or may not even be ctenodactyloids, and all of which are deserving of review. Moreover, the Eocene record of taxa identified as ctenodactyloids extends from Mongolia, Kazakhstan, and China to Thailand, India, and Turkey. There is considerable diversity of opinions on what taxa to include within Ctenodactyloidea and within how many families. Sorting out the confusion that has accumulated over the last few years is well beyond the scope of this report, but is a significant problem that needs to be addressed in a wholesale fashion.

For the purposes of this report, we adopt the general framework of Ctenodactyloidea of Dawson et al. (1984). These authors recognized *Cocomys* as a member of the ctenodactylid lineage, extending the ctenodactyloid record into the early Eocene. Dawson et al. (1984) named three families within the superfamily Ctenodactyloidea. Two are known only from the Eocene of eastern and central Asia, Cocomyidae (including early to middle Eocene *Cocomys*, *Tamquammys*, and *Tsinlingomys*) and Yuomyidae (including middle to late Eocene *Petrokozlovia*, *Yuomys*, *Advenimus*, and *Saykanomys*). The third, Ctenodactylidae, ranges from Oligocene to Recent, and from Asia to several Mediterranean islands and northern Africa. Another probable family of Ctenodactyloidea mentioned by Dawson et al. (1984) is Chapattamyidae from the early and middle Eocene of India and Pakistan, which most researchers since Flynn et al. (1986) have included in the superfamily.

In light of the numerous craniodental features shared by *Exmus mini* and *Cocomys lingchaensis*, and the results of our phylogenetic analysis, which identified these as sister taxa (Fig. 23), we assign *E. mini* to Cocomyidae. In addition to sharing general skull proportions, including a short, robust rostrum and large orbit, these two taxa share features from essentially every major region of the skull, including the rostrum, palate, skull roof, orbital mosaic, mesocranium, and ear region, along with details of the dentition. However, along with these similarities are significant differences that by and large support *E. mini* as a more derived member of Cocomyidae. Among the derived features of *E. mini* foreshadowing the condition in later ctenodactyloids are its more firmly attached bulla and inflated ear region, its larger sphenopalatine vacuity, and its pauciserial incisor enamel (as in *Cocomys*) that may be a transitional stage toward multiserial enamel (as in ctenodactylids). Our assignment of *E. mini* to Cocomyidae impacts two of the diagnostic characters of the family cited by Dawson et al. (1984): P4/p4 non-molariform, without metacone and hypocone, and upper molar protoconule present. The p4 of *E. mini* is molariform; its P4 is non-molariform, but has a small metacone; and its upper molars lack a protoconule.

The broader phylogenetic relationships of *Cocomys* and Cocomyidae remain controversial. Some authors (e.g., Dashzeveg and Meng 1998; Wang 2001a; Van Valen 2004) have embraced ctenodactyloid relationships for *Cocomys* as first postulated by Dawson et al. (1984) and as supported here. Along with the dental resemblances first noted by

Dawson et al. (1984), *Cocomys* and *Exmus* share with later extinct and extant ctenodactylids many cranial features from the skull roof, orbit, mesocranium, and ear region that do not occur in North American paramyids. Other authors have argued for a more basal position for *Cocomys*, either more primitive than (e.g., Marivaux et al. 2002, 2004) or at a multichotomy with the North American paramyids (e.g., Bryant and McKenna 1996; Meng et al. 2003). *Cocomys* is given a novel position in the classification of McKenna and Bell (1997). Without justification, these authors place *Cocomys* in the family Chapattimyidae in a new suborder, Sciuravida, "for the most recent common ancestor of †Ivanantoniidae, †Sciuravidae, †Chapattimyidae, †Cylindrodontidae, Ctenodactylidae, and all its descendants." Our results are clearly at variance with this association. The most recent common ancestor of these diverse rodents would also be the most recent common ancestor of all other rodentiaforms except *Tribosphenomys*, *Sinomylus*, and *Alagomys*. Sciuravidae, included in our analysis, and Cylindrodontidae (currently under study by M.R. Dawson) have a most recent common ancestor among the paramyid-complex. Ivanantonidae are so incompletely known and inconsistently described that they must remain incertae sedis until a more accurate description is provided. Chapattimyidae have been linked with the early ctenodactyloids, especially with the yuomyids, although this relationship has not been firmly established, but placing *Cocomys* within Chapattimyidae is not justified in any phylogenetic analysis. The concept of Sciuravida should be discarded as unsupported by the evidence at hand.

In our phylogenetic analysis (Fig. 23), *Bandaomys* from the early Eocene Wutu Formation falls at the base of the ctenodactyloid/hystricognath clade, just outside *Cocomys* + *Exmus*. *Bandaomys* was originally described as a possible yuomyid by Tong and Dawson (1995) and is more derived than *Cocomys* in the phylogenetic analysis by Dashzeveg and Meng (1998), as well as in the iterations of the Dashzeveg and Meng analysis by Guo et al. (2000) and Wang (2001a). However, in our iteration of the Dashzeveg and Meng analysis (Fig. 22), *Bandaomys*, *Cocomys*, and *Tribosphenomys* fell at a basal multichotomy. Given that *Bandaomys* does not exhibit the basic ctenodactyloid features of cheek teeth increasing in size posteriorly and well developed hypoconulid on the lower molars, especially on m3, we do not consider it to be a ctenodactyloid.

The broader relationships of the living gundis and ctenodactyloids have long been enigmatic. Simpson (1945:213) wrote, "this group vies with or exceeds the bathyergids in uncertainty. . . About all that can be said is that the ctenodactylids are not sciuromorphs, so must be either myomorphs, hystricomorphs, or members of a separate suborder." Wood (1977:133), who considered the earliest member of the Ctenodactylidae to be *Saykanomys* from the middle Eocene of Kazakhstan and Mongolia, argued that the features shared by ctenodactylids and hystricognaths, such as enlarged infraorbital foramen, fused malleus and incus, and multiserial incisor enamel, were convergently acquired, because *Saykanomys* "could not have been close to any hystricognathous form." Subsequently, support for relationships between ctenodactylids and hystricognaths has accumulated from various anatomical systems, such as the fetal membranes (Luckett 1985), reproductive biology (George 1985b), and more recently from DNA sequence analyses (Huchon et al. 2000, 2002; Adkins et al. 2001). In fact, based on the last, a new grouping, Ctenohystrica, has been named (Huchon et al. 2000). Support for this clade has also come from phylogenetic analyses involving fossils (Bryant and McKenna 1996; Marivaux et al. 2002, 2004; Meng et al. 2003) including our own (Fig. 23). However, we caution that none of the analyses including fossil taxa are true tests of the reality of Ctenohystrica, which require inclusion of many more relevant extinct and extant taxa, both within Hystricognathi (Hystricognathiformes) and Ctenodactyloidea. Consequently, although our analysis identified Hystricognathi nested within Ctenodactyloidea, we are not yet willing to refer to ctenodactyloids as paraphyletic or invent (or endorse) a new name for a possible ctenodactyloid/hystricognath clade.

A final topic is the fundamental division within Eocene rodents first proposed as a trichotomy (ischyromyoids, ctenodactylids, and others) by Hartenberger (1980) and modified to a dichotomy by Luckett and Hartenberger (1985). The latter hypothesize that the modern groups arose in Asian ctenodactyloids and North American-Eurasian ischyromyoids, although these authors are not certain how all the modern groups fit within this dichotomy. The DNA sequence analyses of three nuclear genes by Huchon et al. (2002) recognize three major infraordinal rodent clades: squirrel- and dormouse-related taxa (Scuiridae, Aplodontidae, and Gliridae); mouse-related taxa (Muridae, Dipodidae, Castoridae, Geomyidae, Heteromyidae, Anomaluridae, and Pedetidae); and gundi- and Guinea pig-related taxa (Ctenodactylidae and Hystricognathi). However, the relationships among these three clades are poorly resolved. "None of the three bifurcating topologies connecting them involves significantly different log-likelihood…and the results are sensitive to the method of reconstruction and the data set considered (Huchon et al. 2002:1059)." Interestingly, in none of their analyses does the Ctenohystrica clade fall as the outgroup to the other two, which would be the topology most consistent with the hypotheses of Hartenberger (1980) and Luckett and Hartenberger (1985). Our phylogenetic analysis (Fig. 23) is the first morphological one to be consistent with the hypothesis of a fundamental dichotomy within Eocene rodents into a North American-European and an Asian clade. However, we review this result as merely a teaser. The reality of this dichotomy first for the Eocene record and then for linkage with the modern groups will

require considerable additional testing with many more relevant taxa and characters.

ACKNOWLEDGMENTS

We are particularly appreciative of the help provided by Professor Alan Walker, Departments of Anthropology and Biology, and Dr. Tim Ryan, Center for Quantitative Imaging, Pennsylvania State University, who made available the high resolution CT scans of *Exmus*. We also thank Professor Wighart von Koenigswald, Rheinischen Friedrich-Wilhelms-Universität Bonn, Germany, for his report on and figures of the enamel microstructure of *Exmus*. For the loan of specimens, we acknowledge Dr. Jin Meng, American Museum of Natural History, and Dr. Robert Emry, United States National Museum, Smithsonian Institution. The specimens of *Exmus* were collected in 1993 by Dr. Yuan Wang and Wei Zhou, both of IVPP. The main preparation of the specimens was done by Shuhua Xie at IVPP. For various kinds of assistance with the specimens of *Exmus*, we are very grateful to Dr. James Rossie and Alan Tabrum. For pertinent discussions, we thank Drs. Zhe-Xi Luo, Thomas Martin, John Wahlert, and Jin Meng. For their thorough reviews, we thank Jin Meng, William Korth, and John Wahlert. The photographs were taken by the senior author, and most of the figures were completed by Gina Scanlon, with Mark Klingler assisting on figures 14 and 16. This research was supported by National Science Foundation Grant DEB-0129127 to JRW and by the Major Basic Research Project of the Ministry of Science and Technology of China (G2000077707) and the Chinese Academy of Sciences (KZCX-SW-127).

LITERATURE CITED

ADKINS, R.M., E.L. GELKE, D. ROWE, AND R.L. HONEYCUTT. 2001. Molecular phylogeny and divergence time estimates for major rodent groups: evidence from multiple genes. Molecular Biology and Evolution, 18:777–791.

AVERIANOV, A. 1996. Early Eocene Rodentia of Kyrgyzstan. Bulletin du Muséum national d'Histoire naturelle, Paris, 4e série, 18:629–662.

BOHLIN, B. 1946. The fossil mammals from the Tertiary deposits of Taben-buluk, western Kansu. Part II: Simplicidentata, Carnivora, Artiodactyla, Perissodactyla, and Primates. Palaeontologia Sinica New Series C, 8b:1–259.

BRYANT, J.D., AND M.C. MCKENNA. 1996. Cranial anatomy and phylogenetic position of *Tsaganomys altaicus* (Mammalia: Rodentia) from the Hsanda Gol Formation (Oligocene), Mongolia. American Museum Novitates, 3156:1–42.

BUGGE, J. 1971. The cephalic arterial system in mole-rats (Spalacidae), bamboo rats (Rhizomyidae), jumping mice and jerboas (Dipodoidea) and dormice (Gliroidea) with special reference to the systematic classification of rodents. Acta Anatomica, 79:165–180.

———. 1974. The cephalic arterial system in insectivores, primates, rodents and lagomorphs, with special reference to the systematic classification. Acta Anatomica, 87 (supplement 62):1–159.

———. 1985. Systematic value of the carotid arterial pattern in rodents. Pp. 355-379, *in* Evolutionary Relationships Among Rodents, A Multidisciplinary Approach (W.P. Luckett and J.-L. Hartenberger, eds.). Plenum Press, New York.

COCKERELL, T.D.A., L.I. MILLER, AND M. PRINTZ. 1914a. The auditory ossicles of American rodents. Bulletin of the American Museum of Natural History, 33:347–380.

———. 1914b. The auditory ossicles of some African rodents. Zoologische Anzeiger, 44:433–440.

COOPER, G., AND A.L. SCHILLER. 1975. Anatomy of the Guinea Pig. Harvard University Press, Cambridge.

DASHZEVEG, D. 1990a. The earliest rodents (Rodentia, Ctenodactyloidea) of Central Asia. Acta Zoologica Cracoviensia, 33(2):11–35.

———. 1990b. New trends in adaptive radiation of Early Tertiary rodent (Rodentia, Mammalia). Acta Zoologica Cracoviensia, 33(2):37–44.

DASHZEVEG, D., J.-L. HARTENBERGER, T. MARTIN, AND S. LEGENDRE. 1998. A peculiar minute Glires (Mammalia) from the early Eocene of Mongolia. Bulletin of Carnegie Museum of Natural History, 34:194–209.

DASHZEVEG, D., AND J. MENG. 1998. New Eocene ctenodactyloid rodents from the eastern Gobi Desert of Mongolia and a phylogenetic analysis of ctenodactyloids based on dental features. American Museum Novitates, 3246:1–20.

DAWSON, M.R. 1961. The skull of *Sciuravus nitidus*, a middle Eocene rodent. Postilla, 53:1–13.

DAWSON, M.R., AND K.C. BEARD. 1996. New late Paleocene rodents (Mammalia) from Big Multi Quarry, Washakie Basin, Wyoming. Palaeovertebrata, 25:301–321.

DAWSON, M.R., C. LI, AND T. QI. 1984. Eocene ctenodactyloid rodents (Mammalia) of eastern and central Asia. Pp. 138–150, *in* Papers in Vertebrate Paleontology Honoring Robert Warren Wilson (R.M. Mengel, ed.), Carnegie Museum of Natural History, Special Publication 9.

DE BEER, G.R. 1937. The Development of the Vertebrate Skull. Clarendon Press, Oxford.

DIERBACH, A.R. 1985. Zur Morphogenese des Craniums von *Cavia porcellus* L. Teil I. Einfuhrung, Systematik und beschreibender Teil. Gegenbaurs Morphologisches Jahrbuch, 131:441–476.

DIETERLEN, F. 1993. Family Ctenodactylidae. P. 761, *in* Mammal Species of the World (D.E. Wilson and D.M. Reeder, eds.). Smithsonian Institution Press, Washington, D.C.

DORAN, A.H.G. 1878. Morphology of mammalian ossicula auditûs. Transactions of the Linnean Society of London, Second Series, Zoology, 1:391–497.

EVANS, H.E. 1993. Miller's Anatomy of the Dog. W.B. Saunders, Philadelphia.

FLEISCHER, G. 1973. Studien am Skelett des Gehörorgans der Säugetiere, einschließlich des Menschen. Säugetierkunde Mitteilungen, 53:131–239.

FLYNN, L.J., L.L. JACOBS, AND I.U. CHEEMA. 1986. Baluchimyinae, a new ctenodactyloid rodent subfamily from the Miocene of Baluchistan. American Museum Novitates, 2841:1–58.

GAUPP, E. 1908. Zur Entwicklungsgeschichte und vergleichenden Morphologie des Schädels von *Echidna aculeata* var. *typica*. Semon's Zoologishe Forschungsreisen in Australien. Denkshriften der medicinisch-naturwissenschaftliche Gesellschaft zu Jena, 6:539–788.

GEORGE, W. 1985a. Cluster analysis and phylogenetics of five species of Ctenodactylidae (Rodentia). Mammalia, 49:53–63.

———. 1985b. Reproductive and chromosomal characters of ctenodactylids as a key to their evolutionary relationships. Pp. 453–474, *in* Evolutionary Relationships Among Rodents: A Multidisciplinary Approach (W.P. Luckett and J.-L. Hartenberger, eds.). Plenum Press, New York.

GREENE, E.C. 1935. Anatomy of the rat. Transactions of the American Philosophical Society, new series, 27:1–370.

GREGORY, W.K. 1910. The orders of mammals. Bulletin of the American Museum of Natural History, 27:1–524.

GUO, J.-W., Y. WANG, AND X.-A. YANG. 2000. A new early Eocene ctenodactyloid rodent (Rodentia, Mammalia) and the associated mammalian fossils from Danjiangkou, Hubei. Vertebrata PalAsiatica, 38(4):303–313. [in Chinese, English summary]

GUTHRIE, D.A. 1963. The carotid circulation in the Rodentia. Bulletin of the Museum of Comparative Zoology, 128:455–481.

———. 1969. The carotid circulation in Aplodontia. Journal of Mammalogy, 50:1–7.

HARTENBERGER, J.-L. 1969. Les Pseudosciuridae (Mammalia, Rodentia) de l'Éocène moyen de Bouxwiller, Egerkingen et Lissieu. Palaeovertebrata, Montpellier, 3:27–61.

———. 1973. Étude systématique des Theridomyoidea (Rodentia) de l'Éocène supérieur. Mémoires de la Société Géologique de France, 117:1–76.

———. 1980. Données et hypothèses sur la radiation initiale des rongeurs. Palaeovertebrata, Memoire Jubil. René Lavocat:285–301.

HENSON, O.W., JR. 1961. Some morphological and functional aspects of certain structures of the middle ear in bats and insectivores. The University of Kansas Science Bulletin, 42:151–255.

HERSHKOVITZ, P. 1962. Evolution of Neotropical cricetine rodents (Muridae) with special reference to the phyllotine group. Fieldiana, Zoology, 46:1–524.

HILL, J.E. 1935. The cranial foramina in rodents. Journal of Mammalogy, 16:121–129.

HOWELL, A.B. 1926. The Anatomy of the Wood Rat. Williams & Wilkins, Baltimore.

HU, Y. 1995. New late early Eocene ctenodactyloid rodents (Rodentia, Mammalia) from Danjiangkou, Hubei. Vertebrata PalAsiatica, 33(1):24–38 (in Chinese, English summary).

HUCHON, D., F.M. CATZEFLIS, AND E.J.P. DOUZERY. 2000. Variance of molecular datings, evolution of rodents, and the phylogenetic affinities between Ctenodactylidae and Hystricognathi. Proceedings of the Royal Society of London, B267:393–402.

HUCHON, D., O. MADSEN, M.J.J.B. SIBBALD, K. AMENT, M.J. STANHOPE, F. CATZEFLIS, W.W. DE JONG, AND E.J.P. DOUZERY. 2002. Rodent phylogeny and a timescale for the evolution of Glires: evidence from an extensive taxon sampling using three nuclear genes. Molecular Biology and Evolution, 19:1053–1065.

KALTHOFF, D. 2000. Die Schmelzmikrostruktur in den Incisiven der hamsterartigen Nagetiere und anderer Myomorpha (Rodentia, Mammalia). Palaeontographica, A259:1–193.

KLAAUW, C.J. VAN DER. 1931. The auditory bulla in some fossil mammals. Bulletin of the American Museum of Natural History, 62:1–352.

KLINGENER, D. 1964. The comparative myology of four dipodoid rodents (genera *Zapus*, *Napaeozapus*, *Sicista*, and *Jaculus*). Miscellaneous Publications Museum of Zoology, University of Michigan, 124:1–100.

KOENIGSWALD, W. VON, AND M.P. SANDER. 1997. Glossary of terms used for enamel microstructures. Pp. 267–280, *in* Tooth Enamel Microstructures (W. von Koenigswald and M.P. Sander, eds.). A.A. Balkema, Amsterdam.

KORTH, W.W. 1984. Earliest rodent evolution and radiation of rodents in North America. Bulletin of Carnegie Museum of Natural History, 24:1–71.

KORVENKONTIO, V.A. 1934. Mikroskopische Untersuchungen an Nagerincisiven unter Hinweis auf die Schmelzstruktur der Backenzähne. Annales Zoologici Societas Zoologicae-Botanicae Fennicae Vanamo, 2(1):1–274.

LAVOCAT, R. 1967. Observations sur la région auditive des Rongeurs Théridomorphes. Problèmes actuels de Paléontologie. Colloques Internationaux du Centre National de la Recherche Scientifique, 163:491–501.

———. 1973. Les rongeurs du Miocène d'Afrique Orientale. I. Miocène inférieur. Mémoires et Travaux de l'E. P. H. E. Institut de Montpellier, 1:1–284.

LAVOCAT, R., AND J.-P. PARENT. 1985. Phylogenetic analysis of middle ear features in fossil and living rodents. Pp. 333–354, *in* Evolutionary Relationships Among Rodents, A Multidisciplinary Approach (W.P. Luckett and J.-L. Hartenberger, eds.). Plenum Press, New York.

LI, C.-K. 1975. *Yuomys*, a new ischyromyoid rodent genus from the upper Eocene of North China. Vertebrata PalAsiatica, 13:58–70 (in Chinese, English summary).

LI, C., C. CHIU, D. YAN, AND S. HSIEH. 1979. Notes on some early Eocene mammalian fossils of Hengtong, Hunan. Vertebrata PalAsiatica, 17:71–82 (in Chinese, English summary).

LI, C., AND S. TING. 1983. The Paleogene mammals of China. Bulletin of Carnegie Museum of Natural History, 21:1–98.

LI, C.-K., J.-J. ZHENG, AND S.-Y. TING. 1989. The skull of *Cocomys lingchaensis*, an early Eocene ctenodactyloid rodent of Asia. Pp. 179–192, *in* Papers on Fossil Rodents in Honor of Albert Elmer Wood (C.C. Black and M.R. Dawson, eds.). Natural History Museum of Los Angeles County Science Series 33.

LOPATIN, A.V., AND A.O. AVERIANOV. 2004. A new species of *Tribosphenomys* (Mammalia: Rodentiaformes) from the Paleocene of Mongolia. Pp. 169–175, *in* Paleogene Mammals (S.G. Lucas and P.E. Kondrashov, eds.). New Mexico Museum of Natural History and Science Bulletin, 26.

LUCKETT, W.P. 1985. Superordinal and intraordinal affinities of rodents: developmental evidence from the dentition and placentation. Pp. 227–276, *in* Evolutionary Relationships Among Rodents: A Multidisciplinary Approach (W.P. Luckett and J.-L. Hartenberger, eds.). Plenum Press, New York.

LUCKETT, W.P., AND J.-L. HARTENBERGER. 1985. Evolutionary relationships among rodents: comments and conclusions. Pp. 685–712, *in* Evolutionary Relationships Among Rodents: A Multidisciplinary Approach (W.P. Luckett and J.-L. Hartenberger, eds.). Plenum Press, New York.

MACPHEE, R.D.E. 1981. Auditory region of primates and eutherian insectivores. Contributions to Primatology, 18:282 pp.

MARIVAUX, L., M. VIANEY-LIAUD, AND J.-J. JAEGER. 2004. High-level phylogeny of early Tertiary rodents: dental evidence. Zoological Journal of the Linnean Society, 142:105–134.

MARIVAUX, L., M. VIANEY-LIAUD, J.-L. WELCOMME, AND J.-J. JAEGER. 2002. The role of Asia in the origin and diversification of hystricognathous rodents. Zoologica Scripta, 31:225–239.

MARTIN, T. 1992. Schmelzmikrostruktur in den Inzisiven alt- und neuweltlicher hystricognather Nagetiere. Palaeovertebrata Mémoire Extraordinaire, 1992:1–168.

———. 1993. Early rodent incisor enamel evolution: phylogenetic implications. Journal of Mammalian Evolution, 1:227–254.

———. 1997. Incisor enamel microstructure and systematics in rodents. Pp. 163–175, *in* Tooth Enamel Microstructure (W. von Koenigswald and M.P. Sander, eds.). A.A. Balkema, Amsterdam.

———. 1999. Evolution of incisor enamel microstructure in Theridomyidae (Rodentia). Journal of Vertebrate Paleontology, 19:550–65.

MCKENNA, M.C., AND S.K. BELL. 1997. Classification of Mammals Above the Species Level. Columbia University Press, New York.

MCKENNA, M.C., AND J. MENG. 2001. A primitive relative of rodents from the Chinese Paleocene. Journal of Vertebrate Paleontology, 21:565–572.

MEINERTZ, T. 1941. Das oberflächliche Facialisgebiet der Nager. Zoologishce Jahrbucher, Abteilung für Anatomie und Ontogenie der Tiere, 67:119–270.

MENG, J. 1990. The auditory region of *Reithroparamys delicatissimus* (Mammalia, Rodentia) and its systematic implications. American Museum Novitates, 2972:1–35.

———. 2004. Phylogeny and divergence of basal Glires. Pp. 93–109, *in* Tributes to Malcolm C. McKenna: His Students, His Legacy (G.C. Gould and S.K. Bell, eds.). Bulletin of the American Museum of Natural History, 285.

MENG, J., Y. HU, AND C. LI. 2003. The osteology of *Rhombomylus* (Mammalia, Glires): implications for phylogeny and evolution of Glires. Bulletin of the American Museum of Natural History, 275:1–247.

MENG, J., AND A.R. WYSS. 1994. The enamel microstructures of *Tribosphenomys* (Mammalia, Glires): functional and phylogenetic implications. Journal of Mammalian Evolution, 2:185–203.

———. 2001. The morphology of *Tribosphenomys* (Rodentiaformes, Mammalia): phylogenetic implications for basal Glires. Journal of Mammalian Evolution, 8:1–71.

MENG, J., A.R. WYSS, M.R. DAWSON, AND R.-J. ZHAI. 1994. Primitive fos-

sil rodent from Inner Mongolia and its implications for mammalian phylogeny. Nature, 370:134–136.

MOSS-SALENTIJIN, L. 1978. Vestigial teeth in the rabbit, rat and mouse; their relationship to the problem of lacteal dentitions. Pp. 13–29, *in* Development, Function and Evolution of Teeth (P.M. Butler and K.A. Joysey, eds.). Academic Press, London.

MUSSER, G.G., M.D. CARLETON, E.M. BROTHERS, AND A.L. GARDNER. 1998. Systematic studies of oryzomyine rodents (Muridae, Sigmodontinae): diagnoses and distributions of species formerly assigned to *Oryzomys "capito"*. Bulletin of the American Museum of Natural History, 236:1–376.

Nomina Anatomica Veterinaria, 4th edition. 1994. Vienna: Adolf Holzhausen's Successors.

NOVACEK, M.J. 1977. Aspects of the problem of variation, origin and evolution of the eutherian auditory bulla. Mammal Review, 7:131–149.

PARENT, J.-P. 1980. Recherches sur l'oreille moyenne des Rongeurs actuels et fossiles. Anatomie, valeur systématique. Thèse Montpellier, École Pratique des Hautes Études. Mémoires et travaux de l'Institut de Montpellier, 11:1–285.

———. 1983. Anatomie et valeur systématique de l'oreille moyenne des rongeurs actuels et fossiles. Mammalia, 47:93–122.

RINKER, G.C. 1954. The comparative myology of the mammalian genera *Sigmodon*, *Oryzomys*, *Neotoma*, and *Peromyscus* (Cricetinae), with remarks on their intergeneric relationships. Miscellaneous Publications Museum of Zoology, University of Michigan, 83:1–124.

SCHRENK, F. 1989. Zur Schädelentwicklung von *Ctenodactylus gundi* (Rothmann 1776) (Mammalia: Rodentia). Courier Forschungsinstitut Senckenberg, 108:1–241.

SEGALL, W. 1970. Morphological parallelisms of the bulla and auditory ossicles in some insectivores and marsupials. Fieldiana, Zoology, 51:169–205.

SHEVYREVA, N.S. 1976. Paleogene rodents of Asia. Academy of Sciences U.S.S.R., Transactions of the Palaeontological Institute, 158:1–115. [in Russian, English summary]

SIMPSON, G.G. 1945. The principles of classification and a classification of mammals. Bulletin of the American Museum of Natural History, 85:1–350.

SISSON, S. 1910. A Text-book of Veterinary Anatomy. W.B. Saunders, Philadelphia.

STEHLIN, H.G., AND S. SCHAUB. 1951. Die Trigonodontie der simplicidentaten Nager. Schweizerische Paläontologische Abhandlungen, 67:1–385.

SWOFFORD, D.L. 2002. PAUP* Phylogenetic Analysis Using Parsimony (*and Other Methods), version 4.0b10. Sinauer Associates, Sunderland, MA.

TANDLER, J. 1899. Zur vergleichenden Anatomie der Kopfarterien bei den Mammalia. Denkschriften Akademie der Wissenschaft, Wien, mathematisch-naturwissenschaftliche Klasse, 67:677–784.

———. 1901. Zur vergleichenden Anatomie der Kopfarterien bei den Mammalia. Anatomische Hefte, 18:327–368.

THEWISSEN, J.G.M. 1989. Mammalian frontal diploic vein and the human foramen caecum. Anatomical Record, 223:242–244.

TONG, Y., AND M.R. DAWSON. 1995. Early Eocene rodents (Mammalia) from Shandong Province, People's Republic of China. Annals of Carnegie Museum, 64:51–63.

VAN VALEN, L. 2004. Adaptation and the origin of rodents. Pp. 110–119, *in* Tributes to Malcolm C. McKenna: His Students, His Legacy (G.C. Gould and S.K. Bell, eds.). Bulletin of the American Museum of Natural History, 285.

VIANEY-LIAUD, M. 1985. Possible evolutionary relationships among Eocene and lower Oligocene rodents of Asia, Europe and North America. Pp. 277–309, *in* Evolutionary Relationships Among Rodents, A Multidisciplinary Approach (W.P. Luckett and J.-L. Hartenberger, eds.). Plenum Press, New York.

WAHLERT, J.H. 1968. Variability of rodent incisor enamel as viewed in thin section, and the microstructure of the enamel in fossil and Recent rodent groups. Breviora, 309:1–18.

———. 1974. The cranial foramina of protrogomorphous rodents; an anatomical and phylogenetic study. Bulletin of the Museum of Comparative Zoology, 146:363–410.

———. 1983. Relationships of the Florentiamyidae (Rodentia, Geomyoidea) based on cranial and dental morphology. American Museum Novitates, 2769:1–23.

———. 1985. Cranial foramina of rodents. Pp. 311–332, *in* Evolutionary Relationships Among Rodents: A Multidisciplinary Approach (W.P. Luckett and J.-L. Hartenberger, eds.). Plenum Press, New York.

———. 2000. Morphology of the auditory region in *Paramys copei* and other Eocene rodents from North America. American Museum Novitates, 3307:1–16.

WAHLERT, J.H., AND S.L. SAWITZKE. 1988. Muscle insertions and basicranial morphology in rodents. Annals of the New York Academy of Sciences, 529:128–130.

WANG, B.-Y. 1997. The mid-Tertiary Ctenodactylidae (Rodentia, Mammalia) of eastern and central Asia. Bulletin of American Museum of Natural History, 234:1–88.

———. 2001a. Late Eocene ctenodactyloids (Rodentia, Mammalia) from Qujing, Yunnan, China. Vertebrata PalAsiatica, 39:24–42.

———. 2001b. On Tsanganomyidae (Rodentia, Mammalia) of Asia. American Museum Novitates, 3317:1–50.

WASSIF, K. 1948. Studies on the structure of the auditory ossicles and tympanic bone in Egyptian Insectivora, Chiroptera and Rodentia. Bulletin of the Faculty of Science, Fouad I University, Cairo, 27:177–213.

WIBLE, J.R. 1984. The ontogeny and phylogeny of the mammalian cranial arterial pattern. Ph.D. dissertation, Duke University, Durham, NC, 705 pp.

———. 1986. Transformations in the extracranial course of the internal carotid artery in mammalian phylogeny. Journal of Vertebrate Paleontology, 6:313–325.

———. 1987. The eutherian stapedial artery: character analysis and implications for superordinal relationships. Zoological Journal of the Linnean Society, 91:107–135.

———. 1990. Late Cretaceous marsupial petrosal bones from North America and a cladistic analysis of the petrosal in therian mammals. Journal of Vertebrate Paleontology, 10:183–205.

———. 2003. On the cranial osteology of the short-tailed opossum *Monodelphis brevicaudata* (Didelphidae, Marsupialia). Annals of Carnegie Museum, 72:137–202.

WIBLE, J.R., AND T.J. GAUDIN. 2004. On the cranial osteology of the yellow armadillo *Euphractus sexcinctus* (Dasypodidae, Xenarthra, Placentalia). Annals of Carnegie Museum, 73:117–196.

WIBLE, J.R., M.J. NOVACEK, AND G.W. ROUGIER. 2004. New data on the skull and dentition in the Mongolian Late Cretaceous eutherian mammal *Zalambdalestes*. Bulletin of the American Museum of Natural History, 281:1–144.

WIBLE, J.R., G.W. ROUGIER, M.J. NOVACEK, M.C. MCKENNA, AND D. DASHZEVEG. 1995. A mammalian petrosal from the Early Cretaceous of Mongolia: implications for the evolution of the ear and mammaliamorph interrelationships. American Museum Novitates, 3149:1–19.

WOOD, A.E. 1962. The early Tertiary rodents of the family Paramyidae. Transactions of the American Philosophical Society, new series, 52(1):1–261.

———. 1977. The evolution of the rodent family Ctenodactylidae. Journal of the Palaeontological Society of India, 20:120–137.

WOOD, A.E., AND R.W. WILSON. 1936. A suggested nomenclature of the cusps of the cheek teeth of rodents. Journal of Paleontology, 10:388–391.

WOODS, C.A. 1972. Comparative myology of jaw, hyoid, and pectoral appendicular regions of New and Old World hystricomorph rodents. Bulletin of the American Museum of Natural History, 147:115–198..

ADDENDUM

After the final submission of our manuscript, Bezuidenhout and Evans (2005) published a monograph on the anatomy of the woodchuck, with terminology based on the Nomina Anatomica Veterinaria (1992). We were unable to incorporate this useful reference into our paper.

BEZUIDENHOUT, A.J., AND H.E. EVANS. 2005. Anatomy of the Woodchuck (*Marmota monax*). Special Publication of the American Society of Mammalogists, 13:1–180.

TABLE 1. Cranial Measurements (mm)

	Exmus IVPP V7429	*Exmus* IVPP V7430	*Cocomys* IVPP V7399
ONL	35.0	34.3	34.4
ZB	?	18.4*	17.2*
IB	5.6	5.3	5.6
LR	8.8/9.2	9.6*/?	7.3/6.9
BR	9.3	?	8.5
LB	13.0	13.4	13.5
HBC	7.7	?	9.8
BZP	?/2.0	?/2.1*	?
LD	6.7/7.4	?/7.2	6.1/6.3
LBP	6.8*/6.8	7.3/7.1	7.3/7.3
BBP	9.3	8.3	8.4
PPL	15.0	?	16.4
LIF	4.0/3.7	4.1/4.1	3.2/3.3
BIF	3.2	2.3	2.8
ML	22.6/?	?	?
MD	5.5/5.4	?	?
CH	?	?/10.3	?
CPH	13.9/?	?	?
CLMX	7.0/6.8	7.5/?	6.7/?
CLMA	7.8/7.8	8.3/8.2	?

For an illustration of the cranial measurements, see Musser et al. (1998: fig. 2). Left/right side measurements provided for some measurements; *estimated. Abbreviations: **BBP**, breadth of bony palate across first upper molars; **BIF**, breadth of incisive foramina; **BR**, breadth of rostrum; **BZP**, breadth of zygomatic plate; **CH**, ascending ramus height at condyle; **CLMA**, crown length of mandibular tooth row; **CLMX**, crown length of maxillary tooth row (P4–M3); **CPH**, ascending ramus height at coronoid process; **HBC**, height of braincase; **IB**, interorbital breadth; **LB**, lambdoidal breadth; **LBP**, length of bony palate; **LD**, length of diastema; **LIF**, length of incisive foramena; **LR**, length of rostrum; **MB**, mastoid breadth; **MD**, mandibular body depth at last lower premolar; **ML**, mandible length; **ONL**, occipitonasal length; **PB**, palatal breadth at fifth maxillary tooth; **PL**, palatal length; **POL**, pre-orbital length; **PPL**, postpalatal length; **ZB**, greatest zygomatic breadth.

TABLE 2. Dental Measurements (mm)

		Exmus IVPP V7429	*Exmus* IVPP V7430
P3	AP	0.64	?
	T	0.51	?
DP4	AP	1.34	1.47
	T	1.4	1.47
P4	AP	?	1.24*
	T	?	1.75*
M1	AP	1.6	1.79
	T	1.6	1.66
M2	AP	1.73	1.86
	T	1.6	1.74
M3	AP	1.54	1.79
	T	1.34	1.54
dp4	AP	1.4	1.6
	TR	0.96	1.09
	TA	1.09	1.28
p4	AP	?	1.34
	TR	?	1.21
	TA	?	1.28
m1	AP	1.79	1.92
	TR	1.4	1.73
	TA	1.73	1.79
m2	AP	1.98	2.05
	TR	1.73	1.86
	TA	1.86	1.92
m3	AP	2.05	2.11
	TR	1.66	1.92
	TA	1.54	1.66

Abbreviations: **AP**, anteroposterior; **T**, transverse; **TA**, talonoid width; **TR**, trigonid width.
*measured from the CT scans

APPENDIX 1. Scores for *Exmus* and *Cocomys* in the Meng et al. (2003) matrix.

We scored *Exmus* for all 173 craniodental characters and none of the 54 postcranial characters employed by Meng et al. (2003), to which the reader is referred for the original character list, matrix, and analyses. We also changed the scores of *Cocomys* for eight characters. After our eight changes to *Cocomys*, *Exmus* differed from that taxon in only 13 characters. Listed below are the eight changes to *Cocomys* and the 13 characters in which *Exmus* and *Cocomys* differ.

Changes to *Cocomys*
Character 50: Cheek teeth—from "brachydont" (0) to "some unilateral hypsodonty" (1).
Character 81: Entoconid of lower molar—from polymorphic (0/1) to "posteriorly positioned" (0).
Character 88: Coronoid process—from (?) to "somewhat reduced" (1).
Character 94: Coronoid canal—from (?) to "absent" (0).
Character 100: Left and right optic foramina—from "separate" (0) to "confluent anteriorly along the skull midline" (1).
Character 112: Sphenopalatine vacuity—from (?) to "present" (1).
Character 138: Jugal—from (-) to "dorsally overlapping maxilla" (1).
Character 152: Alisphenoid-parietal contact—from "present/absent owing to a narrow squamosal-frontal contact" (0/1) to "present" (0).

Differences between *Cocomys* and *Exmus*
Character 39: Talonid of p4—*Cocomys* "simple" (0); *Exmus* "tricuspate" (1).
Character 42: Labial cusp(s) of P4—*Cocomys* "single" (0); *Exmus* "double, including a smaller metacone" (1).
Character 91: Anterior edge of masseteric fossa—*Cocomys* "extends below m3" (1); *Exmus* "extends below m2" (2).
Character 93: Mandibular condyle—*Cocomys* (?); *Exmus* "anteroposteriorly oriented" (2).
Character 106: Dorsal palatine foramen—*Cocomys* "in palatine" (0); *Exmus* "absent" (3).
Character 110: Alisphenoid canal—*Cocomys* "present" (1); *Exmus* "absent/present" (0/1).
Character 114: Mastoid foramen—*Cocomys* (?); *Exmus* "between mastoid and supraoccipital" (2).
Character 136: Lacrimal facial process—*Cocomys* "absent" (1); *Exmus* "present" (0).
Character 145: Postorbital process of frontal—*Cocomys* "absent" (0); *Exmus* "present" (1).
Character 146: Supraorbital crest—*Cocomys* "absent" (0); *Exmus* "present" (1).
Character 153: Hamulus-bulla contact—*Cocomys* (?); *Exmus* "present" (1).
Character 154: Interparietal—*Cocomys* "present" (1); *Exmus* "absent" (0).
Character 166: Course of distal internal carotid artery on promontorium—*Cocomys* "present" (1); *Exmus* "medial to tympanic cavity" (3)

APPENDIX 2. Scores for *Exmus* in the Dashzeveg and Meng (1998) matrix

We scored *Exmus* for all 26 dental characters employed by Dashzeveg and Meng (1998), to which the reader is referred for the original character list, matrix, and analysis. *Exmus* differed from *Cocomys* in only 4 characters, which are listed below.

Character 2: Posterior zygomatic root—*Cocomys* "below M1" (1); *Exmus* "P4" (2).
Character 5: P4/p4—*Cocomys* "non-molariform" (1); *Exmus* "molariform" (0). Note in the original matrix, Dashzeveg and Meng (1998: 13) reversed the scores for all entries regarding this character. Taxa said to have non-molariform teeth in their character description were incorrectly scored as molariform and vice versa.
Character 8: Molar paraconule (protoconule)—*Cocomys* "present" (0); *Exmus* "absent" (1).
Character 9: Metaloph on M1-M3—*Cocomys* "joining protocone" (0); *Exmus* "toward but not joining protocone" (1).

APPENDIX 3. Taxa selected for phylogenetic analysis reported here and sources of data.

Outgroups
Sinomylus (McKenna and Meng 2001)
Tribosphenomys (Meng et al. 1994; Meng and Wyss 1994, 2001; Lopatin and Averianov 2004)
Alagomys (Dashzeveg 1990b; Tong and Dawson 1995; Dawson and Beard 1996)

Ingroups
Paramys (Korvenkontio 1934; Wood 1962; Wahlert 1974, 2000)
Reithroparamys (Wood 1962; Meng 1990; Martin 1992; AMNH 12561)
Sciuravus (Korvenkontio 1934; Dawson 1961; Wahlert 1974; USNM 18100, 22477)
Protadelomys (Stehlin and Schaub 1951; Hartenberger 1969, 1973; Martin 1999)
Cocomys (Li et al. 1989; Martin 1992; IVPP V7399)
Exmus (this report)
Bandaomys (Tong and Dawson 1995)
**Tamquammys* (Shevyreva 1976; Dawson et al. 1984)
**Advenimus* (Shevyreva 1976; Dawson et al. 1984)
**Yuomys* (Li 1975)
Tataromys (Bohlin 1946; Wang 1997; Martin 1992; MAE S6-94-6438, S6-97-5307; IVPP 91-12788a&b)
Sayimys (Bohlin 1946; Martin 1992)
Ctenodactylus (Martin 1992; CM 45489, 45490, 79249)
Pectinator (CM 85591)
Tsaganomys (Martin 1992; Bryant and McKenna 1995; Wang 2001b)
Paraphiomys (Lavocat 1973; Parent 1980; Martin 1992)
Erethizon (Martin 1992; CM 77907, 92133)
Cavia (Martin 1992; CM 1927, 5293)
Dasyprocta (Martin 1992; CM 5259; Cockerell et al. 1914a)

*Scored for incisor enamel characters by other authors (e.g., Averianov 1996; Dashzeveg and Meng 1998), but we are unaware of primary literature describing the enamel for these rodents. Martin (1993) reported on cf. *Tamquammys*, but we await a report based on a more definitive attribution.

APPENDIX 4. Character list for phylogenetic analysis reported here.

The source for 68 of the 104 characters is Meng et al. (2003). For those 68, we include an "M" and a number in parentheses to represent the number of the character in Meng et al. (2003); an asterisk with these signifies some modification to the original character, such as the addition or subtraction of character states. A multistate character denoted as "ordered" was ordered in the phylogenetic analysis (see Appendix 5).

1. (M2*) Incisor enamel—single-layered with radial enamel (0) or double-layered with Hunter Schreger bands (1).
2. (M3*) Incisor enamel type—radial (0), pauciserial (1), or multiserial (2). [ordered]
3. (M50*) Cheek teeth—brachydont (0), some unilateral hypsodonty (1), or hypsodont (2).
4. (M51) Upper tooth rows—parallel (0), or convergent anteriorly (1).
5. Main cheek teeth cusps—conical (0), or lophed (1).
6. Cheek tooth size increases posteriorly—absent (0), or present (1).
7. Number of permanent upper premolars—3 or more (0), 2 (1), or 1 or none (2). [ordered]
8. (M35*) P3—oval in crown view and multicuspate (0), or small and conical (1).
9. (M42*) Labial cusp(s) of P4—single (0), double, including a smaller metacone (1), or paracone and metacone subequal in size (2).
10. (M44*) Anterior and posterior ridges of P4—weak or incomplete (0), distinct, but low (1), or as high as protoloph and metaloph (2). [ordered]
11. (M45) P4 hypocone—absent (0), small (1), or very large and anteroposteriorly extended (2). [ordered]
12. P4 protoconule—present (0), or absent (1).
13. P4 metaconule—present (0), or absent (1).
14. Upper molar shape—triangular (0), or rectangular (1).
15. (M46) Labial cingulum on upper molars—present (0), or absent (1).
16. (M56*) Upper molar protoloph—weak (0), or strong (1).
17. (M72*) Upper molar metaloph—extending to protocone (0), to hypocone (parallel to protoloph) (1), or posteriorly to join posteroloph (2).
18. Upper molar anteroloph—weak or absent (0), distinct, but low (1), or even with or higher than protoloph. [ordered]
19. (M57*) Upper molar posteroloph—weak or absent (0), distinct, but low (1), or even with or higher than metaloph. [ordered]
20. (M60*) Upper molar mesostyle—absent (0), or present (1).
21. (M64) Upper molar hypocone—weak or absent (0), or strong (1)
22. M1-2 protoconule—present (0), or absent (1).
23. M1-2 metaconule—present (0), or absent (1).
24. (M67*) Upper molar mesoloph—absent (0), or present (1).
25. (M68*) Upper molar hypoflexus—absent or shallow (0), or deep (1).
26. (M69*) Upper molar mure—absent (0), or present (1).
27. p4 hypolophid—absent (0), or present (1).
28. p4 paraconid—present (0), or absent (1).
29. p4 talonid—heel (0), or expanded (1).
30. p4 hypoconid—present (0), or absent (1).
31. p4 hypoconulid—present (0), or absent (1).
32. (M70*) Lower molar hypoflexid—shallow or absent (0), or deep (1).
33. (M77*) Lower molar paraconid—reduced (0), or absent (1).
34. (M78*) Lower molar metaconid—anterior or aligning with protoconid (0), or more posterior than protoconid (1).
35. (M79) Mesoconid of lower molar—absent (0), or present (1).
36. (M81) Entoconid of lower molar—posteriorly positioned (0), or anteriorly shifted (1).
37. Metalophid II of m2—absent (0), short (1), or closes trigonid posteriorly (2).
38. Ectolophid of m2 in little worn teeth—strong connection between protoconid and hypoconid (0), weak or absent posterior to protoconid (1), or shifted lingually (2).
39. Hypoconulid of m1–2—(0) indistinct, or (1) distinct.
40. Hypoconulid of m3—subequal to (0), or greater than that of m2 (1).
41. (M82*) Hypolophid of lower molar—absent (0), incomplete (1), or complete (2). [ordered]
42. (M87) Mental foramina—two or more (0), or one (1).
43. Mental foramen position—anterior foramen below p4 (0), or below diastema (1).
44. (M88*) Coronoid process—large (0), reduced, subequal to condylar process (1), or nearly absent (2). [ordered]
45. Mandibular condyle height—higher than occlusal surface (0), or even with (1).
46. (M90*) Angular process—origin in plane of body (0), or lateral to plane of body (1).
47. (M91*) Anterior edge of masseteric fossa—extends below m3 (0), below m2 (1), or below anterior half of m1 or p4 (2). [ordered]
48. Dorsal margin of masseteric fossa—inclined (0), or horizontal (1).
49. (M95*) Mandibular foramen—at level of tooth row or higher (0), or lower than tooth row (1).
50. (M96*) Incisive foramina—closer to incisors (0), at mid rostrum (1), or nearly as long as diastema (2). [ordered]
51. (M116*) Nasal—broadest posteriorly (0), nearly parallel (1), or broadest anteriorly (2).
52. Nasal—extends farther posteriorly than premaxilla (0), or even with or shorter than premaxilla (1).
53. (M98*) Infraorbital foramen—small (0), or large (hystricomorphous) (1).
54. Palatine on palate—anterior extent to M1 (0), anterior to M1 (1), or posterior to M1 (2).
55. Posterior margin of palate—at or in front of M3 (0), or posterior to M3 (1).
56. (M132*) Orbital wing of the palatine—small, posterior to molars (0), or prolonged anteriorly (1).
57. (M108*) Sphenopalatine foramen—within maxilla (0), between maxilla and palatine (1), or between maxilla and frontal (2).

APPENDIX 4 CONT.

58. Jugal—in anterior and ventral orbital margin (0), or in ventral only (1).
59. (M136*) Lacrimal facial process—small (0), or substantial (1).
60. (M102*) Nasolacrimal foramen—between lacrimal and maxilla (0), within lacrimal (1), or within maxilla (2).
61. (M103*) Nasolacrimal duct—lateral to posterior part of incisor (0), or medial to posterior part of incisor (1).
62. (M104) Lateral vacuity of nasolacrimal duct—absent (0), or present (1).
63. Orbital pocket of lacrimal—absent (0), or present (1).
64. (M127*) Orbits—anterior extent over P4 or more anterior (0), or shifted posteriorly (1).
65. Orbit size—less than 15% skull length (0), or greater than 20% skull length (1).
66. (M146) Supraorbital crest—absent (0), or present (1).
67. (M145*) Postorbital process—absent (0), on frontal (1), or on parietal and squamosal (2). [ordered]
68. Frontoparietal suture—narrow, *V*-shaped (0), flat (1), or broad, *U*-shaped (2).
69. Temporal lines—meet anteriorly to form sagittal crest (0), meet posteriorly to form sagittal crest (1) or sagittal crest absent (2).
70. (M154) Interparietal—absent (0), or present (1).
71. (M153*) Hamulus-bulla relationship—hamulus distant from bulla (0), or extends to or nearly to bulla (1).
72. (M100*) Left and right optic foramina—separate (0), or confluent (1).
73. (M150) Orbital process of alisphenoid—significant (0), or greatly reduced (1).
74. (M151*) Alisphenoid-frontal contact—present (0), or absent (1).
75. (M152*) Alisphenoid-parietal contact—present (0), or absent (1).
76. Pterygoid fossa—shallow (0), or deep (1).
77. (M111) Sphenopterygoid canal—absent (0), or present (1).
78. (M112) Sphenopalatine vacuity—absent (0), or present (1).
79. (M105*) Foramen ovale—within alisphenoid (0), or between alisphenoid and petrosal or ectotympanic (1).
80. Foramen ovale accessorius—absent (0), or present (1).
81. Masticatory and buccinator foramina—absent (1), or present (1).
82. Ectopterygoid crest—short, anterior to foramen ovale (0), or long, extends beyond foramen ovale (1).
83. Alisphenoid tympanic process posterior to foramen ovale—absent (0), or present (1).
84. (M110*) Alisphenoid canal—present (0), or absent (1).
85. (M149*) Glenoid fossa—near anterior extent of ear region (0), or well anterior to ear region (1).
86. (M99*) Postglenoid foramen—within squamosal (0), or between squamosal and ectotympanic or petrosal (1).
87. Piriform fenestra—extensive (0), restricted (1), or absent (2). [ordered]
88. Anteromedial shelf of petrosal—ridge-like (0), flattened (1), or separated from promontorium (2).
89. (M166*) Transpromontorial groove for internal carotid artery—present (0), or absent (1).
90. (M167*) Groove for stapedial artery on promontorium—present (0), or absent (1).
91. (M168*) Stapedial artery—ventral to fenestra cochleae (0), or partially shielding fenestra (1).
92. (M169*) Facial nerve—occupies groove in middle ear (0), or enclosed in canal (1).
93. (M173*) Fenestra cochleae—facing posteroventrally (0), or turning laterally (1).
94. Post-promontorium tympanic sinus—small (0), or enlarged, extending posterior to level of stapedius fossa (1).
95. Epitympanic recess—small (0), or enlarged, extending anterior to level of promontorium (1).
96. Tegmen tympani—small (0), or enlarged, extending ventral to level of promontorium (1).
97. Caudal tympanic process of petrosal—with prolonged posterior horizontal shelf (0), or forms vertical wall (1).
98. (M155*) Mastoid of petrosal—not inflated (0), or inflated (1).
99. (M157) Mastoid exposure on occiput—present (0), or absent (1).
100. Petrosal exposure dorsal to external acoustic meatus—absent (0), present (1), or inflated (2). [ordered]
101. (M159*) Osseous external auditory canal—absent (0), or present (1).
102. Malleus/incus fusion—absent (0), or present (1).
103. Tympanic process of basioccipital—absent or weak (0), or strong (1).
104. Condyloid canal—absent (0), or present (1).

APPENDIX 5. Taxon-character matrix for the phylogenetic analysis reported here.
Codes for polymorphic taxa are: A = 0 & 1 ; B = 0 & 2 ; C = 1 & 2

Sinomylus	0 0 0 0 0 ? 0 0 0 0	0 1 1 1 1 0 0 0 1 A	1 0 0 0 0 0 ? ? ? ?	? ? ? ? ? ? ? ? ? ?	? 0 ? ? ? ? ? ? ? 1
	0 0 0 ? ? ? ? ? 0 ?	0 0 ? 0 ? 0 ? ? ? ?	? ? ? ? ? ? ? ? ? ?	? ? ? ? ? ? ? ? ? ?	? ? ? ? ? ? ? ? ? ?
	? ? ? ?				
Tribosphenomys	0 0 0 0 0 1 1 1 ? ?	? ? ? 0 0 0 0 0 0 0	1 0 0 0 0 0 0 1 0 ?	? 0 A 0 1 0 0 0 0 1	0 A 0 0 ? 0 1 ? 0 ?
	? ? 0 ? ? ? ? ? ? ?	? ? ? 0 ? ? ? ? ? ?	? ? ? ? ? ? ? ? ? ?	? ? ? ? ? ? ? ? ? ?	? ? ? ? ? ? ? ? ? ?
	? ? ? ?				
Alagomys	1 1 0 ? 0 0 ? ? ? ?	? ? ? 0 1 0 ? 0 0 0	0 0 0 0 0 0 0 1 1 0	1 0 1 0 0 0 0 0 1 0	0 A 2 0 ? ? 1 ? ? ?
	? ? ? ? ? ? ? ? ? ?	? ? ? ? ? ? ? ? ? ?	? ? ? ? ? ? ? ? ? ?	? ? ? ? ? ? ? ? ? ?	? ? ? ? ? ? ? ? ? ?
	? ? ? ?				
Paramys	1 1 0 0 0 0 1 1 2 1	0 0 0 1 1 0 0 1 1 1	1 0 0 0 0 1 0 1 1 0	1 0 1 0 1 0 C 0 0 0	A 0 0 0 0 0 1 0 0 0
	1 1 0 0 0 0 0 0 0 0	0 0 0 0 0 0 0 0 0 0	0 0 0 0 0 0 0 0 0 0	0 0 0 0 0 0 0 0 0 0	
	? ? 0 0				
Reithroparamys	1 1 0 0 0 0 1 1 2 1	0 0 0 1 1 0 0 1 1 1	1 0 0 0 0 1 0 1 1 0	1 0 1 0 0 0 2 0 0 0	1 1 0 0 0 0 1 0 0 0
	1 1 0 0 0 ? ? 0 0 ?	0 0 0 0 0 0 0 0 0 0	? 0 0 ? ? 0 0 ? 0 ?	? ? 1 0 0 0 0 2 1 0	1 0 0 1 1 1 0 0 0 0
	0 ? 1 0				
Sciuravus	1 1 0 0 0 0 1 1 2 1	1 0 0 1 1 0 1 1 1 1	1 0 0 0 0 1 1 1 1 0	1 0 1 0 1 0 1 0 0 0	2 A 0 0 0 0 1 0 0 0
	A 1 0 B 0 0 0 0 0 ?	0 0 0 0 0 0 0 0 0 1	? ? 0 0 0 0 0 0 0 ?	0 ? 0 0 0 0 0 0 0 0	0 0 0 0 0 0 0 0 0 ?
	0 ? 0 0				
Protadelomys	1 1 0 0 0 ? 2 ? 2 1	0 1 0 1 1 1 1 1 1 1	1 0 0 0 0 1 1 1 1 0	1 1 1 0 0 1 2 0 0 0	2 ? ? ? ? ? ? ? ? 0
	? ? 1 A 0 ? ? ? ? 0	? 0 ? 0 0 ? ? ? 0 ?	? ? ? ? ? 0 0 1 0 0	0 0 ? ? 0 ? ? ? ? ?	? ? ? ? ? ? ? ? ? ?
	? ? ? ?				
Cocomys	1 1 1 0 0 1 1 1 0 1	1 0 0 1 1 0 0 1 1 1	1 0 0 0 0 0 0 1 1 1	1 0 1 0 1 0 1 1 1 1	0 0 0 0 0 0 0 0 ? 1
	1 1 0 1 0 1 1 0 0 0	0 0 0 0 1 0 0 2 2 1	? 1 0 0 0 1 0 1 0 1	0 1 1 0 0 0 1 1 0 0	0 0 0 1 1 1 1 0 0 0
	0 ? 0 1				
Exmus	1 1 1 0 0 1 1 1 1 1	1 1 1 1 1 0 0 1 1 1	1 1 0 0 0 0 0 1 1 0	0 0 1 0 1 0 1 1 1 1	0 0 0 0 0 0 1 0 0 1
	1 0 0 1 0 1 C 0 1 0	0 0 1 0 1 1 1 2 2 0	1 1 0 0 0 1 0 1 0 1	1 1 1 A 0 0 1 1 1 0	0 0 0 1 1 1 1 0 0 0
	0 0 1 1				
Bandaomys	? ? 0 ? 0 0 ? ? 1 1	1 1 0 1 1 0 0 1 1 1	0 0 0 0 0 0 0 0 1 0	1 0 1 0 1 0 2 1 0 0	1 ? ? ? ? ? ? ? ? ?
	? ? ? ? ? ? ? ? ? ?	? ? ? ? ? ? ? ? ? ?	? ? ? ? ? ? ? ? ? ?	? ? ? ? ? ? ? ? ? ?	? ? ? ? ? ? ? ? ? ?
	? ? ? ?				
Tamquammys	? ? 0 0 0 1 1 1 0 0	1 0 0 1 1 0 0 1 1 0	1 0 0 0 0 1 0 1 1 1	1 0 1 0 1 0 1 1 1 1	2 ? ? ? ? ? 1 ? ? ?
	? ? 1 ? ? ? ? ? ? ?	? ? ? ? ? ? ? ? ? ?	? ? ? ? ? ? ? ? ? ?	? ? ? ? ? ? ? ? ? ?	? ? ? ? ? ? ? ? ? ?
	? ? ? ?				
Advenimus	? ? 1 0 0 1 1 ? 2 1	1 1 0 1 1 0 0 1 1 1	1 0 0 0 0 1 0 1 1 0	0 0 1 0 1 0 1 1 1 1	1 0 0 ? ? 0 A ? ? ?
	? ? 1 ? ? ? ? ? ? ?	? ? ? ? ? ? ? ? ? ?	? ? ? ? ? ? ? ? ? ?	? ? ? ? ? ? ? ? ? ?	? ? ? ? ? ? ? ? ? ?
	? ? ? ?				
Yuomys	? ? 1 ? 0 1 1 A 2 1	0 0 1 1 1 1 0 1 1 1	1 1 1 0 0 1 1 1 1 0	0 1 1 0 1 0 1 0 1 1	2 1 1 ? ? 0 1 0 ? 1
	? ? 1 ? ? ? ? ? ? ?	? ? ? ? ? ? ? ? ? ?	? ? ? ? ? ? ? ? ? ?	? ? ? ? ? ? ? ? ? ?	
	? ? ? ?				

APPENDIX 5 CONT.

Tataromys	1210112?00 011111C220 1110000110 1110001211 2101001001 2012100001? 0011111221 ?100010101 11?00?2?1? ?1?1??1102 1?1?
Sayimys	1210102?00 0111111220 1110110110 1110002200 2112?021?? ??101????? ???1????2?1 1????101?1 ?11?0??2?? ???????1?? 1???
Ctenodactylus	1220112??? ???11??220 11100??110 111100?201 ?112102112 1010102011 0011112121 1101010101 0101012211 ?111111102 1111
Pectinator	??20102??0 01111??220 11101?0110 111100?200 2112102112 1010002011 0011112C21 1101010102 0101012211 ?1?1111102 1?1?
Tsaganomys	1210102?02 0111110220 0110001110 1010011000 1110011001 2002002000 1010001000 1011?00?10 0000002211 ?111100?000 1010
Paraphiomys	1210102?22 2111112220 1111111110 1110011000 1111012001 2010000100 1000101111 1010101100 0000??2211 ?111??1011 110?
Erethizon	1211101?22 2111112220 1111111110 1110012200 2A010A1001 1110000102 10?1000010 1010101110 1001112211 ?111001011 1100
Cavia	1221102?2? 21111?2220 111111?110 1110012?0? ?112012111 1112002111 1101110120 0111111100 0000112211 ?111001012 1100
Dasyprocta	1220102?22 2111112220 1111111110 1111012?00 2111011100 1110000111 1101111110 1111101100 001A112211 ?111001111 1100

APPENDIX 6. Diagnoses of nodes from the strict consensus tree (Fig. 23) resulting from the PAUP analyses of the taxon-character matrix in Appendix 5. Only unequivocal characters are listed.

(*Reithroparamys*, *Paramys*, *Sciuravus*, and *Protadelomys*) + (*Bandaomys* + "ctenodactyloids")
18(1) upper molar anteroloph distinct, but low
20(1) upper molar mesostyle present
37(1) metalophid II of m2 short
41(1) hypolophid of lower molar incomplete

Reithroparamys, *Paramys*, *Sciuravus*, and *Protadelomys*
9(2) P4 paracone and metacone equal in size
12(0) P4 protoconule present
26(1) upper molar mure present
50(0) incisive foramina closer to incisors than cheek teeth
52(1) nasal extends farther posteriorly than premaxilla

Sciuravus + *Protadelomys*
17(1) Upper molar metaloph extends to hypocone (paralell to protoloph)
27(1) p4 hypolophid present
41(2) lower molar hypolophid complete

Paramys (*Sciuravus* + *Protadelomys*)
88(0) anteromedial shelf of petrosal ridge-like
89(0) transpromontorial groove for internal carotid artery present
94(0) post-promontorial tympanic sinus small
95(0) epitympanic recess small
103(0) tympanic process of basioccipital absent or weak

Bandaomys + "ctenodactyloids"
11(1) P4 hypocone small
38(1) ectolophid of m2 in little worn teeth ends posterior to protoconid

"ctenodactyloids"
3(1) cheek teeth with some unilateral hypsodonty
6(1) cheek tooth size increases posteriorly
39(1) hypoconulid of m1-2 distinct
40(1) hypoconulid of m3 greater than that of m2

Cocomys + *Exmus*
41(0) hypolophid of lower molar absent
54(1) palatine on palate anterior to M1
56(1) orbital wing of the palatine prolonged anteriorly
57(1) sphenopalatine foramen between maxilla and palatine
88(1) anteromedial shelf of petrosal flattened

Advenimus (*Tamquammys* (*Yuomys* + Ctenohystrica))
26(1) upper molar mure present
53(1) infraorbital foramen large

Tamquammys (*Yuomys* + Ctenohystrica)
41(2) hypolophid of lower molar complete

Yuomys + Ctenohystrica
11(0) P4 hypocone absent
13(1) P4 metaconule absent
16(1) upper molar protoloph strong
22(1) M1-2 protoconule absent
23(1) M1-2 metaconule absent
32(1) lower molar hypoflexid deep
38(0) ectolophid of m2 in little worn teeth with strong connection between protoconid and hypoconid

Ctenodactylidae
10(0) anterior and posterior ridges of P4 weak or incomplete
17(1) upper molar metaloph extending to hypocone (parallel to protoloph)
38(2) ectolophid of m2 in little worn teeth shifted lingually
55(1) posterior margin of palate posterior to M3
56(1) lacrimal facial process substantial
64(1) orbits shifted posteriorly
66(1) supraorbital crest present
70(1) interparietal present
98(1) mastoid of petrosal inflated
100(2) petrosal exposure dorsal to external acoustic meatus inflated

Ctenodactylus (*Sayimys* + *Pectinator*)
44(2) coronoid process nearly absent
45(1) mandibular condyle height even with occlusal surface
47(2) anterior edge of masseteric fossa extends below anterior half of m1 or p4
48(1) dorsal margin of masseteric fossa horizontal
49(1) mandibular foramen lower than tooth row
50(2) incisive foramina nearly as long as diastema
57(2) sphenopalatine foramen between maxilla and frontal
67(2) postorbital process on parietal and squamosal
74(1) alisphenoid-frontal contact absent
84(1) alisphenoid canal absent

Sayimys + *Pectinator*
6(0) cheek tooth size not increasing posteriorly
25(1) upper molar hypoflexus deep
40(0) hypoconulid of m3 subequal to that of m2

Hystricognathiformes
6(0) cheek tooth size not increasing posteriorly
10(2) anterior and posterior ridges of P4 as high as protoloph and metaloph
36(1) entoconid of lower molar anteriorly shifted
40(0) hypoconulid of m3 subequal to that of m2
46(1) angular process origin lateral to plane of body
61(1) nasolacrimal duct medial to posterior part of incisor
73(1) orbital process of alisphenoid greatly reduced
95(0) epitympanic recess small

Hystricognathi
9(2) P4 paracone and metacone equal in size
11(2) P4 hypocone very large and anteroposteriorly extended
17(2) upper molar metaloph extending posteriorly to join posteroloph
24(1) upper molar mesoloph present
25(1) upper molar hypoflexus deep
44(1) coronoid process reduced, subequal to condylar process
(1) jugal in ventral orbital wall only
77(1) sphenopterygoid canal present
99(1) mastoid exposure on occiput absent
103(0) tympanic process of basioccipital absent or weak

Erethizon (*Cavia* + *Dasyprocta*)
37(2) metalophid II of m2 closes trigonid posteriorly
52(1) nasal extends farther posteriorly than premaxilla
64(1) orbits shifted posteriorly

Cavia + *Dasyprocta*
3(2) cheek teeth hypsodont
48(1) dorsal margin of masseteric fossa horizontal
57(1) lacrimal facial process substantial
62(1) lateral vacuity of nasolacrimal duct present
66(1) supraorbital crest present
72(1) left and right optic foramina confluent
74(1) alisphenoid-frontal contact absent